UILU-ENG-86-2003

CIVIL ENGINEERING STUDIES

STRUCTURAL RESEARCH SERIES NO. 524

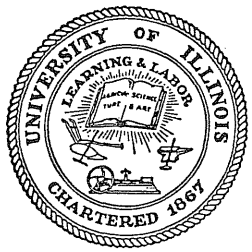

ISSN: 0069-4274

A MIXED EULERIAN-LAGRANGIAN MODEL FOR THE ANALYSIS OF DYNAMIC FRACTURE

By
HYUN M. KOH
and
ROBERT B. HABER

Technical Report of Research
Sponsored by
THE NATIONAL SCIENCE FOUNDATION
Grant No. MEA 84-00654

UNIVERSITY OF ILLINOIS
at URBANA-CHAMPAIGN
URBANA, ILLINOIS
FEBRUARY 1986

A MIXED EULERIAN-LAGRANGIAN MODEL FOR THE ANALYSIS OF DYNAMIC FRACTURE

By

Hyun M. Koh

and

Robert B. Haber

A Technical Report of
Research Sponsored by

THE NATIONAL SCIENCE FOUNDATION
Grant No. MEA 84-00654

University of Illinois
at Urbana-Champaign
Urbana, Illinois

February 1986

ACKNOWLEDGEMENT

This report was prepared as a doctoral dissertation by Mr. Hyun M. Koh and was submitted to the Graduate College of the University of Illinois at Urbana-Champaign in partial fulfillment of the requirements for the degree of Doctor of Philosophy in Civil Engineering. The thesis was done under the supervision of Dr. Robert B. Haber, Associate Professor of Civil Engineering.

The investigation was supported by the National Science Foundation under Grant MEA 84-00654, "Eulerian-Lagrangian Kinematic Models in Fracture Mechanics." The authors wish to thank Drs. A. R. Robinson, D. A. W. Pecknold and W. C. Schnobrich, Professors of Civil Engineering, and Dr. K.-S. Kim, Assistant Professor of Theoretical and Applied Mechanics, for their assistance.

The numerical computations were performed on the Boeing Computer Services Cray X-MP with the support of the National Science Foundation Office of Advanced Scientific Computation. Pre- and post-processing of the numerical data was performed on the VAX and Image Processing System (VIPS) at the University of Illinois at Urbana-Champaign. Access to the VIPS was provided by the Civil Engineering Department, University of Illinois at Urbana-Champaign.

TABLE OF CONTENTS

LIST OF TABLES

LIST OF FIGURES

CHAPTER 1

INTRODUCTION

1.1 Background

Cracks are present in essentially all structural materials, either as natural imperfections or as a result of fabrication processing. When the crack sizes are sufficiently large, their existence can significantly reduce the strength of the material. Under certain conditions the cracks will propagate, slowly or rapidly, to further reduce the material strength or to cause the failure of a structure. Crack growth can result from high load levels, cyclic loading, or as a time-dependent phenomenon at low load levels, associated with creep, stress corrosion or other environmental influences.

The fracture of solids, from a micromechanics viewpoint, can be seen as a process of nucleation, growth and coalescence of voids or microcracks. When the crack size is large compared to the characteristic dimensions of the material microstructure a continuum mechanics theory can be used to explain the mechanism of fracture. In this case, two broad categories of fracture processes can be identified: ductile fracture and brittle fracture. These broad classifications are useful, even though the details of the fracture process will vary with the material, load conditions, temperature and other environmental conditions.

Ductile fracture is associated with large-scale plastic deformation and crack-tip blunting prior to the initiation of crack growth. This implies high rates of energy dissipation and slow fracture velocities. Ductile fracture usually occurs in high-toughness, low-strength materials. Fracture often occurs in a brittle manner if the plastic deformations are confined to

a region which is small compared to a characteristic crack dimension (as in the case in brittle materials such as glass, ceramics and high-strength metallic alloys). Even in ductile materials, brittle fracture can occur when the plastic flow is inhibited by low temperature or triaxial stresses induced by geometric constraints. Brittle fracture generates low rates of energy dissipation. Thus, a sustained level of loading can cause unstable, fast crack propagation at velocities on the order of the material's characteristic wave speeds. Inertia effects become significant when rapid crack propagation causes large material velocities. This study is concerned with brittle fracture, and the following discussion is devoted primarily to problems in brittle fracture.

A major concern in the continuum mechanics of fracture is the determination of a realistic fracture criterion [1]. The energy balance theory, first formulated by Griffith [2], assumes that crack extension will occur when the change in the external work is equal to the sum of the strain energy change and a material-dependent surface fracture energy associated with the creation of new crack surface. Kinetic energy is also considered in the energy balance for dynamic fracture [3]. Irwin [4] and Orowan [5] introduced plastic work as an additional energy dissipation mechanism.

In linear elastic fracture the energy variation due to crack advance can be expressed in terms of the stress intensity factor [6]. The stress intensity factor indicates the strength of the singularity in the stress field at the crack tip. This implies that the stress intensity factor not only defines the local crack-tip stress field but also provides a parameter for a fracture criterion equivalent to the energy balance theory. The form of the stress singularity is common for all stationary cracks in elastic materials, whether the response is static or dynamic [7]. Therefore, the dynamic stress field around a stationary, (or slowly moving) crack tip can

also be characterized by the stress intensity factor. Rapid dynamic brittle fracture involves more complicated features, such as the interaction between reflected stress waves and the crack-tip zone, fracture initiation and arrest, and crack branching [8]. Nevertheless, the order of the singularity in the stress field (for subsonic crack velocities) is the same as for stationary cracks, and a dynamic stress intensity factor provides useful information to describe these problems. Thus, most analytic and experimental studies are directed to the solution and evaluation of the stress intensity factors, in both linear elastic fracture [9,10] and dynamic fracture [11,12,13].

Since analytic procedures are limited to highly idealized geometries and loading conditions, numerical methods play an important role in fracture analysis, particularly for problems involving dynamic brittle fracture. Finite element methods have been used extensively to analyze both linear elastic [14] and dynamic brittle fracture problems [15,16]. Various singular elements provide an efficient way to model crack-tip stress singularities and to compute stress intensity factors. However, existing finite element techniques suffer some drawbacks. It is difficult to model the crack-tip motion and the singular strain and velocity fields properly. Awkward remeshing operations and interpolation of field variables are often required. These can lead to complex solution procedures and, more importantly, to inaccurate results. These problems can be attributed to the inherent properties of finite element procedures based on Lagrangian kinematic models. A major theme in this work is the development of a new kinematic model for dynamic fracture to overcome these problems.

1.2 Objectives and Scope

The objectives of this study are to develop appropriate kinematic models and continuum formulations for the analysis of static and dynamic fracture problems; and to develop effective computational methods based on the continuum formulations.

A special small-deformation form of the Eulerian-Lagrangian kinematic description is developed for modeling static and dynamic fracture problems. The advantages of this kinematic model over conventional Lagrangian models are explored. The mixed Eulerian-Lagrangian kinematic description (ELD) has previously been applied to large-deformation static analysis in solid mechanics problems [17] and the analysis of frictional contact problems [18,19].

Chapter 2 presents a finite element method for computing the energy release rates and the stress intensity factors in linear elastic fracture problems. The Eulerian-Lagrangian kinematic description is specialized to small-deformation problems, and used to derive explicit expressions for the mutual potential energy release rates. Finite element procedures are developed to evaluate integral expressions for the energy release rates and to compute the stress intensity factors. Several pure mode-I and mixed-mode linear elastic fracture problems are analyzed.

The small-deformation form of the Eulerian-Lagrangian kinematic description is extended to elastodynamic problems in Chapter 3. Expressions for relevant field variables in the ELD and their material time derivatives are presented and used to formulate the variational equations of motion. The dynamic ELD introduces more stringent continuity requirements than conventional Lagrangian formulations. A special weak form of the variational equations of motion relaxes the continuity conditions, and is the

basis of finite element formulation using moving isoparametric elements, which is suitable for dynamic problems.

In Chapter 4 the dynamic ELD formulation is applied to rapid crack propagation problems. Moving isoparametric finite element solution procedures are developed that correctly simulate the crack-tip motion and the singular forms of the fields of strain energy density and kinematic energy density. The dynamic stress intensity factor is computed from the energy release rates obtained by either virtual rate expressions or from global energy differences. Numerical examples of dynamic crack propagation are presented. The transient stages of crack acceleration and arrest are studied. The effects of wave propagation on dynamic crack propagation behavior are discussed. Recommendations for further research are given in Chapter 5.

1.3 Notation

Symbols used in this study are defined when they first appear in the text and wherever clarification is necessary. Tensors and matrices are denoted by boldfaced characters. Tensor quantities are expressed in terms of Cartesian basis vectors. Repeated subscript indices imply summation, unless indicated otherwise. The most frequently used symbols are listed below. Quantities in the Eulerian-Lagrangian model are expressed as functions of the reference coordinates, unless specified otherwise.

$\mathbf{B}$	:	Strain-displacement transformation matrix
$\mathbf{C}$	:	Effective damping matrix
$\mathbf{E}$	:	Elasticity matrix
$\mathbf{H}$	:	Matrix of finite element shape functions
$\mathbf{K}$	:	Stiffness matrix

$\bar{K}$, $\hat{K}$: Effective stiffness matrices for explicit and implicit integration

n : Unit surface normal vector

M : Mass matrix

P : Load vector

$\bar{P}$, $\hat{P}$: Effective load vectors for explicit and implicit integration

T : Surface traction vector

U, $\dot{U}$, $\ddot{U}$: Global vector of node displacements and global vectors of the first- and second-order spatial time derivatives of the node displacements

U_e, $\dot{U}_e$, $\ddot{U}_e$: Element vector of node displacements and element vectors of the first- and second-order spatial time derivatives of the node displacements

ξ^N : Local natural coordinate vector, used to describe the reference volume of region N

ϕ_N : Auxiliary coordinate mapping for region N

A : Surface of the material volume V of a structure

A_0 : Surface of a local material volume V_0 around the crack tip

A_T : Portion of a material volume surface on which the tractions are prescribed

A_u : Portion of a material volume surface on which the displacements are prescribed

a : Current length or half length of a crack

a_0 : Initial crack length

a^r : Surface of a reference volume v^r corresponding to A

a_0^r : Surface corresponding to A_0 of a local reference volume v_0^r around a crack tip

a_T^r : Portion of the surface of a reference volume on which the tractions are prescribed

b : Length or half length of a plate, or length of a finite element

b_i, $\hat{b}_i$: Components of the body force vector per unit mass, expressed as functions of the reference and material coordinates

c_i, $i=1,8$: Constants used in Newmark's time integration method

C_D, C_R, C_S : Dilatation, Rayleigh and shear wave speeds

$C_{ijk\ell}$: Components of the elasticity tensor

E : Young's modulus

e_{ij} : Components of the small-deformation strain tensor

F_i : Components of body force per unit volume

G, $G^{(1,2)}$: Potential energy release rate, and mutual potential energy release rate associated with two independent equilibrium states 1 and 2

h : Height or half height of a plate, or height of a finite element

h_α : Finite element shape function for node α

$\tilde{J}$: Determinant of the Jacobian $\tilde{J}$

$\tilde{J}_{ij}$: Jacobian components of the mapping between the reference and material configurations

$\bar{J}_{ij}$: Inverse Jacobian components of the mapping between the reference and material configurations

$\dot{\bar{J}}_{ij}$: Spatial time derivatives of the components $\bar{J}$

K_a : Surface area metric relating differential areas in the reference and material configurations

K_I, K_{II}, K_{III} : Stress intensity factors for modes I, II and III

$K(t,v)$: Time and velocity dependent dynamic stress intensity factor

L : Height of a plate

$M^{(1,2)}$: Mutual potential energy associated with two independent equilibrium states 1 and 2

n_i : Direction cosines of a unit surface normal vector

r : Radial distance from the crack tip

s : Plate thickness for plane stress and plane strain problems, or the circumference at the crack tip for axisymmetric problems

T_i, $\hat{T}_i$: Components of the surface traction vector, expresssed as functions of the reference and material coordinates

$\overline{T}_i$: Components of a prescribed surface traction vector

u_i, $\hat{u}_i$: Displacement components, expressed as functions of the reference and material coordinates

$\dot{u}_i$, $\ddot{u}_i$: First- and second-order spatial time derivatives of the displacement components

$\overset{*}{u}_i$, $\overset{**}{u}_i$: Components of the material velocity and acceleration vectors

$\overline{u}_i$, $\overline{\overset{*}{u}}_i$: Components of prescribed displacement and material velocity vectors

$u_{i\alpha}$, $\dot{u}_{i\alpha}$, $\ddot{u}_{i\alpha}$: Displacement components in direction i at node α and their first- and second-order spatial time derivatives

V : Material volume of a structure

V_0 : Local material volume around a crack tip

v : Crack-tip velocity

v^r : Reference volume corresponding to V

V_0^r : Reference volume corresponding to V_0

$V_{\zeta 0}^r$: Reference volume of crack-tip element ζ

W : Plate width

w, $w^{(1,2)}$: Strain energy density, and mutual strain energy density associated with two independent equilibrium states 1 and 2

$\hat{w}^{(1,2)}$: Mutual strain energy density associated with two independent equilibrium states 1 and 2, expressed as a function of the material coordinates

X_i, $\dot{X}_i$, $\ddot{X}_i$: Components of the material coordinate vector, and their first- and second-order spatial time derivatives

X_i, $\dot{X}_{i\alpha}$, $\ddot{X}_{i\alpha}$: Component in direction i of the material coordinate vector at node α, and its first- and second-order spatial time derivatives

x_i^r : Components of the reference coordinate vector

β : Newmark time integration constant, or constant used in (2.45)

Δ : Symbol denoting incremental quantities

δ : Symbol denoting virtual quantities, or Newmark time integration constant

δ_{ij} : Kronecker delta

ε_{ijk} : Permutation symbol

μ : Shear modulus

ν : Poisson's ratio

Π : Potential energy functional

ρ, $\hat{\rho}$: Mass density expressed as functions of the reference and material coordinates

σ_{ij} : Components of the Cauchy stress tensor

Ω_N^t : Domain of a region N at time t

ω_N^r : Reference volume corresponding to region N

CHAPTER 2

COMPUTATION OF THE STATIC STRESS INTENSITY FACTORS USING THE EULERIAN-LAGRANGIAN KINEMATIC MODEL

2.1 General

A crack in a stressed body causes a significant stress concentration in the vicinity of the crack tip. Inelastic deformation usually develops near the crack tip, except in extreme cases of brittle fracture. When the size of the inelastic deformation zone is small with respect to the crack size and other geometric dimensions, the local stress field can be adequately represented by a function with a singularity of order $r^{-1/2}$, where r is the radial distance from the crack tip [6]. The strength of the singularity is often characterized by the stress intensity factors K_I, K_{II} and K_{III}, corresponding to deformation modes of opening, in-plane sliding and anti-plane sliding of the crack surfaces.

The Griffith fracture criterion is derived from the overall energy balance of a structure. In linear elastic fracture, the energy variation due to crack advance is determined by the local stress and deformation fields near the crack tip; while the surface energy associated with crack growth is assumed to be a property of the material under consideration. This implies that the critical conditions for fracture can be expressed in terms of the stress intensity factors; i.e. fracture will occur when the stress intensity factor attains a critical value [6].

A primary objective of linear elastic fracture analysis is to calculate the stress intensity factors for given crack dimensions, structural geometries and loading conditions. This provides a description of the stress field near the crack tip, and provides information needed for

predicting the onset of crack propagation and the propagation direction [20].

The energy release rate, G, is the energy change per unit crack advance per unit thickness. The stress intensity factors are related to the energy release rate as

$$G = \frac{1-\nu^2}{E}(K_I^2 + K_{II}^2) + \frac{1+\nu}{E}K_{III}^2 \qquad \text{(plane strain)} \qquad (2.1)$$

$$G = \frac{1}{E}(K_I^2 + K_{II}^2 + K_{III}^2) \qquad \text{(plane stress)} \qquad (2.2)$$

where E is Young's modulus and ν is Poisson's ratio. Rice [21] demonstrated that the path-independent J-integral is equivalent to the energy release rate and can be used for the analysis of linear elastic fracture problems. The direct relation between G and the stress intensity factors indicates the equivalence of the energy balance and the critical stress intensity criteria for crack growth. Various analytic solutions of linear elastic fracture problems are listed in [9].

Analytic solution methods can be used for cases of relatively simple geometry; but in practical engineering problems with complex geometries and stress distributions, numerical methods are needed to compute the stress intensity factors. The finite element method is a versatile and powerful technique for the analysis of crack problems with realistic complexity. The virtual crack extension method appears to be the most attractive available finite element method for calculating the energy release rates. Conventional Lagrangian kinematic models, the basis of most finite element elasticity solutions, do not permit the formulation of true energy release

rate expressions because true variations of the crack length are not possible.

In this chapter explicit integral expressions for the energy release rates and stress intensity factors in linear elastic fracture mechanics problems are derived using a mixed Eulerian-Lagrangian kinematic model. This approach was presented previously in [22,23]. Here a more concise development of the general mixed-mode solution method using the mutual potential energy functional is presented. A review of finite element methods for computing the stress intensity factors is given in Section 2.2. Section 2.3 presents the Eulerian-Lagrangian kinematic description for small deformation analysis. Expressions for the potential energy and mutual potential energy functionals are developed using the Eulerian-Lagrangian model. Explicit expressions for the instantaneous mutual potential energy release rates are derived in Section 2.4. Finite element procedures for calculating the stress intensity factors from the mutual energy release rates in mixed-mode fracture problems are developed in Section 2.5. Section 2.6 presents example numerical results for finite element computation of fracture stress intensity factors using the new procedure.

2.2 Review of Finite Element Procedures for Computing the Stress Intensity Factors

The finite element method is a popular technique for the analysis of fracture mechanics problems. The use of various singularity elements [24-32] provides an efficient means for calculating the stress intensity factor (SIF) in elastic crack problems.

Several approaches have been used to evaluate the SIF. First, the SIF may be calculated by substituting computed values of stress or displacement into the known crack-tip field equations [33,34]. This approach can produce

inaccurate results due to the errors inherent to finite element discretization. In order to overcome these disadvantages, Gifford and Hilton [35] proposed a direct approach using assumed-stress hybrid crack-tip elements which contain K_I and K_{II} as unknown stress field parameters. The SIF values are computed directly during the solution process.

Another alternative is to compute the stress intensity factors as functions of the energy release rates associated with crack extension. The energy release rates can be estimated by computing the change in energy of a structure for two neighboring positions of the crack tip. Since discretization errors tend to be self-cancelling when the energy differences are computed, the energy method is reliable and accurate and is the preferred choice of many analysts. Watwood [36] computed the strain energy for two slightly different crack lengths by performing two complete finite element analyses. He employed numerical differentiation to determine the strain energy release rate. Parks [37] and Hellen [38], refined the method so that the energy release rate is calculated without a full second analysis by considering only the elements immediately surrounding the crack tip. Since a true virtual crack extension is not used in these methods, the analyst must provide a finite length of crack extension that will accurately predict the energy release rate. In addition, either the computation and storage of stiffness variation matrices or the use of substructuring and wavefront solution techniques is required. Another means to calculate the energy release rate is the J-integral technique [33]. The J-integral, a path-independent contour integral involving the stress and displacement fields around the crack tip, is equivalent to the energy release rate G for the elastic case [10,21]. Parks demonstrated that his method is an area-analogue of the J-integral.

2.3 The Eulerian-Lagrangian Kinematic Description for Small-Deformation Analysis

In this section a specialization of the Eulerian-Lagrangian kinematic description [17] for small deformation analysis is developed. First, a kinematic model is developed that accommodates changes in both the displacement field and the undeformed geometry. A potential energy expression and the stationary condition for equilibrium are derived using the new description. The mutual potential energy associated with two independent equilibrium states is defined, and the principle of stationary mutual potential energy is stated.

2.3.1 Kinematics

A typical isoparametric finite element shown in Figure 2.1 is used to illustrate a version of the small-deformation Eulerian-Lagrangian model. A fixed, Cartesian global coordinate system is used to describe the material configuration. Here, the material configuration is represented by the isoparametric finite element geometry. A separate reference coordinate system is used to describe an independent reference configuration. These correspond to the element natural coordinate system and the parent element geometry in the isoparametric element version. Position vectors in the global and reference (natural) coordinate systems are denoted by $\mathbf{X}$ and $\mathbf{x}^r$, respectively.

The novel aspect of this kinematic description is that the natural coordinates $\mathbf{x}^r$ are the only independent spatial variables, and both the displacement field $\mathbf{u}$ and the mapping to the material configuration change with time.

$$\mathbf{u} = \mathbf{u}(\mathbf{x}^r, t) \tag{2.3}$$

$$\mathbf{X} = \mathbf{X}(\mathbf{x}^r, t) \tag{2.4}$$

In the above t designates an independent "time-like" parameter. In a conventional isoparametric model the geometric mapping does not change with time. Therefore, the set of material particles in each element is invariable. In the present development the material associated with each parent element can change. This requires a flux of material particles across element boundaries. No attempt is made in this development to define explicitly the displacement field as a function of the global coordinates and time. That is, $\mathbf{u} = \mathbf{u}(X,t)$ is not required.

The Jacobian $\tilde{\mathbf{J}}$ and inverse Jacobian $\bar{\mathbf{J}}$ of the mapping between $\mathbf{X}$ and $\mathbf{x}^r$ have components

$$\tilde{J}_{ij} = \frac{\partial X_i}{\partial x_j^r} \tag{2.5}$$

$$\bar{J}_{ij} = \tilde{J}^{-1}_{ij} = \frac{\partial x_i^r}{\partial X_j} \tag{2.6}$$

The metric tensor $\tilde{\mathbf{J}}$ is the transpose of the familiar Jacobian metric tensor used in isoparametric element formulations.

Assuming an admissible displacement field $\mathbf{u}$ and small deformations, the components of the strain tensor are expressed as

$$e_{ij} = \frac{1}{2}\left(u_{i,k}\,\bar{J}_{kj} + u_{j,k}\,\bar{J}_{ki}\right) \tag{2.7}$$

where a comma between subscripts denotes differentiation with respect to the natural coordinate system.

2.3.2 Potential Energy and Equilibrium

In this subsection an expression for the potential energy of a linearly elastic body is presented and equilibrium conditions are derived from the principle of stationary potential energy. Since $\mathbf{x}^r$ is the independent spatial variable, all integral expressions are written in the coordinate system of the parent element. The potential energy is given by

$$\Pi = \int_{v^r} w \tilde{J} \, dv^r - \int_{v^r} \rho b_i u_i \tilde{J} \, dv^r - \int_{a_T^r} T_i u_i K_a \, da^r \tag{2.8}$$

where $\mathbf{T}(\mathbf{x}^r,t)$ is a surface traction vector per unit area in the undeformed configuration, $\mathbf{b}(\mathbf{x}^r,t)$ is a body force vector per unit mass, the strain energy density is

$$w = \frac{1}{2} \sigma_{ij} e_{ij} \tag{2.9}$$

and the components of the stress tensor are

$$\sigma_{ij} = C_{ijk\ell} e_{k\ell} \tag{2.10}$$

In equation (2.8) $\tilde{J}$ is the determinant of the Jacobian $\tilde{J}$, v^r is the parent element volume, ρ is mass density in the undeformed configuration, a_T^r is the part of the surface of v^r on which surface tractions are prescribed, and K_a is a surface area metric such that a differential area dA in the material configuration is equal to $K_a da^r$.

The equations of equilibrium are derived from the condition $\delta_u \Pi = 0$ for all admissible variations in the displacement field, $\delta u = \delta u(\mathbf{x}^r)$.

$$\int_{v^r} \frac{\partial w}{\partial e_{ij}} \frac{\partial e_{ij}}{\partial u_k} \tilde{J}\, dv^r - \int_{v^r} \rho\, b_k\, \tilde{J}\, dv^r - \int_{a_T^r} T_k\, K_a\, da^r = 0 \qquad (2.11)$$

2.3.3 Mutual Potential Energy

Two independent equilibrium states, labeled 1 and 2, of a linearly elastic body are introduced. Superposition of the two equilibrium states yields another independent equilibrium state, labeled 0. The displacements, body forces and surface forces for equilibrium state 0 are

$$u_i^{(0)} = u_i^{(1)} + u_i^{(2)} \qquad (2.12)$$

$$b_i^{(0)} = b_i^{(1)} + b_i^{(2)} \qquad (2.13)$$

$$T_i^{(0)} = T_i^{(1)} + T_i^{(2)} \qquad (2.14)$$

The potential energy for equilibrium state 0 can be written in the following form.

$$\Pi^{(0)} = \Pi^{(1)} + \Pi^{(2)} + M^{(1,2)} \qquad (2.15)$$

$M^{(1,2)}$ in (2.15) is the mutual potential energy associated with the two independent equilibrium states 1 and 2.

$$M^{(1,2)} = \int_{v^r} w^{(1,2)}\, \tilde{J}\, dv^r - \int_{v^r} \rho(b_i^{(1)}\, u_i^{(2)} + b_i^{(2)}\, u_i^{(1)})\, \tilde{J}\, dv^r$$

$$- \int_{a_T^r} (T_i^{(1)}\, u_i^{(2)} + T_i^{(2)}\, u_i^{(1)})\, K_a\, da^r \qquad (2.16)$$

The mutual potential energy density $w^{(1,2)}$ is defined by

$$w^{(1,2)} = e^{(1)}_{ij} C_{ijk\ell} e^{(2)}_{k\ell} \tag{2.17}$$

The principle of stationary mutual potential energy [36] states that

$$\delta_{u^{(1)}} M^{(1,2)} = 0 \tag{2.18}$$

$$\delta_{u^{(2)}} M^{(1,2)} = 0 \tag{2.19}$$

for arbitrary admissible variations of the equilibrium displacement fields $u^{(1)}$ and $u^{(2)}$.

2.4 Explicit Expressions for the Instantaneous Energy Release Rates

The variation of the mutual potential energy corresponding to a variation of the crack length is used to derive explicit expressions for the instantaneous mutual potential energy release rates. The expressions are general for static mixed-mode fracture problems, and reduce to appropriate expressions for each pure mode case. Isoparametric finite element expressions for virtual crack extensions are presented.

2.4.1 Variational Expressions for Mutual Potential Energy Release Rates

In this section an instantaneous mutual potential energy release rate is obtained from the variation of $M^{(1,2)}$ due to a virtual crack extension. First, expressions for the variation of $M^{(1,2)}$ of an arbitrary fixed material volume are written in the material coordinate system, and then transformed to the reference coordinate system.

Consider a fixed finite material volume V_0 bounded by the surface A_0, which includes a part of the crack surfaces as shown in Figure 2.2. All of the field variables are first defined as functions of the material coordinates, indicated here by a circumflex "^". The variation of $M^{(1,2)}$ due to a virtual crack extension is as follows when expressed in the material coordinate system,

$$\delta M^{(1,2)} = \delta \int_{V_0} \hat{w}^{(1,2)} dV - \delta \int_{V_0} \hat{\rho} \, (\hat{b}_i^{(1)} \, \hat{u}_i^{(2)} + \hat{b}_i^{(2)} \hat{u}_i^{(1)}) \, dV$$

$$- \delta \int_{A_0} (\hat{T}_i^{(1)} \hat{u}_i^{(2)} + \hat{T}_i^{(2)} \hat{u}_i^{(1)}) dA - \delta \int_{\delta A} (\hat{T}_i^{(1)} \hat{u}_i^{(2)} + \hat{T}_i^{(2)} \hat{u}_i^{(1)}) \, dA \qquad (2.20)$$

in which δA is the crack surface created during the virtual crack extension. To simplify the analysis, but without loss of generality, it is assumed that during a virtual crack extension there are no variations of the mass density and body forces in V_0, no variations of the surface tractions on A_0, and that the newly-created crack surfaces are traction-free.

$$\delta \hat{\rho} = \delta \hat{b}_i^{(1)} = \delta \hat{b}_i^{(2)} = 0 \qquad \text{in } V_0 \qquad (2.21a)$$

$$\delta \hat{T}_i^{(1)} = \delta \hat{T}_i^{(2)} = 0 \qquad \text{on } A_0 \qquad (2.21b)$$

$$\hat{T}_i^{(1)} = \hat{T}_i^{(2)} = 0 \qquad \text{on } \delta A \qquad (2.21c)$$

Then equation (2.20) can be simplified.

$$\delta M^{(1,2)} = \delta \int_{V_0} \hat{w}^{(1,2)} dV - \delta \int_{V_0} \hat{\rho} \, (\hat{b}_i^{(1)} \, \delta \hat{u}_i^{(2)} + \hat{b}_i^{(2)} \delta \hat{u}_i^{(1)}) \, dV$$

$$- \int_{A_0} (\hat{T}_i^{(1)} \delta\hat{u}_i^{(2)} + \hat{T}_i^{(2)} \delta\hat{u}_i^{(1)}) dA \qquad (2.22)$$

The fixed material volume V_0 and the surface A_0 map onto the reference volume v_0^r which is bounded by the surface a_0^r. The field variables can be defined as functions of the reference coordinates $\mathbf{x}^r$, as an alternative to the above functions based on the material coordinates. Thus, the displacement function $\hat{\mathbf{u}}^{(n)}(\mathbf{X},t)$ in the material configuration is related to the function $\mathbf{u}^{(n)}(\mathbf{x}^r,t)$ by the inverse geometric mapping.

$$\hat{\mathbf{u}}^{(n)}(\mathbf{X},t) = \mathbf{u}^{(n)}(\mathbf{x}^r(\mathbf{X},t)) \ , \ n = 1,2 \qquad (2.23)$$

A virtual crack extension is modeled by a special variation in the geometric mapping $\delta\mathbf{X}(\mathbf{x}^r,t)$. To maintain equilibrium in the material volume during the virtual crack extension (subject to the conditions (2.21)), there must be variations in the displacement fields $\delta\mathbf{u}^{(n)}(\mathbf{x}^r)$; n = 1, 2. Equation (2.22) is then rewritten in the reference coordinate system as

$$\delta M^{(1,2)} = \int_{v_0^r} (\delta_{u^{(1)}} w^{(1,2)} + \delta_{u^{(1)}} w^{(1,2)}) \, \tilde{J} \, dv^r$$

$$- \int_{v_0^r} \rho \, (b_i^{(1)} \, \delta u_i^{(2)} + b_i^{(2)} \delta u_i^{(1)}) \, \tilde{J} \, dv^r$$

$$- \int_{a_0^r} (T_i^{(1)} \delta u_i^{(2)} + T_i^{(2)} \delta u_i^{(1)}) K_a da^r + \int_{v_0^r} \delta_X (w^{(1,2)} \tilde{J}) \, dv^r \qquad (2.24)$$

where δ_X denotes a variation due to the geometric variation. If the volume V_0 is in equilibrium, the first three integrals in (2.24) vanish for admissible variations $\delta\mathbf{u}^{(1)}$ and $\delta\mathbf{u}^{(2)}$, by the principle of stationary mutual

potential energy ((2.18) and (2.19)). The variation of the mutual potential energy is then simply

$$\delta M^{(1,2)} = \int_{V_0^r} (w^{(1,2)} \, \delta_X \tilde{J} + \delta_X \, w^{(1,2)} \, \tilde{J}) dv^r \tag{2.25}$$

The variation of the geometric mapping is defined as a function of $\mathbf{x}^r$ and the virtual crack length extension δa,

$$\delta \mathbf{X} = \delta \mathbf{X}(\mathbf{x}^r, \delta a) = \delta a \, \bar{\mathbf{X}}(\mathbf{x}^r) \tag{2.26}$$

where $\bar{\mathbf{X}}$ is an admissible variation of the geometric mapping consistent with crack growth. To ensure that a fixed material volume is maintained during the virtual crack extension, the geometric variation must satisfy the constraint

$$X_i \cdot n_i = 0 \quad \text{on } a_0^r \tag{2.27}$$

in which $\mathbf{n}$ is the outward normal to a_0^r. The variations of the Jacobian and inverse Jacobian have components

$$\delta \tilde{J}_{ij} = \delta \frac{\partial X_i}{\partial x_j^r} = \delta X_{i,j} \tag{2.28}$$

$$\delta \bar{J}_{ij} = \frac{\partial x_i^r}{\partial (X_j + \delta X_j)} - \frac{\partial x_i^r}{\partial X_j} = - \bar{J}_{ik} \, \delta X_{k,\ell} \, \bar{J}_{\ell j} \tag{2.29}$$

The variation of the determinant of the Jacobian is given by

$$\delta\tilde{J} = \varepsilon_{ijk} \left(\tilde{J}_{j2}\, \tilde{J}_{k3}\, \delta X_{i,1} + \tilde{J}_{i1}\, \tilde{J}_{k3}\, \delta X_{j,2} + \tilde{J}_{i1}\, \tilde{J}_{j2}\, \delta X_{k,3}\right) \tag{2.30}$$

where ε_{ijk} is the permutation symbol, and

$$\delta_X w^{(1,2)} = -\sigma_{ij}^{(1)}\, u_{i,k}^{(2)}\, \bar{J}_{k\ell}\, \delta X_{\ell,m}\, \bar{J}_{mj} - \sigma_{ij}^{(2)}\, u_{i,k}^{(1)}\, \bar{J}_{k\ell}\, \delta X_{\ell,m}\, \bar{J}_{mj} \tag{2.31}$$

The mutual potential energy release rate associated with a given direction of crack extension is

$$G^{(1,2)} = -\frac{1}{s}\frac{dM^{(1,2)}}{da} = -\frac{1}{s\delta a}\,\delta M^{(1,2)} \tag{2.32}$$

in which a is the length of the crack and s is either the plate thickness for plane stress and plane strain problems, or the circumference at the crack tip for axisymmetric problems.

2.4.2 Isoparametric Finite Element Expressions for the Energy Release Rates

A two-dimensional finite element model of a crack-tip region is shown in Figure 2.3. To evaluate (2.25), the isoparametric elements surrounding the crack tip are chosen as v_0^r, such that

$$v_0^r = \sum_{\zeta=1}^{P} v_{\zeta 0}^r \tag{2.33}$$

where $v_{\zeta 0}^r$ denotes the reference volume of crack-tip element ζ, and P is the number of crack-tip elements. In Figure 2.3a the crack tip is positioned at a material particle labeled C. Eight isoparametric elements are mapped onto the regions labeled E_1 through E_8. In Figure 2.3b the crack tip has extended a distance δa to reach material particle C', and the elements are

now mapped into regions E_1' through E_8' as described by variations in the element geometric mappings $\delta \mathbf{X}(\mathbf{x}^r)$. There is also a variation in the displacement field $\delta \mathbf{u}(\mathbf{x}^r)$ caused by the combined effects of the local variation of the geometric mapping and the change in the overall structural response due to the crack advance. However, as previously stated, $\delta \mathbf{u}(\mathbf{x}^r)$ has no effect on $\delta \Pi$. Note that the virtual node motions in Figure 2.3 satisfy the constraint (2.27).

The displacement field and the element geometry are interpolated using isoparametric shape functions as

$$u_i = h_\alpha \, u_{i\alpha} \; ; \qquad \alpha = 1, \, N \tag{2.34}$$

$$X_i = h_\alpha \, X_{i\alpha} \; ; \qquad \alpha = 1, \, N \tag{2.35}$$

where the shape functions $h_\alpha(\mathbf{x}^r)$ provide C_0 continuity across element boundaries and are differentiable within each element. N is the number of nodes in the element, and $u_{i\alpha}$ and $X_{i\alpha}$ are the displacement and coordinate at node α for direction i. Therefore,

$$\delta X_i = h_\alpha \, \delta X_{i\alpha} \; ; \qquad \alpha = 1, \, N \tag{2.36}$$

and

$$\delta X_{i,j} = h_{\alpha,j} \, \delta X_{i\alpha} \; ; \qquad \alpha = 1, \, N \tag{2.37}$$

The terms $\delta X_{i\alpha}$ are expressed as functions of δa,

$$\delta X_{i\alpha} = \frac{\partial X_{i\alpha}}{\partial a}\,\delta a = D_{i\alpha}\,\delta a \tag{2.38}$$

where the terms $D_{i\alpha}$ describe the motion of node α in direction i associated with a unit crack extension in a specified direction. In other words $D_{i\alpha}h_{\alpha} = \bar{X}_i$.

Consider the crack-tip elements in Figure 2.3. A virtual crack extension at the crack tip δa is assumed to occur in the X_1-direction, thus the change in the X_1 node coordinate at the crack tip is $\delta X_{1C} = \delta a$. If singular quarter-point isoparametric elements [24,25,27] are used, it is important to preserve the form of the stress singularity during the virtual crack extension to maintain accuracy. This condition is met by adding the additional constraints $\delta X_{i\gamma} = 3/4\ \delta a$ where the subscript γ ranges over the quarter-point nodes. In this case, the terms $D_{1\alpha}$ are given by

$$D_{1\alpha} = \begin{cases} 1 & \text{(For the degree-of-freedom (d.o.f.) in the } X_1\text{- direction at the crack-tip node)} \\ 3/4 & \text{(For the d.o.f. in the } X_1\text{-direction at quarter-point nodes)} \\ 0 & \text{(Otherwise)} \end{cases} \tag{2.39}$$

and $D_{2\alpha} = D_{3\alpha} = 0$. Similar constraints can be developed for other directions of virtual crack growth, as in cases of colinear extension of slanted cracks.

A finite element expression for the mutual potential energy release rate is obtained by combining equations (2.25), (2.30) - (2.32), (2.37) and (2.38):

$$G^{(1,2)} = -\frac{1}{s}\left(\sum_{\zeta=1}^{P} \int_{V_{\zeta 0}^{r}} [A_1^{(1,2)} + A_2^{(1,2)}]\, dv^{r}\right) \tag{2.40}$$

where

$$A_1^{(1,2)} = w^{(1,2)} \varepsilon_{ijk} (\tilde{J}_{j2} \tilde{J}_{k3} h_{\alpha,1} D_{i\alpha} + \tilde{J}_{i1} \tilde{J}_{k3} h_{\alpha,2} D_{j\alpha} + \tilde{J}_{i1} \tilde{J}_{j2} h_{\alpha,3} D_{i\alpha}) \; ; \quad \alpha = 1, N \tag{2.41}$$

and

$$A_2^{(1,2)} = - [\sigma_{ij}^{(1)} u_{i,k}^{(2)} + \sigma_{ij}^{(2)} u_{i,k}^{(1)}] \bar{J}_{k\ell} h_{\alpha,m} \bar{J}_{mj} \tilde{J} D_{\ell\alpha} \; ; \quad \alpha = 1, N \tag{2.42}$$

Finite element matrices for evaluating (2.40) are given in Appendix A.

2.5 Calculation of the Stress Intensity Factors from the Mutual Potential Energy Release Rates

The variation of the potential energy for equilibrium state 0 due to the change of the geometric mapping is expressed using superposition of the two independent equilibrium states 1 and 2 as

$$\delta\Pi^{(0)} = \delta\Pi^{(1)} + \delta\Pi^{(2)} + \delta M^{(1,2)} \tag{2.43}$$

The relations between the potential energy release rates and the stress intensity factors for equilibrium states 1, 2 and 0 can be written as [39]

$$G^{(n)} = \beta[\{K_I^{(n)}\}^2 + \{K_{II}^{(n)}\}^2] \; ; \quad n = 1, 2 \tag{2.44}$$

$$G^{(0)} = \beta[\{K_I^{(1)} + K_I^{(2)}\}^2 + \{K_{II}^{(1)} + K_{II}^{(2)}\}^2]$$

$$= G^{(1)} + G^{(2)} + 2\beta \left[K_I^{(1)} K_I^{(2)} + K_{II}^{(1)} K_{II}^{(2)}\right] \tag{2.45}$$

where

$$\beta = \begin{cases} \dfrac{1 - \nu^2}{E} & \text{(plane strain)} \quad (2.46a) \\ \dfrac{1}{E} & \text{(plane stress)} \quad (2.46b) \end{cases}$$

From (2.32), (2.43) and (2.45), the relation between the mutual potential energy release rate and the stress intensity factors is obtained.

$$G^{(1,2)} = 2\beta \left[K_I^{(1)} K_I^{(2)} + K_{II}^{(1)} K_{II}^{(2)}\right] \tag{2.47}$$

For mixed-mode crack problems, analytic near-field displacement solutions for each pure mode behavior are used to isolate K_I and K_{II}. Let $u^{(1)}$ be the equilibrium displacement field for a cracked structure subjected to a set of actual loads, and let $u^{(2a)}$ and $u^{(2b)}$ be the analytic near-field displacement solutions for pure mode-I and pure mode-II behavior such that $K_I^{(2a)} = K_{II}^{(2b)} = 1.0$ and $K_{II}^{(2a)} = K_I^{(2b)} = 0$. These solutions are well known and given in [9,10]. Then the actual stress intensity factors are computed from the relations

$$G^{(1,2a)} = 2\beta K_I^{(1)} \tag{2.48}$$

$$G^{(1,2b)} = 2\beta K_{II}^{(1)} \tag{2.49}$$

The method can be easily implemented in a conventional finite element program. First, a conventional analysis is performed to compute $u^{(1)}$ for

the actual loads. Then routines are added to evaluate the analytic mode-I and mode-II displacement solutions [9,10] at the crack-tip element nodes and to compute $G^{(1,2a)}$ and $G^{(1,2b)}$ by numerical integration of (2.40) over the crack-tip elements. Only a small number of elements need be included since $D_{i\alpha} = 0$ for most elements. Finally, the stress intensity factors are computed using (2.48) and (2.49).

Two approaches can be used to calculate the stress intensity factors for pure mode-I behavior. One approach is to use the analytic mode-I near-field displacement solution for equilibrium state 2 in the above procedure. Another way is to use the actual finite element solution for both equilibrium states 1 and 2, such that $K_I^{(1)} = K_I^{(2)}$ and $K_{II}^{(1)} = K_{II}^{(2)} = 0$. The relation between the energy release rate and the stress intensity factor becomes

$$G^{(1,2)} = 2\beta \{K_I^{(1)}\}^2 \tag{2.50}$$

Similar approaches are possible for pure mode-II and pure mode-III behavior.

The latter approach is equivalent to the procedure developed in [22], in which the stress intensity factor is directly calculated from the potential energy release rate rather than the mutual potential energy release rate. The total energy release rate is then obtained by evaluating the expression

$$G = -\frac{1}{s\delta a}\delta\Pi$$

$$= -\frac{1}{s}\left(\sum_{\zeta=1}^{P} \int_{v_{\zeta 0}^r} (A_1 + A_2)\, dv^r\right) \tag{2.51}$$

over singular quarter-point isoparametric elements using the finite element solution. In this case the relation between the energy release rate and the pure mode-I stress intensity factor is

$$G = \beta K_I^2 \tag{2.52}$$

Note that the mutual potential energy here is equal to twice the potential energy, so that $G^{(1,2)} = 2G$. A_1 and A_2 in (2.51) are defined as

$$A_1 = w \varepsilon_{ijk} (\tilde{J}_{j2} \tilde{J}_{k3} h_{\alpha,1} D_{i\alpha} \tilde{J}_{i1} \tilde{J}_{k3} h_{\alpha,2} D_{j\alpha} + \tilde{J}_{i1} \tilde{J}_{j2} h_{\alpha,3} D_{k\alpha}); \ \alpha = 1, N \tag{2.53}$$

and

$$A_2 = - \sigma_{ij} u_{i,k} \bar{J}_{k\ell} h_{\alpha,m} \bar{J}_{mj} \tilde{J} D_{\ell\alpha} \ ; \ \alpha = 1, N \tag{2.54}$$

where w is defined in (2.9). Finite element matrices for evaluating (2.51) are given in Appendix A.

2.6 Numerical Examples

The new finite element technique is applied to several crack geometries under plane stress, plane strain and axisymmetric conditions. Selected results are presented to demonstrate the accuracy of the method and the low sensitivity of the method to the degree of mesh refinement.

2.6.1 Mode-I Cracks in Plates and Bars

Several well-known mode-I problems are presented to demonstrate the accuracy of the method. Rectangular plates with single edge cracks, double edge cracks, and central cracks and a round bar with a circumferential crack are analyzed for uniform tension loading. Dimensions and expressions for K_I in terms of a correction factor f(a/b) for finite geometries are given in Figure 2.4 for each configuration. The finite element meshes used to model the upper half of each structure are indicated in Figure 2.5. The meshes contain a total of 55 linear strain triangular elements and 134 nodes. Quarter-point singularity elements were used for the crack-tip elements and a conventional three-point scheme [40] was used for numerical integration of the element stiffnesses and energy release rates.

In Table 2.1, values of the correction factor f(a/b) computed with the new method are compared with analytic solutions [9] and alternative finite element solutions by Hellen [38] for cracks of varying lengths in a plate. The results are in good agreement with the analytic solutions, and are virtually identical to Hellen's solutions. Note that the analytic solutions are based on plates with infinite lengths, whereas both finite element solutions are based on finite plate dimensions.

Results for a cracked round bar subjected to uniform tension are presented in Table 2.2. Energy release rates were computed using both the plane stress and plane strain assumptions for behavior at the crack tip. Again, the results are in close agreement with previous analytic solutions [41] and Hellen's finite element computations [38].

2.6.2 Sensitivity to Mesh Refinement

A single edge crack with a/b equal to 0.3 in a plate with L/b = 2.5 was analyzed to study the sensitivity of the new method to mesh refinement at the crack tip. Five different meshes were used, ranging from a coarse mesh with 18 linear strain triangular elements to a fine mesh with 40 elements. The ratio of the crack-tip element width to the plate width h/b was varied from 0.3 to 0.025. The element aspect ratios were not varied and taken to be equal to the aspect ratio L/b of the plate. The analysis results are shown in Figure 2.6.

It has been shown [42] that the convergence rate for stress intensity factors computed by energy methods without special singularity elements is linear with respect to the element size for plane problems with $r^{-1/2}$ singularities. The results reported for the new method using conventional (non-singular) crack-tip elements confirm this conclusion. When singular elements were used the maximum deviation from Hellen's solution was only 3.6 percent and the solution was stable and virtually identical to Hellen's solution for values of h/b below 0.1. The choice of numerical integration scheme was found to have no significant influence on the accuracy of the results. Therefore, the three-point scheme is recommended on the basis of efficiency. The results indicate that accurate solutions can be obtained using fairly coarse meshes. A minimum of two or three elements along the length of the crack is recommended.

2.6.3 A Cracked Plate Under Shear Loading

The analysis of an edge crack in a rectangular plate subjected to a uniformly distributed shear stress (Figure 2.7) is presented as an example of a mixed-mode problem. The reference solutions for K_I and K_{II}, calculated

by Wilson using a boundary collocation method [39], are K_I = 34.0 psi in.$^{1/2}$ and K_{II} = 4.55 psi in.$^{1/2}$. The structure was analyzed with five different meshes, ranging from a coarse mesh with 52 elements to a fine mesh with 132 elements. The results are in excellent agreement with the reference solutions, giving maximum deviations from the reference values of K_I and K_{II} of 1.6 percent and 0.4 percent, respectively, for the coarsest mesh. In contrast to the results reported for the contour integral technique [39], the present method produces reliable results even when applied very close to the crack tip. In Figure 2.7 r is the radius of the contour used to evaluate the integral in [39] and h is the width of the crack-tip elements used in the new method. It should be noted that the errors in the results from [39] were obtained by changing the radius of the contour integral without changing the finite element mesh. However, for the present method, the increasing errors for $h/a > 0.2$ are attributed to the coarse meshes required by the use of larger crack-tip elements.

2.6.4 A Tension Specimen with a 45° Crack

A rectangular tension specimen with a single edge crack inclined at 45° to the direction of loading is analyzed as a second example of mixed-mode behavior. The problem geometry and finite element mesh are shown in Figure 2.8. Finite element solutions for K_I and K_{II}, given by Yau et al. [39], using the contour integral approach, are K_I = 7.197 psi in.$^{1/2}$ and K_{II} = 3.277 psi in.$^{1/2}$. A mesh of 30 elements and 103 nodes was used. The present solution method, using a mesh with 52 elements and 125 nodes, predicts K_I = 7.202 psi in.$^{1/2}$ and K_{II} = 3.279 psi in.$^{1/2}$.

2.6.5 An Attachment Lug with a Double Crack

A two-dimensional attachment lug configuration, investigated by Liu and Kan [43], is shown in Figure 2.9. A symmetric double-crack pattern is assumed to represent the pattern of fatigue crack growth, and a concentrated load is used to represent the force of a pin reacting against the lug. The results presented in Figure 2.10 and 2.11 correspond to a hole diameter D = 0.25 W. Quasi-static growth of the crack is considered by varying the ratio of a/D and assuming that the crack direction remains horizontal. The combined normalized stress intensity factor, calculated by the present method, is compared with Figure 2.10 with an approximate solution proposed by Liu and Kan [43]. Results for the individual stress intensity factors are shown in Figure 2.11.

2.7 Chapter Summary

A finite element technique has been presented for calculating energy release rates and the stress intensity factors in elastic crack problems. Explicit expressions for the energy release rates were obtained using the isoparametric specialization of the small-deformation Eulerian-Lagrangian kinematic model. It is possible to obtain explicit energy rate expressions because the continuous mixed kinematic model allows variation of the geometric mapping to represent a true virtual crack extension.

Relatively few elements are involved in the energy rate computations, so the cost is generally less than a few percent of the cost of the initial elastic analysis. The method can be implemented with very little programming effort by adding a subroutine to any existing finite element code. The efficiency of the method is competitive with existing techniques and is not dependent on specialized substructuring or equation solving

algorithms. A major advantage of the method is its low sensitivity to the details of the finite element mesh geometry. Accurate results are obtained, even for relatively coarse meshes, without strict limitations on the size of the crack-tip elements. Therefore, the method can be used in unfamiliar situations with confidence.

The method could be used in practical engineering problems, such as the design and maintenance of structures in which fatigue crack propagation is a significant concern. Cyclic loads may cause a crack to propagate slowly, even if the applied stresses are well below the elastic limit, until unstable growth occurs. Empirical equations [44], relating the crack propagation rate to the crack length, require computation of the stress intensity factors during the process of fatigue crack propagation. The method can provide useful estimates of the fatigue life of structural components.

CHAPTER 3

ELASTODYNAMIC FORMULATION OF THE EULERIAN-LAGRANGIAN KINEMATIC DESCRIPTION

3.1 General

Dynamic analysis in solid mechanics is usually based on a Lagrangian kinematic description in which the motion of particles is measured from a known material configuration. In finite element analysis, this implies that the material geometric discretization is selected a priori and the finite element mesh is required to follow the material motion.

There are certain problems that require frequent or continuous remeshing if the mesh is forced to follow the material motion. These include situations in which either the structural geometry, material interfaces or the domain of the boundary conditions change with time; and may pertain to either large- or small-deformation behavior. For example, in dynamic crack propagation the material particle associated with the crack tip changes as the crack propagates, and it would be impossible to describe the crack-tip motion correctly without a remeshing process. The displacement and velocity fields need to be updated correctly for the new material discretization to accomplish the remeshing. This is usually done approximately in a conventional Lagrangian description using interpolation techniques [45]. Incremental contact behavior is another example that calls for some form of remeshing [18]. A special form of an Eulerian description has been applied to mode-I dynamic crack propagation problems using a moving coordinate system centered at the crack tip [46]. The finite element mesh is translated as a rigid body to follow the crack-tip motion. This procedure is

restricted to semi-infinite strips whose surfaces are parallel to the direction of crack growth. Also, appropriate dynamic boundary conditions must be determined for the leading and trailing edges of the finite element mesh.

The mixed Eulerian-Lagrangian kinematic description (ELD) [17,18] provides an alternative to conventional remeshing procedures to overcome these problems. A general development of the ELD is presented in [17] for large-deformation analysis. A specialization of the ELD to small-deformation behavior is the basis of explicit expressions for energy release rates used to analyse mixed-mode crack problems in Chapter 2. To date, the ELD has been applied primarily to static problems.

In this chapter the ELD is extended to the analysis of small-deformation dynamic problems. Section 3.2 presents the dynamic Eulerian-Lagrangian kinematic description for small-deformation theory, and the formulation of the variational equations of motion is described in Section 3.3. A weak form of the variational equations of motion is developed, suitable for approximate solution procedures using assumed displacement fields. Section 3.4 illustrates the application of the dynamic ELD to isoparametric finite element models.

3.2 The Dynamic Eulerian-Lagrangian Kinematic Description for Small-Deformation Analysis

This section presents the kinematic quantities used in the dynamic Eulerian-Lagrangian model. A convenient fixed domain, defined in a special reference coordinate system, is selected as the spatial reference domain. The mapping of the reference configuration onto an actual material domain, defined in the global coordinate system, varies with time. All field variables and field equations are expressed as functions of the reference coordinates. Material and spatial time rates and the relation between the two rates are defined.

3.2.1 Kinematics

The small-deformation ELD kinematic model is illustrated in Figure 3.1. The material configuration at time t is denoted by the volume V. Since there is no distinction between the geometries of deformed and undeformed configurations in small deformation problems, material particles are identified at all times by a single position vector $\mathbf{X}$ defined in a fixed Cartesian coordinate system. A convenient spatial reference configuration is selected which is invariant in time. The reference configuration does not necessarily represent an actual deformed state of the material volume. The reference position vector and volume, $\mathbf{x}^r$ and v^r, are defined in a separate reference coordinate system. The reference coordinates $\mathbf{x}^r$ are the only independent spatial variables; and both the displacement field $\mathbf{u}$ and the mapping to the material configuration change with time.

$$\mathbf{u} = \mathbf{u}(\mathbf{x}^r, t) \tag{3.1}$$

$$\mathbf{X} = \mathbf{X}(\mathbf{x}^r, t) \tag{3.2}$$

The following notation for differential operators is used.

$$\frac{\partial(\ )}{\partial X_i} = (\ )_{;i} \quad , \quad \frac{\partial(\ )}{\partial x_i^r} = (\ )_{,i} \tag{3.3}$$

Then

$$X_{i;j} = x^r_{i,j} = \delta_{ij} \tag{3.4}$$

where δ_{ij} is the Kronecker delta. The Jacobian of the mapping from $\mathbf{x}^r$ to $\mathbf{X}$ has components

$$\tilde{J}_{ij} = X_{i,j} \tag{3.5}$$

and the inverse (or Eulerian) Jacobian components are

$$\bar{J}_{ij} = x^r_{i;j} = \tilde{J}^{-1}_{ij} \tag{3.6}$$

The differential volumes dV and dv^r, in the material and reference configurations respectively, are related by

$$dV = \tilde{J}\, dv^r \tag{3.7}$$

where $\tilde{J}$ is the determinant of the Jacobian components $\tilde{J}_{ij}$,

$$\tilde{J} = \varepsilon_{ijk}\, \tilde{J}_{i1} \tilde{J}_{j2} \tilde{J}_{k3} \tag{3.8}$$

in which ε_{ijk} is the permutation symbol. It is assumed that the determinant of the Jacobian is positive at all points in the structure. The differential areas dA and da^r in the material and reference configurations are related by

$$dA = K_a\, da^r \tag{3.9}$$

The components of the small-deformation strain tensor are

$$\varepsilon_{ij} = \frac{1}{2}(u_{i,k}\, \bar{J}_{kj} + u_{j,k}\, \bar{J}_{ki}) \tag{3.10}$$

3.2.2 Time Rate Expressions

Time derivatives in the two coordinate systems are written as

$$\left.\frac{\partial(\ )}{\partial t}\right|_{\mathbf{X}\ \text{fixed}} = (\overset{*}{\ }) \quad ; \qquad \text{Material time derivatives} \tag{3.11}$$

$$\left.\frac{\partial(\ )}{\partial t}\right|_{\mathbf{x}^r\ \text{fixed}} = (\overset{\cdot}{\ }) \quad ; \qquad \text{Spatial time derivatives} \tag{3.12}$$

It is obvious, from (3.11) and (3.12), that

$$\overset{*}{X}_i = 0 \quad \text{and} \quad \overset{r}{\dot{x}}_i = 0 \tag{3.13}$$

The following important relation between the material and spatial time derivatives is obtained from (3.13) and the chain rule.

$$(\overset{*}{\ }) = (\overset{\cdot}{\ }) - (\ )_{;j}\ \dot{X}_j \tag{3.14a}$$

or

$$(\overset{*}{\ }) = (\overset{\cdot}{\ }) - (\ )_{,k}\ \bar{J}_{kj}\ \dot{X}_j \tag{3.14b}$$

The spatial time derivative of the inverse Jacobian is expressed as (see equation (25) in [17]),

$$\dot{\bar{J}}^t_{ij} = \lim_{\Delta t \to 0} \frac{1}{\Delta t} \left(\bar{J}^{t+\Delta t}_{ij} - \bar{J}^t_{ij}\right)$$

$$= \lim_{\Delta t \to 0} \frac{1}{\Delta t} \left\{-\bar{J}^t_{ik}\ \Delta X_{k,\ell}\ \bar{J}^t_{\ell j} + O(\Delta X^2)\right\}$$

$$= \lim_{\Delta t \to 0} \frac{1}{\Delta t} \{-\bar{J}^t_{ik} \dot{X}_{k,\ell} \bar{J}^t_{\ell j} (\Delta t) + O(\Delta t^2)\}$$

$$= -\bar{J}^t_{ik} \dot{X}^t_{k,\ell} \bar{J}^t_{\ell j} \tag{3.15}$$

where superscripts t and t+Δt denote variables evaluated at times t and t+Δt, respectively.

The material velocity and acceleration, described in the reference configuration, are derived from (3.14) and (3.15). The velocity of a material particle is

$$\overset{*}{u}_i = \dot{u}_i - u_{i;j} \dot{X}_j \tag{3.16a}$$

or

$$\overset{*}{u}_i = \dot{u}_i - u_{i,k} \bar{J}_{kj} \dot{X}_j \tag{3.16b}$$

and its acceleration is

$$\overset{**}{u}_i = \ddot{u}_i - 2 \dot{u}_{i;j} \dot{X}_j + 2 u_{i;j} \dot{X}_{j;k} \dot{X}_k - u_{i;j} \ddot{X}_j + u_{i;jk} \dot{X}_j \dot{X}_k \tag{3.17a}$$

or

$$\overset{**}{u}_i = \ddot{u}_i - 2 \dot{u}_{i,k} \bar{J}_{kj} \dot{X}_j + 2 u_{i,k} \bar{J}_{k\ell} \dot{X}_{\ell,m} \bar{J}_{mj} \dot{X}_j$$

$$- u_{i,k} \bar{J}_{kj} \ddot{X}_j + u_{i,\ell m} \bar{J}_{\ell j} \bar{J}_{mk} \dot{X}_j \dot{X}_k \tag{3.17b}$$

3.3 Formulation of the Variational Equations of Motion Using the Dynamic Eulerian-Lagrangian Kinematic Description

A general elastodynamic problem is first defined in the material configuration. The results of the previous section are used to formulate the variational equations of motion in the reference configuration. A weak form of the equations of motion is developed to relax the continuity requirements on the field variables. Specializations of the equations for finite bodies and unidirectional variations of the geometric mapping are discussed.

3.3.1 The Elastodynamic Problem

The equilibrium and constitutive relations for a general elastodynamic problem, written in the material configuration, are

$$\sigma_{ij;j} + F_i = \rho \overset{**}{u}_i \tag{3.18}$$

$$\sigma_{ij} = C_{ijk\ell}\, e_{k\ell} \tag{3.19}$$

where F_i are components of body force per unit volume, σ_{ij} are components of the Cauchy stress tensor, and $C_{ijk\ell}$ are components of the elasticity tensor. The mass density ρ is assumed to be uniform over the volume V. The strain-displacement relations are defined in (3.10). The displacement and traction boundary conditions are

$$u_i = \bar{u}_i(\mathbf{x}^r, t) \qquad \text{on } A_u \tag{3.20}$$

$$\sigma_{ij}\, n_j = T_i = \bar{T}_i(\mathbf{x}^r, t) \qquad \text{on } A_T \tag{3.21}$$

in which $\bar{u}_i$ and $\bar{T}_i$ are prescribed displacements and surface tractions, A_u and A_T are surface regions in the material configuration on which displacements and tractions are prescribed, and n_j are the direction cosines of the surface normal vector. The initial conditions for the dynamic problem are

$$u_i(\mathbf{x}^r,0) = \bar{u}_i(\mathbf{x}^r) \qquad \text{in } V \tag{3.22}$$

$$\overset{*}{u}_i(\mathbf{x}^r,0) = \overline{\overset{*}{u}}_i(\mathbf{x}^r) \qquad \text{in } V \tag{3.23}$$

where $\bar{u}_i$ and $\overline{\overset{*}{u}}_i$ are prescribed displacements and velocities at $t = 0$.

3.3.2 The Variational Equations of Motion

Let $\delta\mathbf{u}$ denote a kinematically admissible variation of the displacements at time t. The variational statement for the problem in the material configuration is

$$\int_V \sigma_{ij;j}\,\delta u_i\,dV + \int_V F_i\,\delta u_i\,dV - \int_V \rho\,\overset{**}{u}_i\,\delta u_i\,dV$$

$$= \int_{A_T} (\sigma_{ij}\,n_j - \bar{T}_i)\,\delta u_i\,dA \tag{3.24}$$

Application of the Gauss theorem to the first integral and the relation $\delta e_{ij} = \frac{1}{2}(\delta u_{i;j} + \delta u_{j;i})$ leads to

$$\int_V \sigma_{ij}\,\delta e_{ij}\,dV - \int_V F_i\,\delta u_i\,dV - \int_{A_T} \bar{T}_i\,\delta u_i\,dA$$

$$+ \int_V \rho\,\overset{**}{u}_i\,\delta u_i\,dV = 0 \tag{3.25a}$$

or, by substitution of (3.17a)

$$\int_V \sigma_{ij}\,\delta e_{ij}\,dV - \int_V F_i\,\delta u_i\,dV - \int_{A_T} \bar{T}_i\,\delta u_i\,dA + \int_V \rho\,\ddot{u}_i \delta u_i\,dV$$

$$-\int_V 2\,\rho\,\dot{u}_{i;j}\,\dot{X}_j\,\delta u_i\,dV + \int_V 2\,\rho\,u_{i;j}\,\dot{X}_{j;k}\,\dot{X}_k\,\delta u_i\,dV$$

$$-\int_V \rho\,u_{i;j}\,\ddot{X}_j\,\delta u_i\,dV + \int_V \rho\,u_{i;jk}\,\dot{X}_j\,\dot{X}_k\,\delta u_i\,dV = 0 \qquad (3.25b)$$

The last integral in (3.25b) includes a second-order spatial derivative of the displacements, which would require the trial functions in an assumed-displacement solution procedure to be C_1-continuous. This requirement can be inconvenient in finite element solutions, so the Gauss theorem is applied to relax the continuity requirement to C_0 trial functions.

$$\int_V \rho\,\ddot{u}_{i;jk}\,\dot{X}_j\,\dot{X}_k\,\delta u_i\,dV = \int_A \rho\,\dot{u}_{i;j}\,\dot{X}_j\,\dot{X}_k\,n_k\,\delta u_i\,dA$$

$$-\int_V \rho\,\ddot{u}_{i;j}\,\{(\dot{X}_j\,\dot{X}_k)_{;k}\,\delta u_i + \dot{X}_j\,\dot{X}_k\,\delta u_{i;k}\}\,dV \qquad (3.26)$$

The variational equation of motion expressed in the material configuration is obtained from (3.25b) and (3.26)

$$\int_V \sigma_{ij}\,\delta e_{ij}\,dV - \int_V F_i\,\delta u_i\,dV - \int_{A_T} \bar{T}_i\,\delta u_i\,dA + \int_V \rho\,\ddot{u}_i\,\delta u_i\,dV$$

$$-\int_V 2\,\rho\,\dot{u}_{i;j}\,\dot{X}_j\,\delta u_i\,dV + \int_V \rho\,u_{i;j}\,\dot{X}_{j;k}\,\dot{X}_k\,\delta u_i\,dV$$

$$- \int_V \rho\, u_{i;j}\, \ddot{X}_j\, \delta u_i\, dV + \int_A \rho\, u_{i;j}\, \dot{X}_j\, \dot{X}_k\, n_k\, \delta u_i\, dA$$

$$- \int_V \rho\, u_{i;j}\, \dot{X}_j\, \dot{X}_{k;k}\, \delta u_i\, dV - \int_V \rho\, u_{i;j}\, \dot{X}_j\, \dot{X}_k\, \delta u_{i;k}\, dV = 0 \qquad (3.27)$$

It is convenient to describe the equations of motion in the reference volume, because the displacement field and the geometry mapping are defined by functions of the reference coordinates. Equation (3.27) is rewritten in the reference coordinate system using the relations (3.7) and (3.9).

$$\int_{v^r} \sigma_{ij}\, \delta e_{ij}\, \tilde{J}\, dv^r - \int_{v^r} F_i\, \delta u_i\, \tilde{J}\, dv^r - \int_{a_T^r} \bar{T}_i\, \delta u_i\, K_a\, da^r$$

$$+ \int_{v^r} \rho\, \ddot{u}_i\, \delta u_i\, \tilde{J}\, dv^r - \int_{v^r} 2\, \rho\, \dot{u}_{i,k}\, \bar{J}_{kj}\, \dot{X}_j\, \delta u_i\, \tilde{J}\, dv^r$$

$$+ \int_{v^r} \rho\, u_{i,k}\, \bar{J}_{k\ell}\, \dot{X}_{\ell,m}\, \bar{J}_{mj}\, \dot{X}_j\, \delta u_i\, \tilde{J}\, dv^r - \int_{v^r} \rho\, u_{i,k}\, \bar{J}_{kj}\, \ddot{X}_j\, \delta u_i\, \tilde{J}\, dv^r$$

$$+ \int_{a^r} \rho\, u_{i,k}\, \bar{J}_{kj}\, \dot{X}_j\, \dot{X}_\ell\, n_\ell\, \delta u_i\, K_a\, da^r$$

$$- \int_{v^r} \rho\, u_{i,k}\, \bar{J}_{kj}\, \dot{X}_j\, \dot{X}_{\ell,m}\, \bar{J}_{m\ell}\, \delta u_i\, \tilde{J}\, dv^r$$

$$- \int_{v^r} \rho\, u_{i,k}\, \bar{J}_{kj}\, \dot{X}_j\, \dot{X}_\ell\, \delta u_{i,m}\, \bar{J}_{m\ell}\, \tilde{J}\, dv^r = 0 \qquad (3.28)$$

where a_T^r is a surface area in the reference configuration corresponding to A_T. Equation (3.28) is a variational statement in the reference coordinate system that can serve as the basis of weak formulations of general linear elastodynamic problems.

The variational equation of motion (3.28) can be simplified for certain special cases. The spatial rate of the material coordinates on the surface of a finite body are constrained by

$$\dot{\mathbf{X}} \cdot \mathbf{n} = 0 \tag{3.29}$$

to prevent material motion across the physical boundaries of the structure. In this case the second surface integral in (3.28) vanishes. Note that (3.29) does not hold when the reference configuration is mapped onto a subdomain of a large structure as in [46]. In this case, some portions of a^r do not represent physical structure boundaries. When the mapping changes only in the X_1-direction, as in the analysis of mode-I dynamic fracture problems, equation (3.28) reduces to

$$\int_{v^r} \sigma_{ij}\, \delta e_{ij}\, \tilde{J}\, dv^r - \int_{v^r} F_i\, \delta u_i\, \tilde{J}\, dv^r - \int_{a_T^r} \bar{T}_i\, \delta u_i\, K_a\, da^r$$

$$+ \int_{v^r} \rho\, \ddot{u}_i\, \delta u_i\, \tilde{J}\, dv^r - \int_{v^r} 2\rho\, \dot{u}_{i,k}\, \bar{J}_{k1}\, \dot{X}_1\, \delta u_i\, \tilde{J}\, dv^r$$

$$- \int_{v^r} \rho\, u_{i,k}\, \bar{J}_{k1}\, \ddot{X}_1\, \delta u_i\, \tilde{J}\, dv^r$$

$$- \int_{v^r} \rho\, u_{i,k}\, \bar{J}_{k1}\, (\dot{X}_1)^2\, \delta u_{i,m}\, \bar{J}_{m1}\, \tilde{J}\, dv^r = 0 \tag{3.30}$$

It is easily verified that the variational equations of motion (20) in [46] for uniform ρ is equivalent to (3.30) if a moving spatial domain centered at the crack tip is chosen as the reference configuration in the dynamic ELD formulation. It should be noted that this equivalence is only valid for the

special case of constant-velocity, uniform motion of the spatial domain. In fact, the equation in [46] is not valid for general non-uniform motions.[1]

3.4 Specialization to Isoparametric Finite Element Models

This section presents a specialization of the dynamic ELD kinematic model to isoparametric finite element formulations. Finite element expressions are written for a general three-dimensional linear elastodynamic problem using the weak form of the variational equations of motion (3.28). In general, the motion of a spatial domain can be either known or unknown in advance. In this section the finite element formulation is only developed for a known mesh motion, but extension to the case of unknown motion is also discussed.

Computational aspects of various finite element time integration schemes are discussed, and finite element equations, for both explicit and implicit time integration, are presented.

3.4.1 Isoparametric Finite Element Model

In the isoparametric specialization of the ELD a mapping is established between a mesh of isoparametric elements and an actual material domain. The

---

[1] The left-hand side of equation (20) in [46] is missing the term $\int_V \rho\, c\, \frac{\partial c}{\partial x_1} \frac{\partial ui}{\partial x_1}\, \delta u_i dV$ which arises from a convective term in the spatial time derivative of $\partial u_i / \partial x_i$ for the case of general non-uniform motion. This integral cancels with the corresponding right-hand side term. For uniform motion these terms are zero, and have no effect.

kinematic model is depicted in Figure 2.1. The parent element geometry is selected as the spatial reference configuration for each element. A local natural coordinate system is used as the reference coordinate system in each parent element. Motion of the finite element mesh is represented by changes in the isoparametric mapping. The displacement field, the element geometry and other field variables are interpolated using isoparametric shape functions as,

$$u_i = h_\alpha u_{i\alpha} \quad , \quad \mathbf{u} = \mathbf{H}\,\mathbf{U}_e \tag{3.31a}$$

$$\dot{u}_i = h_\alpha \dot{u}_{i\alpha} \quad , \quad \dot{\mathbf{u}} = \mathbf{H}\,\dot{\mathbf{U}}_e \tag{3.31b}$$

$$\ddot{u}_i = h_\alpha \ddot{u}_{i\alpha} \quad , \quad \ddot{\mathbf{u}} = \mathbf{H}\,\ddot{\mathbf{U}}_e \tag{3.31c}$$

$$\delta u_i = h_\alpha \delta u_{i\alpha} \quad , \quad \delta\mathbf{u} = \mathbf{H}\,\delta\mathbf{U}_e \tag{3.31d}$$

$$X_i = h_\alpha X_{i\alpha} \quad , \quad \mathbf{X} = \mathbf{H}\,\mathbf{X}_e \tag{3.31e}$$

$$\dot{X}_i = h_\alpha \dot{X}_{i\alpha} \quad , \quad \dot{\mathbf{X}} = \mathbf{H}\,\dot{\mathbf{X}}_e \tag{3.31f}$$

$$\ddot{X}_i = h_\alpha \ddot{X}_{i\alpha} \quad , \quad \ddot{\mathbf{X}} = \mathbf{H}\,\ddot{\mathbf{X}}_e \tag{3.31g}$$

where h_α are element shape functions, the subscripts $i\alpha$ indicate the component in direction i at node α, and α ranges from 1 to the number of nodes in the element. The matrix H is the usual interpolation matrix containing the element shape functions, and column matrices with subscript e contain quantities measured in the global coordinate system, but evaluated at the element nodes.

Equations (3.31) are used to obtain a discrete form of (3.28)

$$\delta \mathbf{U}^T \sum \Big(\int_{v_e^r} \mathbf{B}^T \mathbf{E} \mathbf{B}\, \tilde{J}\, dv_e^r + \int_{v_e^r} \rho\, \mathbf{H}^T \mathbf{D} \mathbf{G}\, \tilde{J}\, dv_e^r - \int_{v_e^r} \rho \mathbf{H}^T \ddot{\mathbf{A}} \mathbf{G}\, \tilde{J}\, dv_e^r$$

$$+ \int_{a_e^r} \rho\, \mathbf{H}^T \dot{\mathbf{A}} \mathbf{G}\, A_1 K_a\, da_e^r - \int_{v_e^r} \rho\, \mathbf{H}^T \mathbf{S} \mathbf{G}\, \tilde{J}\, dv_e^r - \int_{v_e^r} \rho\, \mathbf{G}^T \dot{\mathbf{A}}^T \dot{\mathbf{A}} \mathbf{G}\, \tilde{J}\, dv_e^r \Big)\, \mathbf{U}$$

$$+ \delta \mathbf{U}^T \sum \Big(\int_{v_e^r} \rho\, \mathbf{H}^T \mathbf{H}\, \tilde{J}\, dv_e^r \Big)\, \ddot{\mathbf{U}} + \delta \mathbf{U}^T \sum \Big(- \int_{v_e^r} 2\rho\, \mathbf{H}^T \dot{\mathbf{A}} \mathbf{G}\, \tilde{J}\, dv_e^r \Big)\, \dot{\mathbf{U}}$$

$$= \delta \mathbf{U}^T \sum \Big(\int_{v_e^r} \mathbf{H}^T \mathbf{F}_e\, \tilde{J}\, dv_e^r + \int_{a_T^r} \mathbf{H}^T \bar{\mathbf{T}}_e\, K_a\, da_e^r \Big) \qquad (3.32)$$

in which the summation symbol indicates assembly over the number of elements, and v_e^r and a_e^r are volume and area in the parent element geometry. The column matrices $\mathbf{U}$, $\dot{\mathbf{U}}$ and $\ddot{\mathbf{U}}$ are assembled forms of the corresponding element matrices. $\mathbf{B}$ and $\mathbf{E}$ are the strain-displacement transformation and elasticity matrices. Other matrices and the scalar quantity A_1 are defined in Appendix B. The reader is cautioned that $\dot{\mathbf{U}}$ and $\ddot{\mathbf{U}}$ do not contain material velocities and accelerations, but rather first- and second-order spatial time derivatives of displacement at the finite element nodes.

The finite element equations for arbitrary $\delta\mathbf{U}$ are obtained from equation (3.32) as

$$\mathbf{M}\, \ddot{\mathbf{U}} + \mathbf{C}\, \dot{\mathbf{U}} + \mathbf{K}\, \mathbf{U} = \mathbf{P} \qquad (3.33)$$

where $\mathbf{M}$ is a consistent mass matrix, $\mathbf{C}$ and $\mathbf{K}$ are nonsymmetric "effective damping" and stiffness matrices, and $\mathbf{P}$ is a load vector. Matrix expressions for $\mathbf{M}$, $\mathbf{C}$, $\mathbf{K}$ and $\mathbf{P}$ are presented in Appendix B. Alternatively, a lumped mass

matrix can be used. The basis of a choice between a consistent and lumped mass matrix, and computational strategies for nonsymmetric matrices are documented in [45-47].

3.4.2 Explicit Integration Equations

The solution to (3.33) can be obtained by either implicit or explicit time integration methods. The analysis of dynamic problems in which the effect of wave propagation is important requires a small integration time step for an accurate solution. Thus, accuracy considerations, rather than stability requirements, might control the step size for explicit integration methods. Using the central difference method the explicit integration equations are

$$\bar{\mathbf{K}}^t \, \mathbf{U}^{t+\Delta t} = \bar{\mathbf{P}}^t \tag{3.34}$$

where

$$\bar{\mathbf{K}}^t = \frac{1}{\Delta t^2} \mathbf{M}^t + \frac{1}{2\Delta t} \mathbf{C}^t \tag{3.35}$$

$$\bar{\mathbf{P}}^t = \mathbf{P}^t - (\mathbf{K}^t - \frac{2}{\Delta t^2} \mathbf{M}^t) \, \mathbf{U}^t - (\frac{1}{\Delta t^2} \mathbf{M}^t - \frac{1}{2\Delta t} \mathbf{C}^t) \, \mathbf{U}^{t-\Delta t} \tag{3.36}$$

Matrices in (3.35) and (3.36) are dependent on the solution at time t. Thus, the usual advantage of explicit integration methods (i.e., only one factorization of $\bar{\mathbf{K}}$ is required) vanishes in the case of a moving finite element mesh.

3.4.3 Implicit Integration Equations

Implicit time integration methods for (3.33) are based on equilibrium at time $t + \Delta t$. The first- and second-order spatial rates of the displacements are approximated in Newmark's method as

$$\dot{U}^{t+\Delta t} = \dot{U}^{t} + c_7 \ddot{U}^{t} + c_8 \ddot{U}^{t+\Delta t} \tag{3.37}$$

$$\ddot{U}^{t+\Delta t} = c_1 (U^{t+\Delta t} - U^{t}) - c_3 \dot{U}^{t} - c_4 \ddot{U}^{t} \tag{3.38}$$

where the integration constants c_i are defined using the Newmark parameters β and δ,

$$c_1 = 1/(\beta\Delta t^2),\ c_2 = \delta/(\beta\Delta t),\ c_3 = 1/(\beta\Delta t),\ c_4 = 1/(2\beta)-1,$$

$$c_5 = \delta/\beta-1,\ c_6 = \frac{\Delta t}{2}(\delta/\beta-2),\ c_7 = \Delta t(1-\delta),\ c_8 = \delta\Delta t \tag{3.39}$$

The implicit integration equations are then written as

$$\hat{K}^{t+\Delta t}\ U^{t+\Delta t} = \hat{P}^{t+\Delta t} \tag{3.40}$$

where

$$\hat{K}^{t+\Delta t} = K^{t+\Delta t} + c_1 M^{t+\Delta t} + c_2 C^{t+\Delta t} \tag{3.41}$$

$$\hat{P}^{t+\Delta t} = P^{t+\Delta t} + M^{t+\Delta t} (c_1 U^{t} + c_3 \dot{U}^{t} + c_4 \ddot{U}^{t})$$

$$+ C^{t+\Delta t} (c_2 U^{t} + c_5 \dot{U}^{t} + c_6 \ddot{U}^{t}) \tag{3.42}$$

Matrices in equations (3.41) and (3.42) are evaluated based on the geometry at time $t + \Delta t$. This presents no problem for cases in which the history of mesh motion is known. For cases where the element mesh motion is not known (e.g., crack propagation prediction, free surface and moving boundary [18] problems), the variational equation (3.28) can be rewritten using incremental expressions for both the displacement and the mapping. This renders equation (3.28) nonlinear with two sets of unknown variables: increments in the displacements $\Delta \mathbf{u}$ and in the mapping $\Delta \mathbf{X}$. One way of solving the problem is to approximate $\Delta \mathbf{X}$ based on conditions at time t, and then treat the problem as a known mesh motion problem. Iteration might improve the prediction of the mesh motion. Another way is to add $\Delta \mathbf{X}$ as unknown solution variables and solve a linearized form of (3.28). This procedure requires additional constraint equations, derived from appropriate criteria (e.g., crack propagation criteria or moving boundary definitions), to determine the mesh motion. The solution can be obtained by either implicit or explicit time integration methods; but explicit methods, based on known geometry at time t, produce simpler finite element expressions. Further study and tests are needed to demonstrate the practicality of the method for problems with unknown mesh motions.

3.5 Chapter Summary

The dynamic Eulerian-Lagrangian kinematic model for the analysis of elastodynamic problems has been developed. Expressions are derived for field variables and material time derivatives using the new kinematic description. The variational equations of motion are written in a form suitable for use with isoparametric finite elements and either explicit or implicit time integration methods.

The ELD formulation is particularly effective for analysing problems in which the structural geometry, material interfaces or the domain of the boundary conditions change with time. The ELD allows the finite element mesh to change continuously without a discrete remeshing process, so the displacement and velocity fields remain continuous in the time domain. The dynamic ELD finite element formulation results in a nonsymmetric stiffness matrix, as is common in other moving mesh procedures using a Lagrangian model [45,46].

Finite element equations using the ELD require the evaluation of the velocity and acceleration fields of the moving mesh. Thus, it is necessary to establish finite element models of the moving mesh velocity and acceleration fields, in addition to the mesh deformation. These are presented in Chapter 4, in which the dynamic ELD formulation is applied to the analysis of dynamic crack propagation problems.

CHAPTER 4

DYNAMIC CRACK PROPAGATION ANALYSIS USING THE EULERIAN-LAGRANGIAN KINEMATIC MODEL

4.1 General

Brittle fracture often involves fast crack propagation at velocities on the order of the material's characteristic wave speeds. This generates rapid material particle motions, and inertia effects become important. Inertia effects are also significant in bodies with stationary cracks that are subjected to impact or explosive loads. Stress waves, generated by either a running crack or dynamic loads, propagate through the medium and reflect at the boundaries. The propagation of stress waves influences the history of the crack-tip stress field and, consequently, effects the motion of the crack.

The near-tip dynamic stress field in a linearly elastic solid is described as a function of the dynamic stress intensity factor, the crack tip velocity, and spatial coordinates local to the crack tip. The spatial dependence of the stress distribution is common for all (subsonic) elastodynamic crack problems, so the crack velocity and the stress intensity factors completely characterize the near-tip stress field [48,49].

$$\sigma_{ij} = \frac{K_I(t)}{(2\pi r)^{1/2}} \sum_{ij}^{I}(\theta,v) + \frac{K_{II}(t)}{(2\pi r)^{1/2}} \sum_{ij}^{II}(\theta,v) + O(1) \qquad (4.1)$$

The first two terms in (4.1) dominate as r goes to zero, where r is the radial distance from the crack tip and v is the crack-tip speed. The functions $\sum_{ij}^{I}(\theta,v)$ are velocity-dependent and reduce to the corresponding expressions for the stationary crack when v = 0. These functions are given

in [49]. For a running crack in a half plane, the dynamic stress intensity factor can be expressed as the product of a universal function of the instantaneous crack-tip velocity and the stress intensity factor for a stationary crack, of length equal to the instantaneous length of the running crack, in a half plane subjected to the same load history [50].

$$K(t,v) = k(v)\, K(t,0) \tag{4.2}$$

The universal function k(v) is given in [51]. The relation is a general result for arbitrary load histories and non-uniform crack-tip motion [52]. It is also valid for running cracks in finite bodies until the time at which reflected waves return to the crack tip.

Crack-tip motion is generally assumed to follow an energy balance criterion, i.e. a crack propagates in such a way that the dynamic energy release rate is equal to a specific fracture energy. The specific fracture energy is a characteristic property of the material under consideration, and is known to be dependent only on the instantaneous crack-tip velocity [11,12,53]. For a uniformly running crack under pure mode-I conditions, the dynamic energy release rate can be expressed as a function of the crack-tip speed and the dynamic stress intensity factor [54],

$$G = \frac{1}{2\mu} f(v) \cdot K_I^{\,2} \tag{4.3}$$

where μ is the shear modulus and f(v) is a velocity-dependent factor given in (4.22). This is valid for all symmetric loading conditions and geometric configurations, and also for a non-uniformly running crack [8]. Nishioka and Atluri have proposed relationships between the modal stress intensity

factors and energy release rates for mixed-mode problems [55]. This study is concerned primarily with dynamic fracture under pure mode-I conditions.

A major concern in the study of dynamic brittle fracture is the solution and measurement of the dynamic stress intensity factor, because the behavior of a crack is determined by the local stress field near the crack tip. A detailed review of available analytic solutions is given in [56], and recent developments are described in [11,12,13,57]. Existing analytic solutions are limited to idealized geometries and loading conditions, because of mathematical complexity. As discussed in [11], simple analytic analysis is not adequate for realistic problems, particularly for problems in which the effects of wave propagation are important. Consequently, a reliable numerical analysis method for dynamic fracture is needed.

In this chapter the dynamic Eulerian-Lagrangian kinematic description is applied to the analysis of elastodynamic fracture problems. A dynamic moving isoparametric finite element method, based on the special weak form of the variational equations of motion developed in Chapter 3, is used for the analysis. Section 4.2 reviews existing finite element methods. Simplified forms of the finite element equations for the analysis of mode-I problems in finite bodies are given in Section 4.3. Section 4.4 presents solution procedures for dynamic crack propagation using the Eulerian-Lagrangian finite element method. The simulation of singular fields near the crack tip and techniques for modeling crack propagation are explained. Computational methods for extracting energy release rates and stress intensity factors are described. In Section 4.5 numerical examples of dynamic crack propagation analysis are presented. The transient stages of crack acceleration and crack arrest are studied in detail, and the effects of wave propagation on dynamic crack growth behavior are discussed.

4.2 Review of Finite Element Methods for the Analysis of Dynamic Crack Propagation

The earliest finite element methods for dynamic crack propagation use a node decoupling technique with a simple nodal force release mechanism [58-63]. In this approach the inter-element forces at the crack-tip node are prescribed to decay from their values at the instant prior to the release of the old crack-tip node, to zero when the crack tip reaches the next node. The energy release rate is computed by numerical differentiation of the change in global energy. This procedure often produces inaccurate results when explicit time integration is employed, since the prescribed nodal force is not generally in dynamic equilibrium with the state of stress in the adjoining finite elements. Also, the effect of impulse stress waves generated by the instantaneous application of the prescribed nodal force reduces the accuracy of the method. Kanninen [15] concluded, based on available methods at the time, that the finite element method was not appropriate for modeling crack propagation.

Bazant, et al. [46] have proposed a special finite element procedure based on a moving coordinate system centered at the crack tip. The finite element mesh is translated as a rigid body to follow the crack-tip motion. As discussed in Chapter 3, this procedure is restricted to semi-infinite strips whose surfaces are parallel to the direction of crack propagation. Also, appropriate dynamic boundary conditions must be determined for the leading and trailing edges of the finite element mesh. More refined finite element methods have been proposed, but they still suffer some disadvantages; e.g., limited applicability and inaccurate modeling of the special characteristics of dynamic crack propagation behavior. These are documented in [16] and [64].

Recently, significant progress has been made by Nishioka and Atluri [45] who use a "moving singular element procedure" to model dynamic crack propagation. In their method, a special singular element is formulated using analytic asymptotic solutions for the singularities near the crack tip together with a variational statement that accounts for the motion of the singular element. To simulate crack propagation, only the conventional finite elements immediately surrounding the singular element are distorted, so that no geometric distortion is applied to the moving crack-tip element. Thus, only limited remeshing is required at each time step. The dynamic stress intensity factor, which is embedded as an unknown parameter in the singular element formulation, is computed directly in the solution process. The numerical results obtained with moving singular elements are compared with those obtained using quarter-point singular isoparametric elements in [65]. Later, Atluri applied a path integral [66] to the moving singular element procedure [67]. A similar moving singular element procedure has been reported by Gunther et al. [64].

Most finite element methods used in dynamic fracture problems use a Lagrangian kinematic model, in which the geometric discretization is selected a priori for a material configuration, and the finite element mesh is required to follow the material motion during a time step. This is disadvantageous, particularly for modeling fast crack propagation, since it requires local remeshing between time steps and frequent overall remeshing. Interpolation of the displacement and velocity fields is required whenever any remeshing is performed. These problems are reduced or eliminated by the dynamic ELD finite element formulation described in the next section.

4.3 The Dynamic Eulerian-Lagrangian Finite Element Method

The elastodynamic version of the Eulerian-Lagrangian kinematic description (ELD), developed in Chapter 3, is an alternative to conventional Lagrangian descriptions for problems in which the geometry of the structure, the material interfaces, or the domains of the boundary conditions change with time. A weak form of the variational equations of motion, written in the reference coordinate system, was presented for linear elastodynamic problems. This form can be simplified for cases in which the geometric mapping changes only in the X_1-direction in bodies with finite geometry (see equation (3.30)). Finite element equations, suitable for the analysis of mode-I dynamic fracture problems, are obtained by discretizing the simplified continuum form of the variational equation. Motion of the finite element mesh is represented by continuous changes in the isoparametric element mappings. The stiffness equations produced by the dynamic ELD are reviewed next.

Implicit integration equations based on the dynamic ELD are formed using Newmark's method,

$$\hat{\mathbf{K}}^{t+\Delta t}\,\hat{\mathbf{U}}^{t+\Delta t} = \hat{\mathbf{P}}^{t+\Delta t} \tag{4.4}$$

where

$$\hat{\mathbf{K}}^{t+\Delta t} = \mathbf{K}^{t+\Delta t} + c_1\,\mathbf{M}^{t+\Delta t} + c_2\,\mathbf{C}^{t+\Delta t} \tag{4.5}$$

$$\hat{\mathbf{P}}^{t+\Delta t} = \mathbf{P}^{t+\Delta t} + \mathbf{M}^{t+\Delta t}\,(c_1\,\mathbf{U}^t + c_3\,\dot{\mathbf{U}}^t + c_4\,\ddot{\mathbf{U}}^t) + \mathbf{C}^{t+\Delta t}\,(c_2\,\mathbf{U}^t + c_5\,\dot{\mathbf{U}}^t + c_6\,\ddot{\mathbf{U}}^t) \tag{4.6}$$

The column matrices $\mathbf{U}^t$, $\dot{\mathbf{U}}^t$, $\ddot{\mathbf{U}}^t$ in (4.6) are the vector of node displacements and its first- and second-order spatial time derivatives; and the terms c_i are integration constants defined in Chapter 3. The matrices $\mathbf{K}^t$, $\mathbf{C}^t$, $\mathbf{M}^t$ and $\mathbf{P}^t$ are defined as

$$\mathbf{K}^t = \sum \Big(\int_{v_e^r} \mathbf{B}^T\mathbf{E}\mathbf{B}\ \tilde{J}\ dv_e^r - \int_{v_e^r} \rho\ \mathbf{H}^T\ddot{\mathbf{A}}\mathbf{G}\ \tilde{J}\ dv_e^r - \int_{v_e^r} \rho\ \mathbf{G}^T\dot{\mathbf{A}}^T\dot{\mathbf{A}}\mathbf{G}\ \tilde{J}\ dv_e^r \Big) \tag{4.7}$$

$$\mathbf{C}^t = \sum \Big(- \int_{v_e^r} 2\rho\ \mathbf{H}^T\dot{\mathbf{A}}\mathbf{G}\ \tilde{J}\ dv_e^r \Big) \tag{4.8}$$

$$\mathbf{M}^t = \sum \Big(\int_{v_e^r} \rho\ \mathbf{H}^T\mathbf{H}\ \tilde{J}\ dv_e^r \Big) \tag{4.9}$$

Equations (4.7)-(4.9) are evaluated based on the geometry at time t. To evaluate (4.5) and (4.6) the mesh geometry, velocity and acceleration at time $t+\Delta t$ must be either known or estimated based on conditions at time t. The required information can be generated using variable geometric mappings, controlled by crack-tip motion, as described in the following section. Expressions for the matrices and scalar quantities used in (4.7)-(4.9) are given in Appendix B.

4.4 Finite Element Solution Procedures for Dynamic Crack Propagation

This section presents a new finite element method for modeling dynamic fracture problems using the ELD kinematic model, and special techniques for computation of the dynamic energy release rate and the stress intensity factor. Quarter-point singular isoparametric elements simulate the singular

fields near the crack tip. Procedures for simulating crack propagation are discussed, and advantages of the dynamic ELD model with respect to conventional Lagrangian models are noted.

4.4.1 Singular Fields Near the Crack Tip

The strain field near a crack tip in a linearly elastic material possesses a singularity of order $r^{-1/2}$, for stationary cracks and cracks propagating at subsonic speeds, where r is the radial distance from the crack tip. This singular form can be incorporated in finite element models by using quarter-point isoparametric elements [25]. The strain in the isoparametric elements are expressed as

$$e_{ij} = \frac{1}{2} (u_{i,k} \bar{J}_{kj} + u_{j,k} \bar{J}_{ki}) \tag{4.10}$$

The singular strain field results from a singular Jacobian at the crack tip, which is produced simply by placing side nodes at the quarter point. The displacement gradients in the natural element coordinate system are nonsingular.

For a running crack, there is also a singularity of order $r^{-1/2}$ in the material velocity field surrounding the crack tip. Quarter-point isoparametric elements based on a conventional Lagrangian kinematic description do not generate the desired singularity, because the material velocity field is simply interpolated as,

$$\begin{aligned} \overset{*}{u}_i &= \dot{u}_i \\ &= h_\alpha \dot{u}_{i\alpha} \end{aligned} \tag{4.11}$$

where h_α are element shape functions, and subscripts $i\alpha$ indicate the component in direction i at node α. The subscript α ranges from 1 to the number of nodes in the element. Finite element methods using conventional Lagrangian kinematic models generally require special singular elements [45,64] to incorporate the singular velocity field. These elements are formulated using analytic solutions for infinite bodies. They can be difficult to incorporate in general finite element programs, because they introduce incompatibilities in the displacement model at the interface between the singular elements and the rest of the mesh. Approximate satisfaction of the compatibility requirement is obtained by a least squares minimization of error [45], or by introducing additional boundary displacement functions [64].

When quarter-point isoparametric crack-tip elements are used with the dynamic ELD to model running cracks, the appropriate singular form is automatically generated in the material velocity field. Using the relation between material and spatial time derivatives (3.14b), the material velocity is expressed in the element natural coordinate system as

$$\overset{*}{u}_i = \dot{u}_i - u_{i,k}\, \bar{J}_{kj}\, \mathring{X}_j \tag{4.12}$$

The convective term in (4.12) introduces the singularity through the Jacobian components. The singularity in the velocity field vanishes, as is expected, for zero crack-tip velocity. Thus, the combination of singular quarter-point isoparametric elements with the dynamic ELD is suitable for all subsonic crack-tip velocities. This model is relatively easy to implement. It is interelement compatible, and there is no need to formulate special crack-tip elements.

4.4.2 A Geometric Model for Crack Propagation

In finite element procedures crack growth motion is usually modeled incrementally, by shifting the crack-tip node to a new material location at each time step. This requires at least a local remeshing prior to every time step, and frequent over-all remeshing. Interpolation of the displacement and velocity fields are required whenever any remeshing is performed. These problems can be reduced or eliminated by using the dynamic ELD finite element procedure, as described in this section.

Crack growth is modeled by continuous Eulerian mesh motion, rather than by discrete remeshing operations. This eliminates the need to remesh and interpolate between every time step. The need for over-all remeshing is greatly reduced, and often eliminated, by smoothly distributing the mesh motion over a selected region of the structure. A two-level mapping is used to describe the Eulerian motion. The actual Eulerian mapping is defined locally by the isoparametric mapping and node coordinates for each individual finite element, as described in Chapter 3. Auxiliary regional mappings are used to relate node coordinate changes to the crack-tip motion. Appropriate regions and mappings are selected prior to analysis for this purpose.

The mapping process is illustrated in Figure 4.1. A topological subdivision is established that describes the structure as a series of regions, whose shapes vary with time. The volume occupied by a typical region N at time t is designated $\Omega_N^{t_1}$. Figure 4.1 shows the geometry change of Ω_N from time t_1 to time t_2. An independent reference parent volume ω_N^r, described by natural coordinates ξ^N, is established for each Ω_N. A coordinate mapping $\phi_N: \omega_N^r \rightarrow \Omega_N$ is then used to describe the geometry of each region through time.

$$X_N = \phi_N(\xi^N, t) \tag{4.13}$$

The changes of the mappings through time are constrained to follow the crack growth.

Nodes at the corners of the finite elements are assumed to represent fixed locations ξ in the parent regions. The coordinates and motion of the corner nodes are calculated by (4.13). To avoid undesirable distortions, side node positions are not computed directly from the mapping ϕ. Instead, straight sides are assumed; and appropriate proportional spacing (mid-side or quarter-point for singular crack-tip elements) is used to determine the side node locations, based on the mapped locations of the element corner nodes.

In the present implementation, the parent regions are unit squares that map to quadrilateral regions of the actual structure via a bilinear mapping. Other mappings, such as transfinite mappings [68], could be useful; especially for curved crack geometries. The four corner nodes of a region control the bilinear mapping. Simple geometric relations are established to link the motion of the region corner nodes to the motion of the crack-tip node. In this way the motion of every finite element node can be expressed explicitly as a function of the crack-tip motion. Using the ELD finite element model described in Chapter 3, the position, velocity and acceleration of any fixed spatial location $\mathbf{x}^r$ within a given element can then be written as an explicit function of the crack-tip motion.

4.4.3 Computation of the Dynamic Energy Release Rates

In this section procedures for computing the dynamic energy release rates are described. Two distinct cases are considered: a stationary crack subject to general dynamic loading and a propagating crack in a dynamic

field. For a stationary crack, an instantaneous "virtual energy release rate" due to a virtual crack extension is used because there is no actual energy flux into the stationary crack tip. For a propagating crack, the dynamic energy release rate is extracted from the real global change in internal energy and external work between time steps.

4.4.3.1 Stationary Crack

This section presents a continuum formulation of the integral expressions for an instantaneous virtual energy release rate for a general dynamic mixed-mode problem. In Section 2.4.1 the variation of the mutual potential energy due to a virtual crack extension was derived for a stationary crack subject to a static stress field. Here dynamic effects are incorporated by including inertia forces as part of the body force expression. In contrast to a growing crack, a stationary crack does not generate a singular distribution of inertia forces around its tip. Therefore, the singular forms of the stress and strain fields are unaffected by the inertia forces and a virtual energy release rate can be used to compute the stress intensity factor by the same procedure outlined in Section 2.4.1.

Consider a fixed finite material volume V_0 bounded by the surface A_0, which includes part of the crack surfaces, as shown in Figure 2.2. All of the field variables are first defined as functions of the material coordinates, indicated here by a circumflex "^". The variation of the mutual potential energy due to a virtual crack extension, expressed in the material coordinate system and including inertia forces as a part of the body forces, is

$$\delta M^{(1,2)} = \delta \int_{V_0} \hat{w}^{(1,2)} dV - \delta \int_{V_0} \hat{\rho} \left((\hat{b}_i^{(1)} - \hat{\ddot{u}}_i^{(1)}) \hat{u}_i^{(2)} \right.$$

$$+ (\hat{b}_i^{(2)} - \hat{\ddot{u}}_i^{(2)})\, \hat{u}_i^{(1)})\, dV \; - \delta \int_{A_0} (\hat{T}_i^{(1)} \hat{u}_i^{(2)}$$

$$+ \hat{T}_i^{(2)} \hat{u}_i^{(1)})\, dA - \delta \int_{\delta A} (\hat{T}_i^{(1)} \hat{u}_i^{(2)} + \hat{T}_i^{(2)} \hat{u}_i^{(1)})\, dA \qquad (4.14)$$

in which δA is the newly-created crack surface. Now $\hat{b}^{(1)}$ and $\hat{b}^{(2)}$ represent all body forces other than the inertia forces. To simplify the analysis, but without loss of generality, it is assumed that during a virtual crack extension there are no variations of the surface tractions on A_0 or the mass density and body forces in V_0, and that the newly-created crack surfaces are traction-free. It is also assumed that there is no change in the material acceleration field during a virtual crack extension.

$$\delta\hat{\rho} = \delta\hat{b}_i^{(1)} = \delta\hat{b}_i^{(2)} = 0 \qquad \text{in } V_0 \qquad (4.15a)$$

$$\delta\hat{T}_i^{(1)} = \delta\hat{T}_i^{(2)} = 0 \qquad \text{on } A_0 \qquad (4.15b)$$

$$\hat{T}_i^{(1)} = \hat{T}_i^{(2)} = 0 \qquad \text{on } \delta A \qquad (4.15c)$$

$$\delta\hat{\ddot{u}}_i^{(1)} = \delta\hat{\ddot{u}}_i^{(2)} = 0 \qquad \text{in } V_0 \qquad (4.15d)$$

Then equation (4.14) can be simplified.

$$\delta M^{(1,2)} = \delta \int_{V_0} \hat{w}^{(1,2)} dV - \delta \int_{V_0} \hat{\rho}\, ((\hat{b}_i^{(1)} - \hat{\ddot{u}}_i^{(1)})\, \delta\hat{u}_i^{(2)}$$

$$+ (\hat{b}_i^{(2)} - \hat{\ddot{u}}_i^{(2)})\, \delta\hat{u}_i^{(1)})\, dV$$

$$- \int_{A_0} (\hat{T}_i^{(1)} \delta \hat{u}_i^{(2)} + \hat{T}_i^{(2)} \delta \hat{u}_i^{(1)}) \, dA \qquad (4.16)$$

The fixed material volume V_0 and the surface A_0 map onto the reference volume v_0^r which is bounded by the surface a_0^r. The field variables can be defined as functions of the reference coordinates $\mathbf{x}^r$, as an alternative to the above functions based on the material coordinates. Thus, the displacement function $\hat{\mathbf{u}}^{(n)}(\mathbf{X},t)$ and the acceleration function $\hat{\ddot{\mathbf{u}}}^{(n)}(\mathbf{X},t)$ in the material configuration are related to the functions $\mathbf{u}^{(n)}(\mathbf{x}^r,t)$ and $\ddot{\mathbf{u}}^{(n)}(\mathbf{x}^r,t)$ by the inverse geometric mapping. There is no difference between $\ddot{\mathbf{u}}^{(n)}(\mathbf{x}^r,t)$ and $\mathbf{u}^{**(n)}(\mathbf{x}^r,t)$ for a stationary crack.

$$\hat{\mathbf{u}}^{(n)}(\mathbf{X},t) = \mathbf{u}^{(n)}(\mathbf{x}^r(\mathbf{X},t)) \;, \; n = 1,2 \qquad (4.17a)$$

$$\hat{\ddot{\mathbf{u}}}^{(n)}(\mathbf{X},t) = \hat{\ddot{\mathbf{u}}}^{(n)}(\mathbf{x}^r(\mathbf{X},t)) \;, \; n = 1,2 \qquad (4.17b)$$

A virtual crack extension is modeled by a special variation in the geometric mapping $\delta\mathbf{X}(\mathbf{x}^r,t)$. To maintain equilibrium in the material volume during the virtual crack extension (subject to the conditions (4.15)), there must be variations in the displacement fields $\delta\mathbf{u}^{(n)}(\mathbf{x}^r)$; n = 1, 2. Equation (4.16) is then rewritten in the reference coordinate system as

$$\delta M^{(1,2)} = \int_{v_0^r} (\delta_{u^{(1)}} w^{(1,2)} + \delta_{u^{(1)}} w^{(1,2)}) \, \tilde{J} \, dV$$

$$- \int_{v_0^r} \rho \, ((b_i^{(1)} - \ddot{u}_i^{(1)}) \, \delta u_i^{(2)} + (b_i^{(2)} - \ddot{u}_i^{(2)}) \, \delta u_i^{(1)}) \, \tilde{J} \, dv^r$$

$$- \int_{a_0^r} (T_i^{(1)} \delta u_i^{(2)} + T_i^{(2)} \delta u_i^{(1)}) \, K_a \, da^r + \int_{v_0^r} \delta_X (w^{(1,2)} \tilde{J}) \, dv^r \qquad (4.18)$$

where δ_X denotes a variation due to the geometric variation. If the volume V_0 is in equilibrium, the first three integrals in (4.18) vanish for admissible variations $\delta u^{(1)}$ and $\delta u^{(2)}$, by the principle of stationary mutual potential energy ((2.18) and (2.19)). The variation of the mutual potential energy is then simply

$$\delta M^{(1,2)} = \int_{v_0^r} (w^{(1,2)} \, \delta_X \, \tilde{J} + \delta_X \, w^{(1,2)} \, \tilde{J}) \, dv^r \qquad (4.19)$$

Equation (4.19) is the same expression as (2.25), and the virtual energy release rate can be evaluated using the finite element expressions given in Section 2.4.2.

For pure mode-I cases, the virtual energy release rate can be written, as in Section 2.5, as

$$G = -\frac{1}{s\delta a} \delta \Pi$$

$$= -\frac{1}{s\delta a} \int_{v_0^r} (w \, \delta_X \tilde{J} + \delta_X w \, \tilde{J}) \, dv^r \qquad (4.20)$$

4.4.3.2 Propagating Crack

The real energy release rate for a propagating crack is here calculated from a finite difference expression based on the global energy difference between time steps. For a crack increment Δa between time steps an average energy release rate is

$$G = \frac{\Delta P - \Delta W - \Delta K}{s\Delta a} \tag{4.21}$$

where ΔP is the change in external work, ΔW the change in strain energy and ΔK the change in kinetic energy between time steps. The instantaneous energy release rate is obtained in the limit as Δa goes to zero. Equation (4.21) is used to compute the dynamic stress intensity factor at the mid-point of a time increment. This procedure usually produces accurate results in finite element methods since discretization errors tend to be self-cancelling when the energy difference is computed. However, problems may be encountered as the crack velocity approaches zero, as noted in Section 4.5.3.

4.4.4 Computation of the Dynamic Stress Intensity Factor

In the present method the dynamic stress intensity factor is computed from the dynamic energy release rate using a relation given in [54]. For pure mode-I propagation, the proper relation is (4.3), where

$$f(v) = \frac{\alpha_D(1 - \alpha_S^2)}{4\alpha_D\alpha_S - (1 + \alpha_S^2)^2} \tag{4.22}$$

$$\alpha_D^2 = 1 - \left(\frac{v}{C_D}\right)^2 \quad ; \quad \alpha_S^2 = 1 - \left(\frac{v}{C_S}\right)^2 \tag{4.23}$$

$$C_S^2 = \frac{\mu}{\rho} \tag{4.24}$$

$$C_D^2 = \begin{cases} \dfrac{2\mu}{\rho}\left(\dfrac{1-\nu}{1-2\nu}\right) & ; \text{ plane strain} \quad (4.25a) \\ \dfrac{2\mu}{\rho}\left(\dfrac{1}{1-\nu}\right) & ; \text{ plane stress} \quad (4.25b) \end{cases}$$

Here, v is the crack propagation speed, C_S the shear wave speed and C_D the dilatation wave speed. When v goes to zero, i.e. for a stationary crack,

$$f(0) = \begin{cases} 1 - \nu & ; \text{ plane strain} \quad (4.26a) \\ \dfrac{1}{1+\nu} & ; \text{ plane stress} \quad (4.26b) \end{cases}$$

and (4.3) becomes equivalent to (2.48).

4.5 Numerical Examples

In this section the dynamic ELD moving finite element method is applied to the analysis of mode-I dynamic crack propagation problems. Finite element solutions are presented, and compared to analytic predictions and other numerical results using conventional kinematic descriptions.

4.5.1 Crack Propagation in a Finite Strip with Prescribed Boundary Displacements

A square plate with an edge crack of length a_0 is subjected to statically applied prescribed displacements under plane strain conditions. After a given time, t = 0, the crack propagates with constant velocity while the prescribed displacements are maintained. The following dimensions and material properties are used (see Figure 4.2): W = 40 mm, 2h = 40 mm, a_0 = 8 mm, E = 7.56 x 10^{10} N/m^2, ν = 0.286, μ = 2.94 x 10^{10} N/m^2, ρ = 2.45 x 10^3 Kg/m^3. The dilatation wave speed C_D is 6.33 Km/sec, the shear wave speed C_S is 3.46 Km/sec and the Rayleigh surface wave speed C_R is 3.2 Km/sec. Three different crack velocities are considered: v = 0.2 C_S, 0.4 C_S and 0.6 C_S; where v is the crack-tip velocity. This problem is a transient, finite body version of Nilsson's problem [69].

Nilsson presents steady-state solutions for the problem of a semi-infinite crack propagating with constant velocity in an infinite strip.

A mesh of quadratic triangular isoparametric elements is used to model the upper half of the structure. Four quarter-point singular elements [25] are used to model the crack-tip region. As discussed in section 4.4.1, quarter-point isoparametric singular elements correctly model the singularities in the stress field and in the material velocity field for a dynamically propagating crack, while maintaining displacement compatibility at the interface between the singular and conventional elements. The finite element mesh used for $v = 0.4\ C_S$ is shown in Figure 4.3. The mesh in Figure 4.3a represents the initial crack geometry. As the crack propagates, the mesh changes continuously to model the crack growth according to the procedure in section 4.4.2. The final mesh at a/W = 0.5 is shown in Figure 4.3b.

Finite element solutions were obtained using implicit integration with Newmark's parameters $\delta = 0.5$ and $\beta = 0.25$. The initial crack length a_0 is 8 mm , and the change in crack length per integration time step is $\Delta t \cdot v = 0.2$ mm for all three velocities. The dynamic energy release rate is obtained by considering the increments in global energy and work during a time step, and the dynamic stress intensity factor (SIF) is computed from the energy release rate by the relation (4.3). The SIF values plotted in Figures 4.4 - 4.6 are normalized by the SIF, $K_I^{\infty}(0)$, of a stationary, semi-infinite crack in an infinite strip. For plane strain,

$$K_I^{\infty}(0) = \frac{u_0 E}{h^{1/2}(1 - \nu^2)} \tag{4.27}$$

where u_0 is the prescribed boundary displacement [69].

According to (4.2), the SIF immediately after the crack begins to propagate should be $k(v)K_I(0)$, where $k(v)$ is the universal function of crack-tip velocity given in [51], and $K_I(0)$ is the SIF for a stationary crack of length a_0. Normalized values of $k(v)K_I(0)$, obtained by numerical evaluation of $k(v)$ and finite element solutions for $K_I(0)$, are marked in Figures 4.4 - 4.6. For all crack-tip velocities studied, the present method predicts values of SIF virtually identical to $k(v)K_I(0)$ immediately after the crack starts propagating. A detailed study of the transition period in which the crack tip accelerates from zero to a constant velocity is presented in the next section. The SIF predicted by the present method increases steadily until the time t_f when the first reflected waves arrive at the crack tip. In the long term, the SIF exhibits small oscillations near Nilsson's steady-state solution, until the crack approaches the far edge of the plate.

Numerical results obtained with a moving singular element procedure [65,70] are presented for comparison. In Figures 4.4 - 4.6 results for a special singular element with propagation eigen functions [70] are plotted as a solid curve, and results for the usual quarter-point isoparametric elements with global energy balance computation [65] are plotted as a dashed curve. Upward arrows indicate the times at which a remeshing process is performed in the moving singular element procedure. For $v = 0.2\ C_S$ both results are nearly identical, so only the results of the propagation eigen function method are plotted. The propagation eigen function results do not match the analytic prediction of an instantaneous drop in the SIF as the crack begins to propagate. The SIF values are overestimated, and the error is larger for higher crack-tip velocities. A disturbance in the SIF is reported in [65] for the quarter-point isoparametric element procedure at higher crack-tip velocities each time remeshing is performed. This might be

an artifact of the displacement discontinuities (in time) that are produced by remeshing operations in a conventional Lagrangian description. In the dynamic ELD formulation the displacement field evolves continuously as the mesh moves, and no disturbance of the SIF is observed.

4.5.2 A Detailed Study of the Crack Acceleration Period

In this section the convergence of the present method to the analytic prediction at the initiation of crack propagation in the previous example is investigated. In an analytic analysis the crack at rest suddenly starts to propagate with a finite speed. As Eshelby observed [71], this is not improper since no inertia is associated with a brittle crack tip. Therefore, the crack speed can change discontinuously. Equation (4.2) implies that the dynamic stress intensity factor value is instantly reduced from its static value, $K_I(0)$, by the factor $k(v)$, immediately after the crack begins to propagate.

In the present study, the crack is assumed to accelerate smoothly from zero velocity to a constant speed of $0.4\ C_S$ during a short transition period t_{tr}. The case of an instantaneous change of the crack-tip velocity is attained in the limit as t_{tr} goes to zero. The crack-tip velocity varies according to a cubic function, such that there is zero acceleration at the beginning and end of the transition period. Three different transition times are considered: $t_{tr}^{(1)} = \Delta t$, $t_{tr}^{(2)} = 1/2\ \Delta t$ and $t_{tr}^{(3)} = 1/4\ \Delta t$, where Δt is the time step size used in the previous example, i.e. $\Delta t = 0.1443$ sec. The geometry, prescribed displacements and material properties are identical to those in the previous example. Reduced time step sizes $\Delta \bar{t}$ are used to capture the details of the transient response. The time step sizes used in the analyses are $\Delta \bar{t}^{(1)} = \Delta \bar{t}^{(2)} = 1/8\ \Delta t$ and $\Delta \bar{t}^{(3)} = 1/16\ \Delta t$.

Values of the SIF, normalized by $K_I^{\infty}(0)$, are plotted in Figure 4.7. The times t_D, t_S and t_R marked in Figure 4.7 indicate the times when the dilatation, shear and Rayleigh waves generated by the initial crack-tip motion pass out of the crack-tip elements. In all three cases, the new method predicts SIF values virtually identical to the analytic prediction, $k(v)K_I(0)$, after the dilatation, shear and Rayleigh wave fronts completely leave the crack-tip elements. However, erratic response is observed prior to t_D, particularly for shorter transition times. This response is attributed to the inability of the singular element shape functions to correctly model the strong wave fronts while they are within the crack-tip elements. However, good results are obtained once the waves pass the singular elements (after the times t_D, t_S and t_R). The use of smaller crack-tip elements reduces the times t_D, t_S and t_R; and thus produces reliable results after a short time. For best results, a transition time t_{tr} roughly equal to t_D is recommended. A minimum of four steps should be used during the transition period, while larger time steps may be used after the solution has stabilized following the transition.

4.5.3 A Crack Arrest Problem

In this section crack arrest behavior in a square plate subjected to statically applied prescribed displacements under plane strain conditions is investigated. The dimensions and material properties are identical to those used in the problem in Section 4.5.1. An edge crack begins to propagate with constant velocity at time t = 0 while the prescribed displacements are maintained, as in the previous example; but suddenly arrests at a time designated t_A. Results for the case in which the running crack velocity is 0.4 C_s and the crack arrest time t_A = 2.382 μsec are presented. In the numerical simulation, the crack decelerates over a short time period equal

to a regular integration time step (Δt = 0.1443 μsec). The crack-tip velocity is assumed to change smoothly from its running velocity to zero velocity according to a cubic function, similar to the assumptions for the crack acceleration period. Sixteen reduced time steps were used during the deceleration period to capture the details of the crack arrest behavior.

Values of the SIF, normalized by the value $K_I^{\infty}(0)$ defined in (4.27), are plotted in Figure 4.8. The times t_{CD}, t_{CS} and t_{CR} marked in Figure 4.8 indicate the times when dilatation, shear and Rayleigh waves generated by the initial crack-tip motion travel to the nearest free boundary and reflect back to the arrested crack tip. The times t_{AD}, t_{AS} and t_{AR} are the times at which the dilatation, shear and Rayleigh waves generated by the crack arrest travel to the nearest free boundary and reflect back to the crack tip. A prediction of the SIF at the instant of crack arrest (prior to the time when the first reflected waves return to the crack tip) can be obtained from the analytic result (4.2) and a finite element solution for $K(t_A,v)$. This prediction is indicated by $K(t_A,0)$ in Figure 4.8. The present method produces an instantaneous jump in the SIF virtually identical to the predicted value at the instant of crack arrest. This close agreement was also obtained for a simulation using a different velocity for the running crack. Immediately after crack arrest, a continued rise of the SIF due to material inertia is predicted. In the long-term, the SIF oscillates around the static stress intensity factor associated with the arrested crack length, denoted by K_S in Figure 4.8, as expected. This was confirmed in the simulation for times up to t = 25.0 μsec, although Figure 4.8 shows only the SIF history for a short time after arrest. The value of K_S shown in Figure 4.8 was computed by the finite element method described in Chapter 2 using the arrested crack length and the static stress field produced by the prescribed boundary displacements. The same type of oscillation of the SIF

after crack arrest has been observed in experiments where the effects of wave reflections are significant [72].

It should be noted that a problem did arise in the numerical computation of the SIF during the deceleration period. As the crack-tip velocity approaches zero, the finite difference approximation of the energy release rates can lead to unreliable predictions of the SIF. The sum of the kinetic and strain energy rates is computed from

$$\frac{\delta(K + W)}{\delta a} = \frac{\delta(K + W)}{\delta t} \frac{\delta t}{\delta a} \tag{4.28}$$

The term $\delta(K+W)$ tends to zero as the crack-tip velocity v approaches zero. Small errors in the finite difference approximation of $\frac{\delta(K + W)}{\delta t}$ will lead to large errors in the computed values of the SIF as v goes to zero because

$$\lim_{v \to 0} \frac{\delta t}{\delta a} = \infty \tag{4.29}$$

In Figure 4.8 the SIF at the mid-point of the deceleration period is plotted. Erratic values for the SIF were computed at only the last three of the sixteen small time steps used during the deceleration period. For $t \geq t_A$ the explicit method of Section 4.4.3.1 was used to compute the SIF. No problems were encountered in the calculation of the SIF subsequent to t_A.

4.5.4 Crack Propagation in a Finite Plate with Stress-Wave Loading

A rectangular plate with a central crack of length $2a_0$, shown in Figure 4.9, is subjected to uniformly distributed tensile traction stresses p_0 under plane strain conditions. The time-dependent stress loading p_0 is defined by

$$p_0 = \sigma_{22} H(t) \tag{4.30}$$

where H(t) is the Heaviside unit step-function. Dimensions and material properties are (see Figure 4.9): W = 104 mm, L = 40 mm, $2a_0$ = 24 mm, E = 7.56 x 10^{10} N/m^2, ν = 0.286, μ = 2.94 x 10^{10} N/m^2, ρ = 2.45 x 10^3 Kg/m^3. The crack, with an initial length of $2a_0$, remains stationary until a time, t = 4.4 μsec, shortly after the stress wave arrives. The crack then begins to propagate at both tips with a constant velocity v = 1.0 Km/sec.

The upper-right quadrant of the structure is modeled with a mesh of LST isoparametric elements, and quarter-point isoparametric elements are used as crack-tip elements. The time step size used is Δt = 0.2 μsec; and δ = 0.5 and β = 0.25 are the Newmark time integration parameters. At time t = 4.4 μsec the crack tips accelerate from zero velocity to v = 1.0 Km/sec using the smooth acceleration scheme described in the previous example. A single regular time step is used as the transition period t_{tr}, which is subdivided into eight reduced time steps. Reduced time steps are continued for an additional regular time step after the crack tips achieve full velocity.

The SIF values plotted in Figure 4.10 are normalized by the static SIF for a crack of initial length $2a_0$ in an infinite body, $\sigma_{22}(\pi a_0)^{1/2}$. The notation for specific times marked in Figure 4.10 is explained as follows.

t_L : the time for the dilatation waves to travel from the boundary where the time-dependent tension is applied to the stationary crack tip.

t_C : the time when the crack starts to propagate.

t_{LD}, t_{LS}, t_{LR} : t_L plus the time taken by the dilatation, shear and Rayleigh waves first scattered by a stationary crack tip to reach the other crack tip.

t_{CD}, t_{CS}, t_{CR} : t_C plus the time taken by the dilatation, shear and Rayleigh waves emanating from a crack tip at t_C to reach the other crack tip.

t_{LOL} : the time for the dilatation waves to travel from the boundary where the time-dependent tension is applied to the opposite side, and reflect back to a moving crack tip.

t_{COL} : the time taken by the dilatation waves emanating from a crack tip at t_C to travel to the nearest boundary and reflect back to the same crack tip.

The analytic solution for the SIF for a stationary crack in an infinite body subjected to stress-wave loading is given by Freund [50] as

$$K(t,0) = 2(2/\pi)^{1/2} \sigma_0 \omega_0 (t - t_L)^{1/2} \qquad (4.31)$$

where ω_0 is given in [50], and σ_0 is $2\sigma_{22}$ in this problem. For a propagating crack the corresponding analytic solution is [50]

$$K(t,v) = 2(2/\pi)^{1/2} \sigma_0 \omega_0 k(v) (t - t_L)^{1/2}$$

$$= k(v) K(t,0), \qquad t > t_L \qquad (4.32)$$

For the finite body problem, the analytic solutions are only valid prior to the time at which reflected waves reach the crack tips. Normalized values

of K_I obtained by numerical evaluation of the analytic expressions for k(v) and ω_0 given in [50,51], are plotted in Figure 4.10 as a solid curve. Results obtained with the new method are also plotted, and are in excellent agreement with the analytic solutions until there is significant interaction of the reflected waves with the crack tip.

Numerical results by Nishioka and Atluri [70] using a moving singular element procedure are also presented in Figure 4.10 for comparison. Their results were obtained using a special singular element based on propagation eigen functions. Upward arrows indicate the times at which over-all re-meshing is performed in the Nishioka and Atluri solution. The procedure does not predict an instantaneous drop in the SIF as the crack starts to propagate; and values of the SIF slightly higher than the analytic results are observed for some time thereafter. It is worth noting that an inaccurate solution at the time when the crack begins to propagate can reduce the accuracy of the solution at subsequent times, when reflected stress waves generated by the moving crack return to the crack tip.

4.6 Chapter Summary

A moving finite element method, based on the dynamic Eulerian-Lagrangian kinematic model, has been used for the analysis of brittle dynamic fracture problems. The finite element equations, developed in Chapter 3 for a general three-dimensional linear elastodynamic problem, were simplified for cases in which the geometric mapping changes only in the X_1-direction, in finite bodies. This model is suitable for the analysis of mode-I dynamic crack propagation. A history of the mesh motion, based on the crack propagation history, is assumed to be known.

The isoparametric finite element version of the dynamic ELD provides a simpler and more effective model of dynamic crack propagation behavior than

conventional Lagrangian kinematic models. Commonly-used quarter-point singular isoparametric elements automatically capture the singularities in both the material velocity field and the stress field at the crack tip. The convective terms in the dynamic ELD model ensure that the proper singular form is generated in the velocity field. The mesh motion used to model crack growth can be distributed over a selected region of the structure using an auxiliary mapping. This greatly reduces - and often eliminates - the need for discrete remeshing of the over-all structure; and local remeshing between time steps is completely eliminated. Since the mesh motion is introduced continuously in the ELD kinematic model, there is no need to interpolate field variables between time steps, as in Lagrangian remeshing procedures.

The dynamic stress intensity factor is computed from either a dynamic energy release rate, based on a global energy difference computation; or from an instantaneous energy rate expression associated with a virtual crack extension. Finite element discretization errors tend to be self-cancelling in the energy methods. Numerical examples of mode-I dynamic crack propagation demonstrate the advantages of the ELD with respect to conventional kinematic descriptions. Excellent agreement is achieved with analytic predictions. The dynamic ELD finite element model performs well, even for cases in which the motion of the crack tip is discontinuous, such as sudden crack propagation at a finite speed. Potential applications of the method to additional problems in the analysis of brittle dynamic fracture are discussed in the next chapter.

CHAPTER 5

CONCLUSIONS AND RECOMMENDATIONS FOR FURTHER STUDY

This study has presented a small-deformation Eulerian-Lagrangian kinematic description for the analysis of static and dynamic brittle fracture. Three novel accomplishments can be identified: The development of a computational method for extracting virtual energy release rates in linear elastic fracture mechanics; formulation of an elastodynamic version of the ELD in continuum form and its specialization to moving isoparametric finite element analysis; and the analysis of rapid brittle fracture using the dynamic ELD moving isoparametric finite element method.

Explicit expressions for mutual potential energy release rates and mixed-mode stress intensity factors for linear elastic fracture mechanics problems were presented in Chapter 2. The ELD kinematic model allows a geometric variation to represent a true virtual crack extension. Thus, a true variational formulation of the energy release rates is possible. The need for finite difference approximation of the energy release rates, required in conventional Lagrangian virtual crack extension methods, is eliminated. The instantaneous energy release rates are evaluated directly from integral expressions defined over quarter-point singular isoparametric elements. The method produces very accurate results, even for a relatively coarse mesh and for an integration domain close to the crack tip.

The small-deformation version of the ELD was extended to dynamic problems in Chapter 3. Time rate expressions for various field variables were derived using the dynamic ELD kinematic model; and a continuum formulation of the variational equations of motion was developed. The variational equations of motion based on the ELD model introduce more stringent continuity conditions than conventional Lagrangian formulations. A special

weak form of the variational equations was derived to overcome these problems and to provide a suitable basis for dynamic moving isoparametric finite element formulations. Finite element expressions for a general three-dimensional dynamic problems were presented using both implicit and explicit time integration methods. The method is particularly effective for analysing problems in which the structural geometry, material interfaces or the domains of the boundary conditions change with time.

In Chapter 4 the dynamic moving isoparametric finite element method has been applied to the analysis of dynamic brittle fracture problems. The dynamic ELD model applied to moving isoparametric elements provides a more effective means for modeling crack propagation behavior than conventional Lagrangian models. The convective terms in the dynamic ELD model, in conjunction with singular quarter-point isoparametric elements, produce the proper singular forms in both the stress and material velocity fields. There is no need to use special non-conforming singular elements, as with conventional Lagrangian finite element models. Crack growth is modeled by mesh motion, which is smoothly distributed over a selected region of the structure using an auxiliary geometric mapping. The need for local remeshing between every time step, required in Lagrangian procedures, is completely eliminated; and the need for over-all discrete remeshing is greatly reduced or eliminated. The mesh motion is introduced in continuous form in the dynamic ELD model, so there is no need to interpolate field variables as in Lagrangian remeshing procedures.

In general, the ELD kinematic model provides a more effective approach to brittle fracture problems than conventional Lagrangian models. This is attributed to the fact that geometric changes due to crack growth cannot be modeled directly by Lagrangian models, while these changes and their effects

on material motion can be incorporated in a natural way using the mixed Eulerian-Lagrangian kinematic model.

In the present study, the ELD model is used primarily for the analysis of two-dimensional brittle fracture problems. However, there are many problems that cannot be adequately described by two-dimensional models. These include crack initiation and branching, where the initial cracks or branches do not penetrate the thickness. Cracks in three-dimensional bodies, such as weldments, are another important example. Since the present formulations are developed in three-dimensions, the new methods can be applied to three-dimensional analysis with the use of appropriate three-dimensional isoparametric singular elements [73,74]. Three-dimensional quarter-point isoparametric elements should be used with caution, since negative Jacobians can occur due to geometric distortion when these elements are used to model a curved crack front [75]. Mixed-mode behavior is important in three-dimensional problems. A procedure for extracting the dynamic stress intensity factor for each fracture mode of a propagating crack is needed for this type of problem.

An explicit computational method for extracting the instantaneous dynamic energy release rate of a propagating crack would be of great interest. The continuum formulation for a stationary crack developed in this study might be extended to the case of a propagating crack by accounting for the velocity field of the moving mesh induced by the actual crack-tip velocity. A version of this procedure based on an extended mutual energy procedure, incorporating a kinetic energy term, might provide an efficient means for the analysis of mixed-mode problems.

Many fracture problems involve nonlinear or rate-dependent material behavior. These include problems involving large-scale yielding, metals

creeping at high temperature, and fracture in various viscoelastic materials. Large-deformation effects may also be significant in these problems. Large deformations in linear materials pose no special problems, as the general ELD [17] was first formulated for this class of problem. However, rate-based constitutive laws do add an additional degree of difficulty. First, the ELD model does not directly incorporate material stress and strain rates. Convective terms must be introduced to convert spatial deformation rates to material rates. Following application of the constitutive relations, the predicted material stress rates must be converted back to spatial rates. These operations can introduce more difficult continuity requirements than those encountered in the linear elastodynamic formulation.

Another possible extension of the present study is the analysis of the temperature field around a moving crack tip, and its effects on the near-tip stress field. An appropriate finite element modeling of the heat transfer equations [76], including Eulerian convective terms could be developed. Even in brittle fracture, the difference between the elastic energy release at the crack tip and the specific fracture energy of the material is mostly converted to heat [77]. Thermal stresses, associated with temperature changes at the moving crack tip, can effect significant stress redistribution at higher crack velocities. Insufficient time for heat conduction at high crack velocities results in an adiabatic heat rise [78,79]. As a first step, a simple linear analysis of the heat transfer problem, assuming that the material thermal properties are independent of temperature, could be useful.

The dynamic moving finite element model in this study is restricted to cases of known mesh motion. This is useful for interpreting experimental tests with the goal of developing crack propagation criteria. However, this restriction would prevent the use of the method for predicting fracture

behavior. As discussed in Chapter 3, the dynamic ELD can be extended to cases of unknown mesh motion. The variational equations of motion can be rewritten using incremental expressions for both the displacements and the mapping. The resulting equations are nonlinear with two sets of unknown variables. The equations in linearized form can be solved iteratively using additional constraint equations derived from appropriate criteria; e.g., crack propagation criteria and moving boundary definitions. This would be useful for investigating crack growth initiation, arrest and direction criteria; particularly for propagation-type direction criteria [20], which are based on conditions after an increment of crack extension. In Lagrangian models the crack is constrained to grow along predetermined element grid lines, so extensive mesh refinement or frequent remeshing is required. In the ELD model, the finite element mesh can move an arbitrary distance in any direction.

The use of computer graphics to prepare data and to interpret the complex transient results of dynamic moving finite element analyses is of great interest. Automatic mesh generation techniques have been used in this study to expedite the pre-processing of the finite element data and to automatically define the geometric mapping used to describe the crack-tip motion. Color computer graphics displays are very useful for post-processing the results of finite element analyses. Color displays of stress, strain and strain energy density distributions have been used. Three-dimensional color animation techniques are under development for depicting transient dynamic fracture behavior, such as the interaction between reflected stress waves and the crack-tip zone.

TABLES

Table 2.1. Correction Factor f(a/b) for Cracks in a Plate

Crack geometry	a/b	Present method L/b=1.0	Present method L/b=2.5	Analytic solution L/b=∞	Analytic solution L/b=∞	Analytic solution L/b=1.0	Hellen L/b=1.0	Hellen L/b=2.5
Single edge crack	0.1	1.18	1.18	1.19*	1.20**		1.22	1.19
	0.2	1.36	1.36	1.37	1.37		1.36	1.36
	0.3	1.65	1.65	1.66	1.68		1.65	1.65
	0.4	2.10	2.10	2.12	2.14		2.10	2.10
	0.5	2.80	2.80	2.82	2.86		2.81	2.81
	0.6	4.00	4.00	--	--		4.01	4.01
Double edge crack	0.1	1.12				1.13**	1.13	
	0.2	1.14				1.13	1.14	
	0.3	1.18				1.14	1.18	
	0.4	1.19				1.16	1.19	
	0.5	1.18				1.14	1.18	
	0.6	1.15				1.10	1.14	
Central crack	0.1	1.01	1.00	1.00***			1.02	1.01
	0.2	1.05	1.02	1.03			1.05	1.02
	0.3	1.12	1.05	1.07			1.12	1.05
	0.4	1.21	1.11	1.13			1.21	1.11
	0.5	1.33	1.18	1.21			1.33	1.18
	0.6	1.48	1.30	1.35			1.48	1.30

* Gross
** Bowie
*** Paris and Sih

Table 2.2 Correction Factor f(a/b) in a Notched Round Bar, L/b=2.5

	Present method		Analytic	Hellen's solution	
a/b	plane strain	plane stress	solution[1]	plane strain	plane stress
0.1	0.214	0.204	0.210	0.213	0.203
0.2	0.260	0.248	0.251	0.256	0.243
0.3	0.268	0.255	0.259*	0.265	0.253
0.4	0.260	0.248	0.255	0.259	0.247
0.5	0.241	0.230	0.240	0.243	0.232

[1] Bueckner, L/b=∞

* a/b=0.293

FIGURES

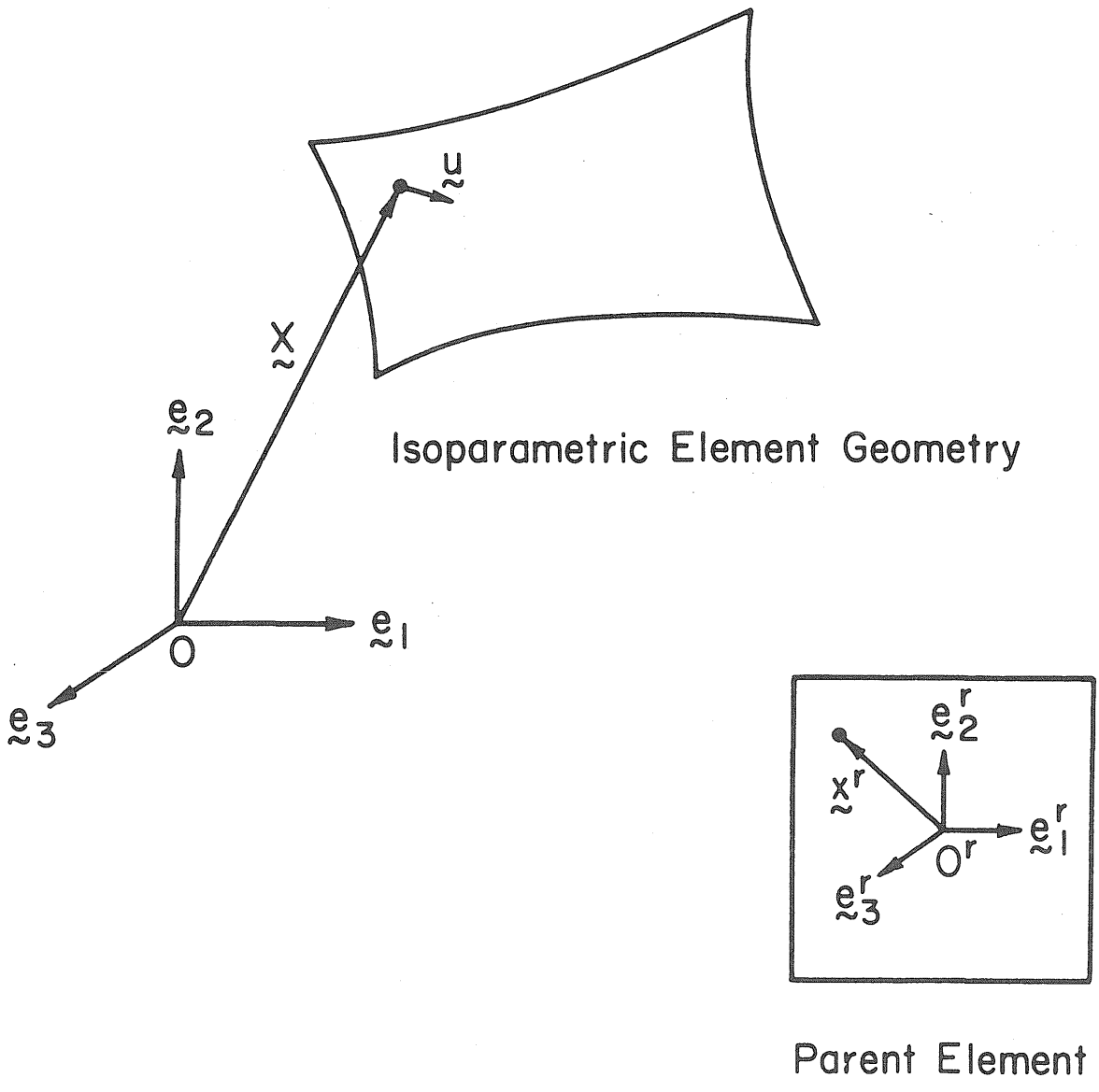

Figure 2.1 The Specialization of the Small-Deformation ELD to Isoparametric Finite Elements

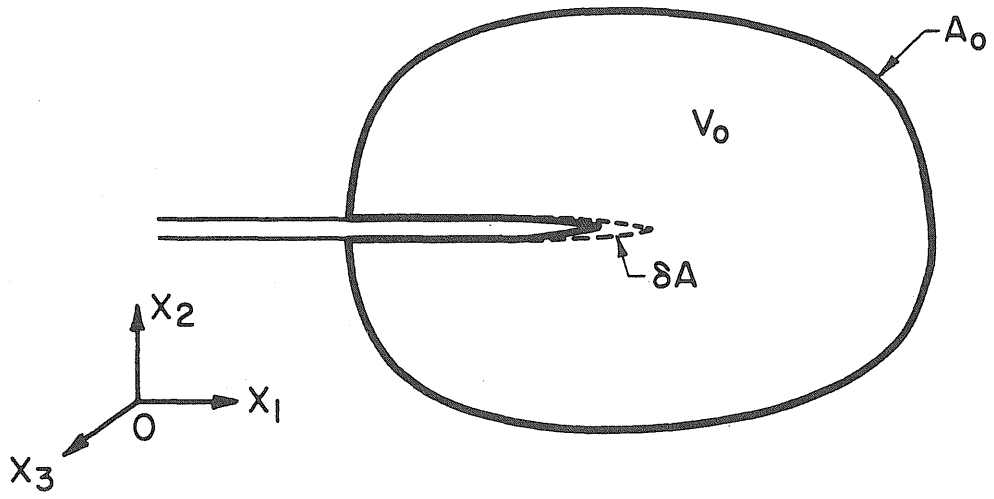

(a) Two Configurations of the Material Volume

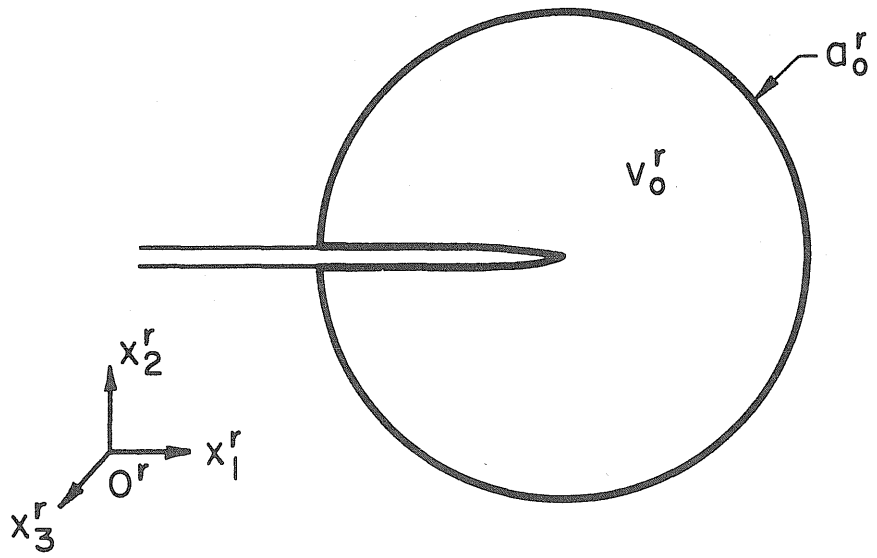

(b) Reference Volume

Figure 2.2 A Fixed Material Volume Surrounding the Crack-Tip Region; (a) the Material Volume, Before and After Virtual Crack Extension, (b) the Reference Volume

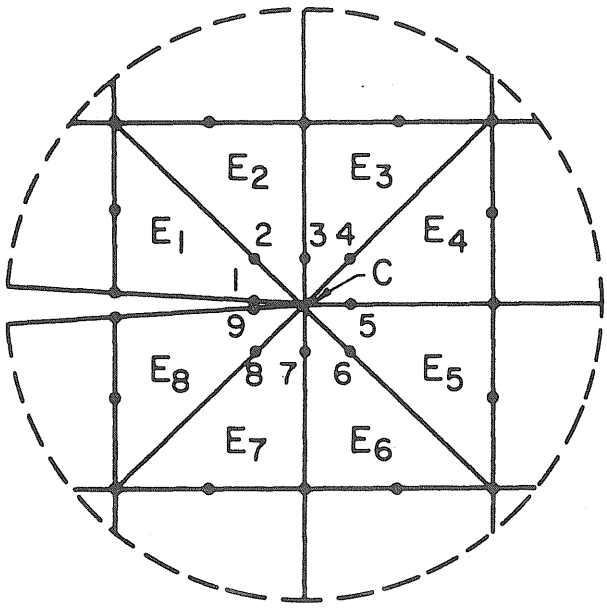

(a) Crack Prior to Extension

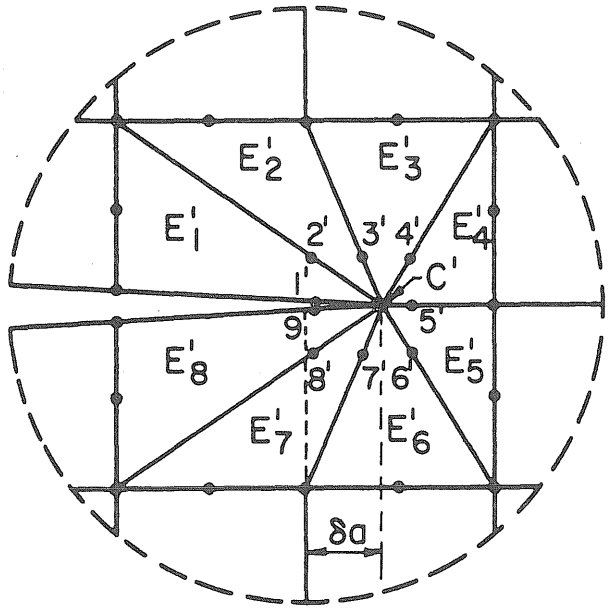

(b) Virtual Extension of Crack

Figure 2.3 Finite Element Model of a Virtual Crack Extension in the Fixed Material Volume

Single Edge Crack

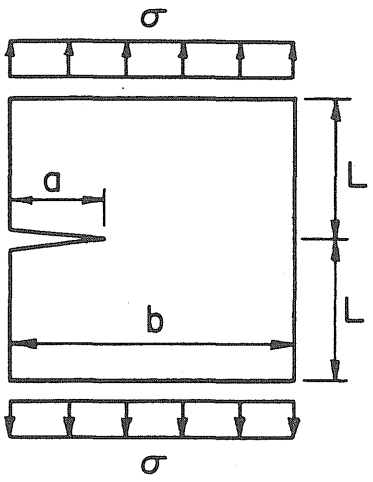

$$K_I = \sigma\sqrt{a\pi}\, f(a/b)$$

Double Edge Crack

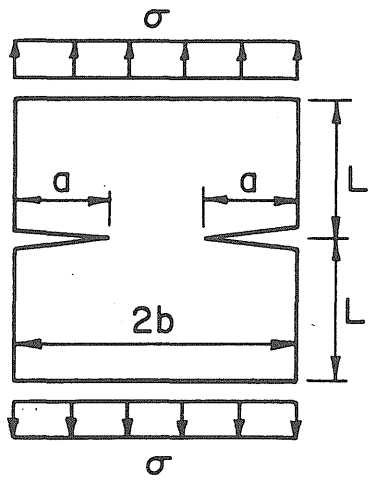

$$K_I = \sigma\sqrt{a\pi}\left(\frac{2b}{\pi a}\tan\frac{\pi a}{2b}\right)^{1/2} f(a/b)$$

Central Crack

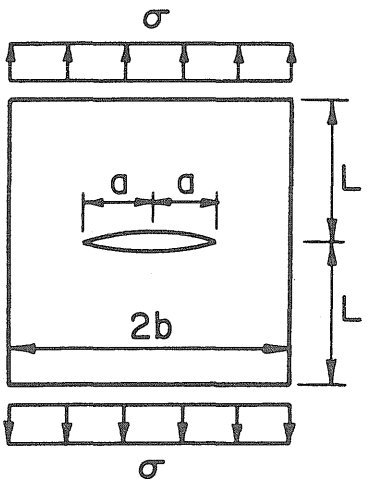

$$K_I = \sigma\sqrt{a/\pi}\, f(a/b)$$

Cracked Round Bar

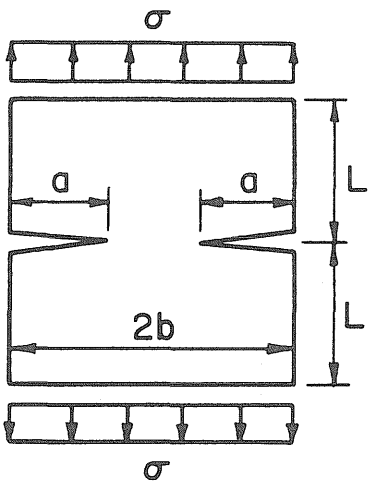

$$K_I = \sigma_{net}\sqrt{2b\pi}\, f(a/b)$$

Figure 2.4 Dimensions and Stress Intensity Factors for Mode-I Crack Problems

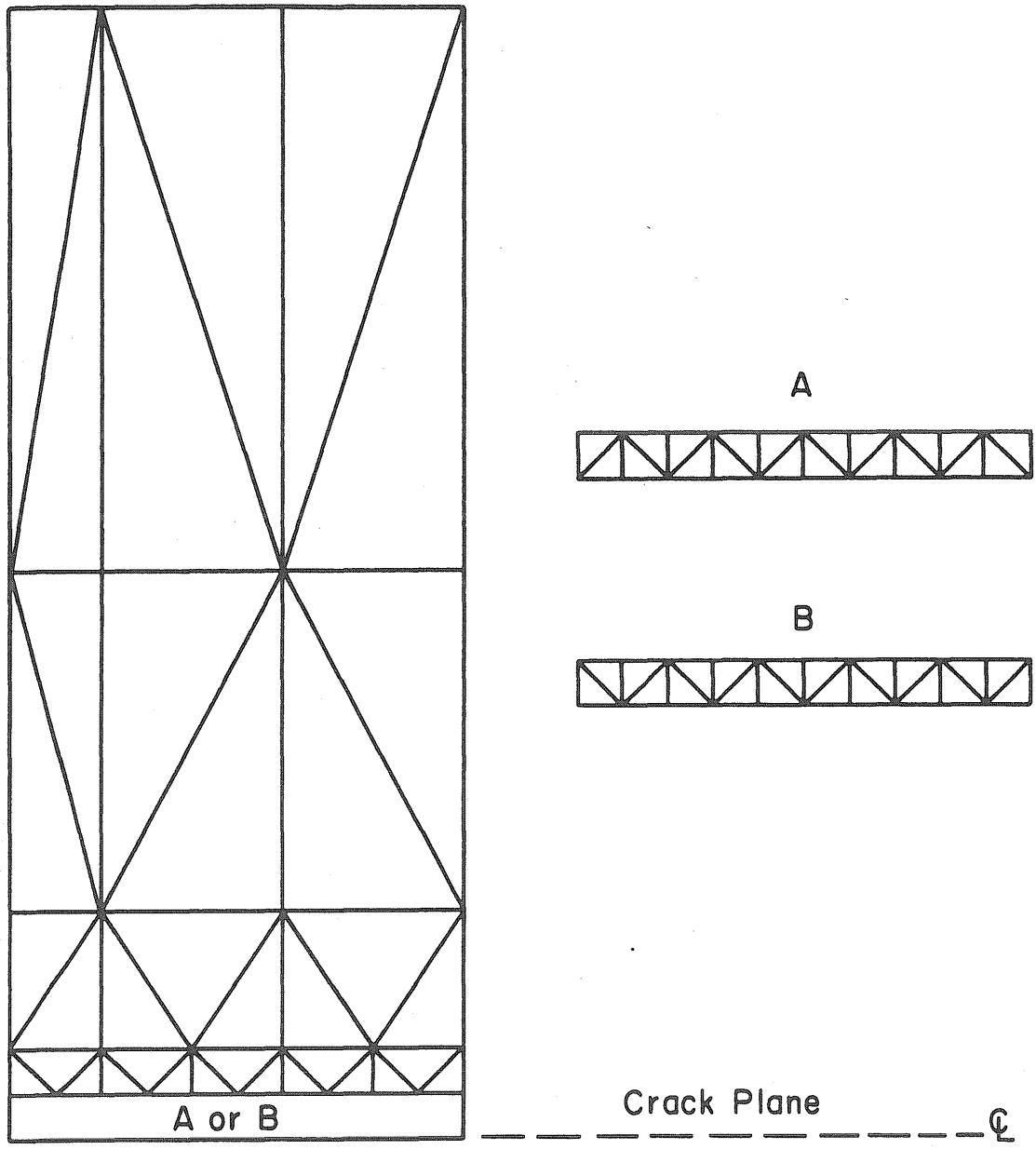

Figure 2.5 Finite Element Meshes for Mode-I Problems

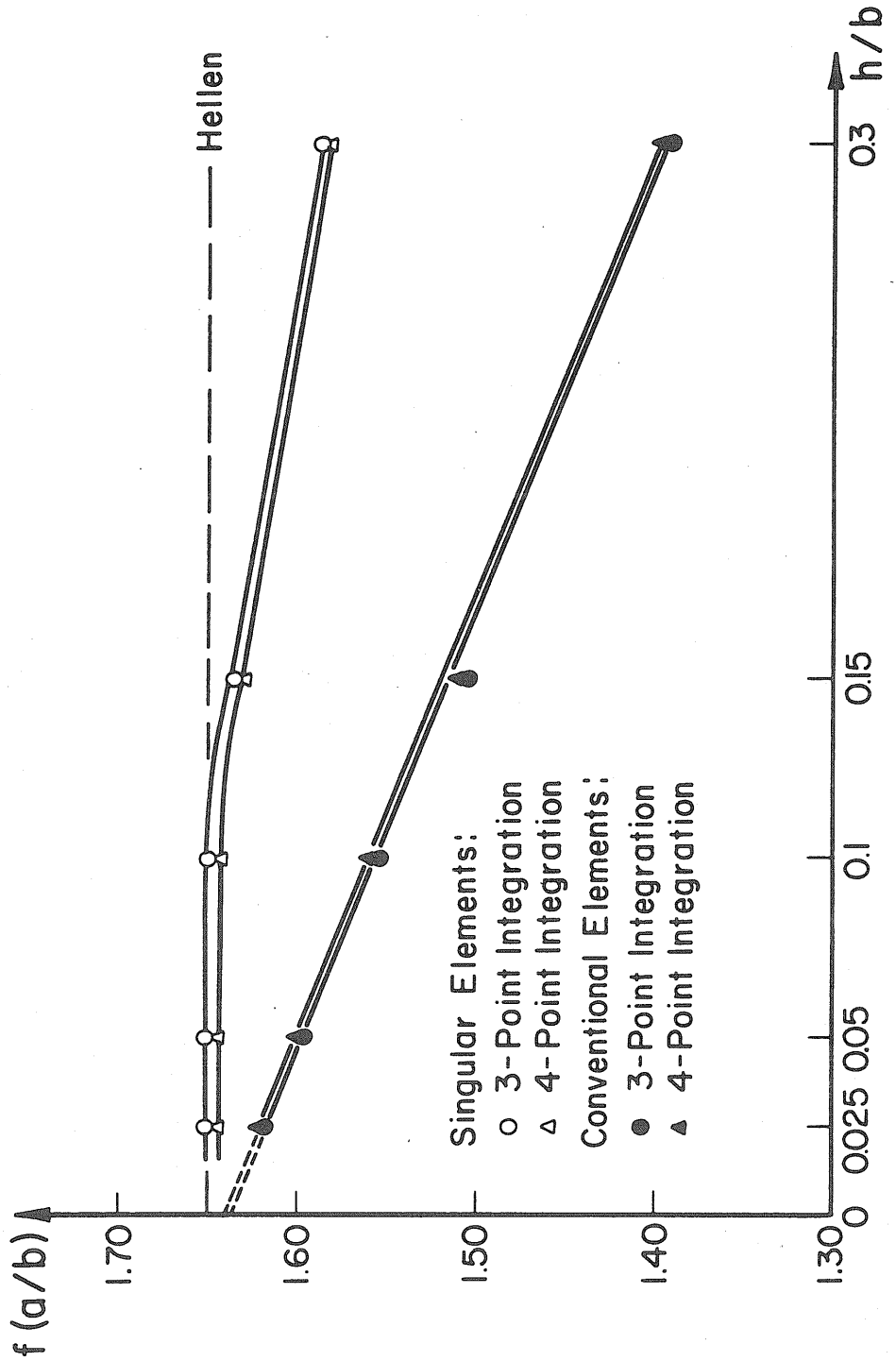

Figure 2.6 The Effect of Mesh Refinement on the Accuracy of Mode-I Solutions

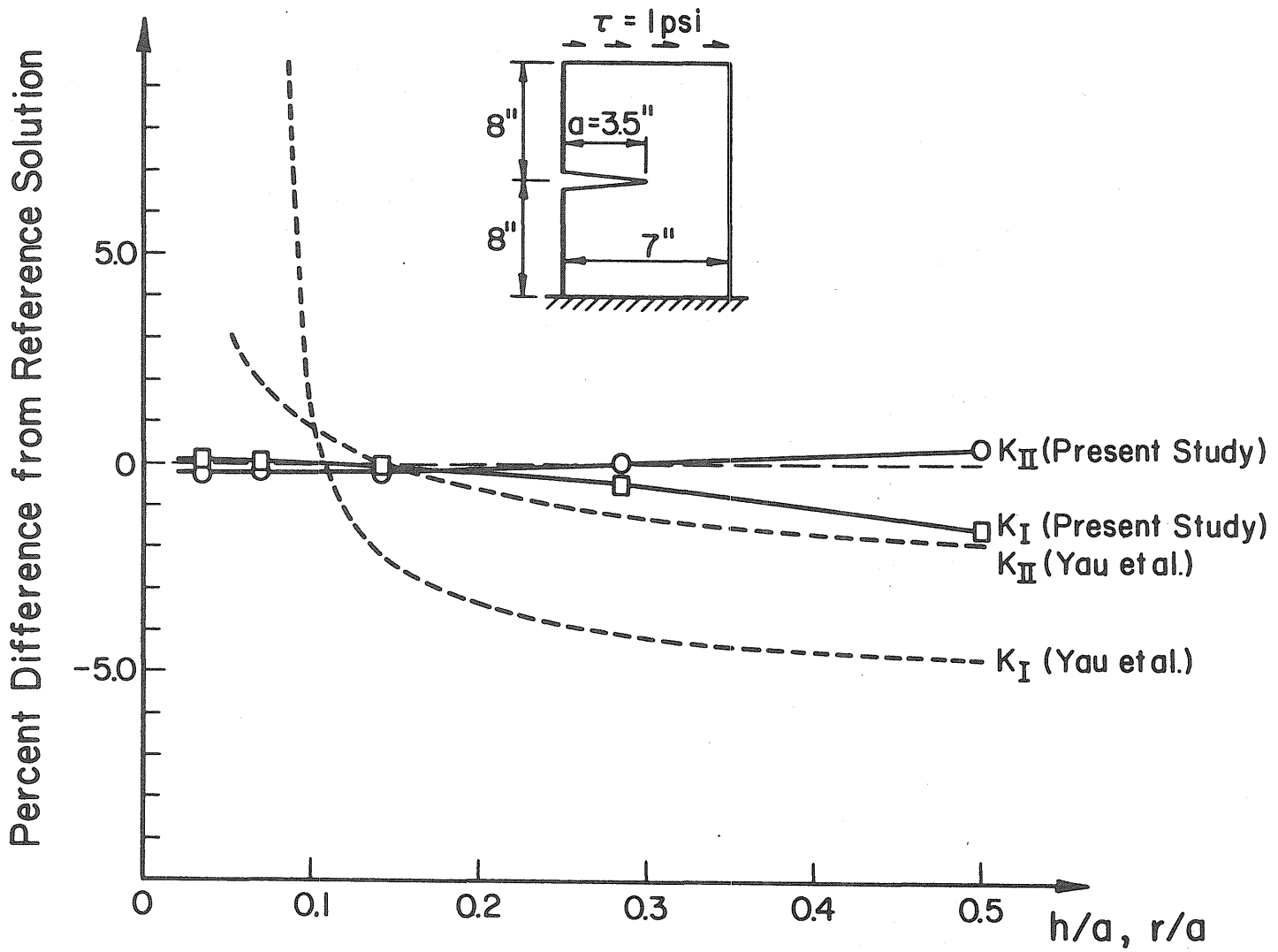

Figure 2.7 The Effect of Varying the Domain of Integration on the Solution Accuracy for the Problem of a Cracked Plate Under Shear Loading

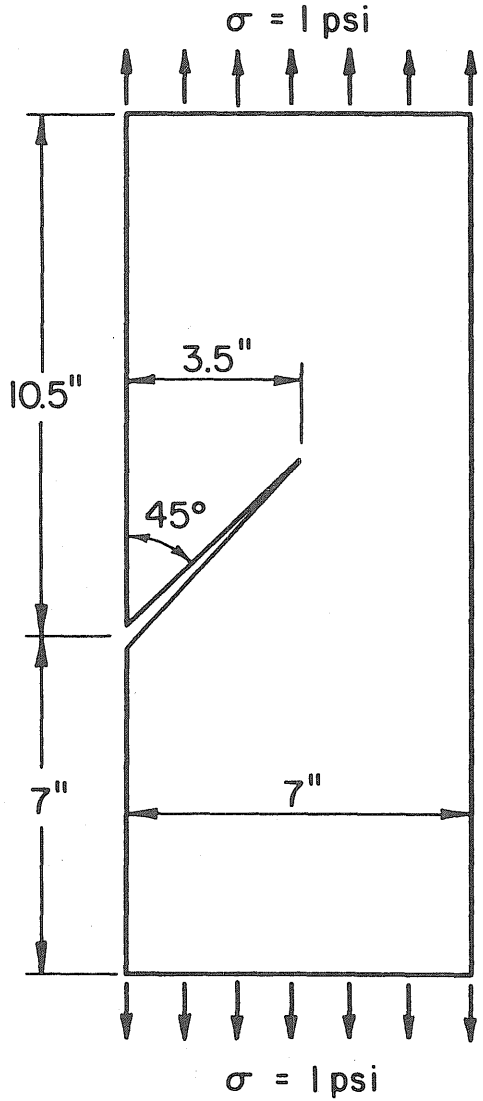

Dimensions and Loading

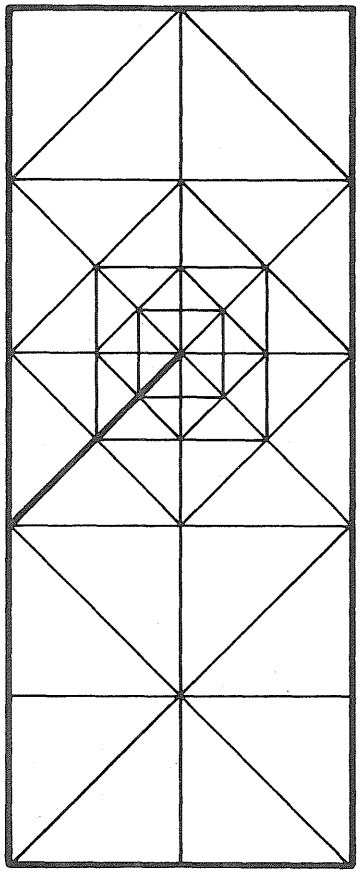

Finite Element Mesh

Figure 2.8 A Tension Specimen with a 45° Crack

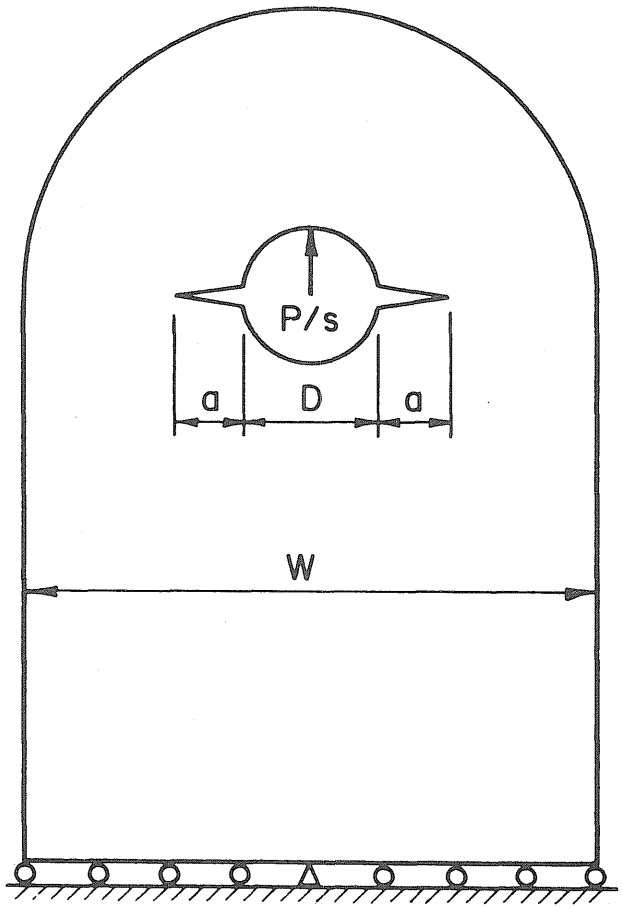

Dimensions and Loading

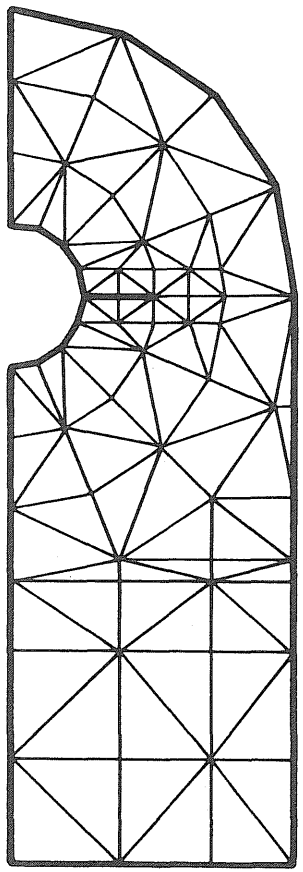

Finite Element Mesh

Figure 2.9 An Attachment Lug with a Double Crack

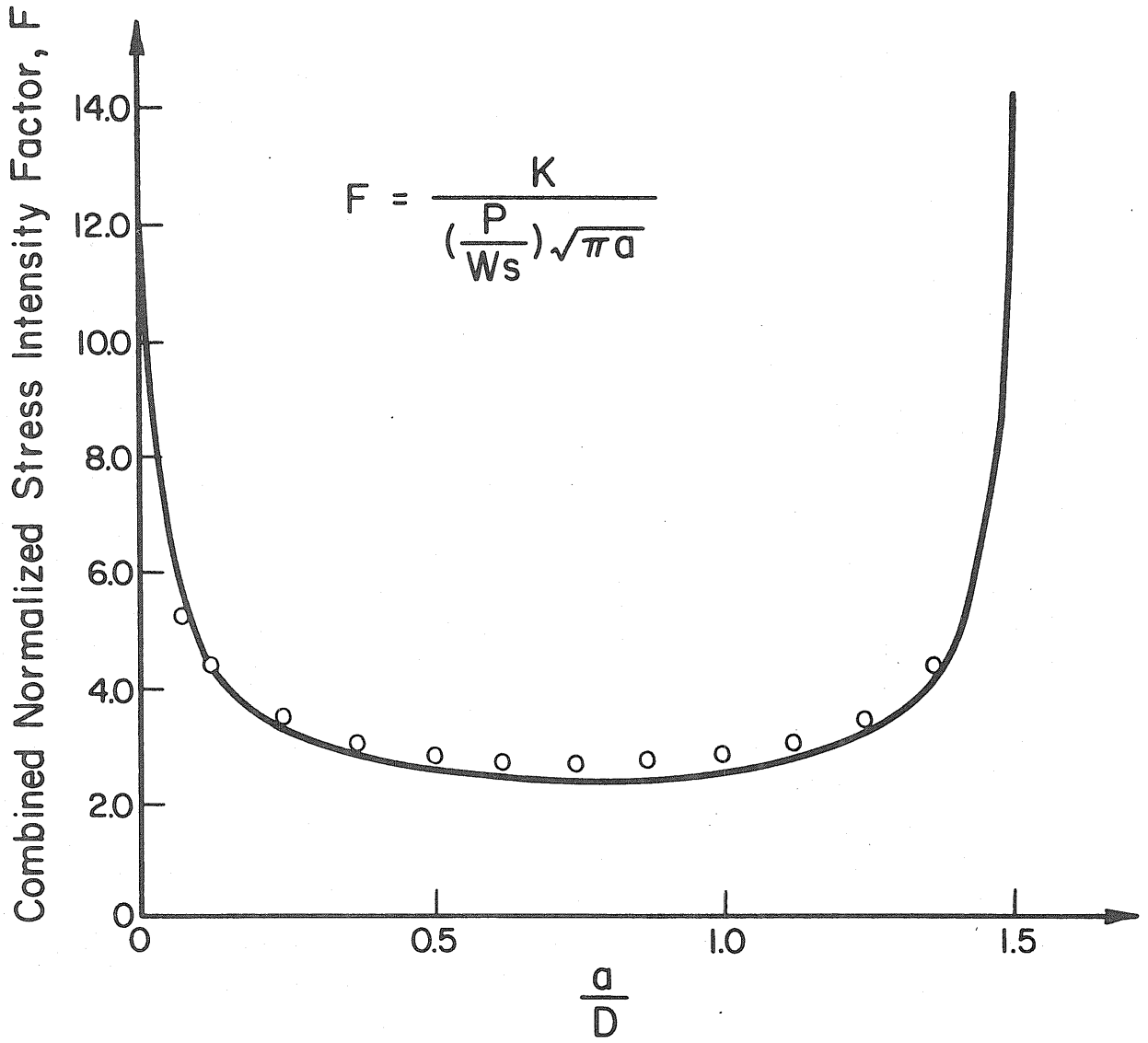

Figure 2.10 The Combined Stress Intensity Factor vs. Crack Length

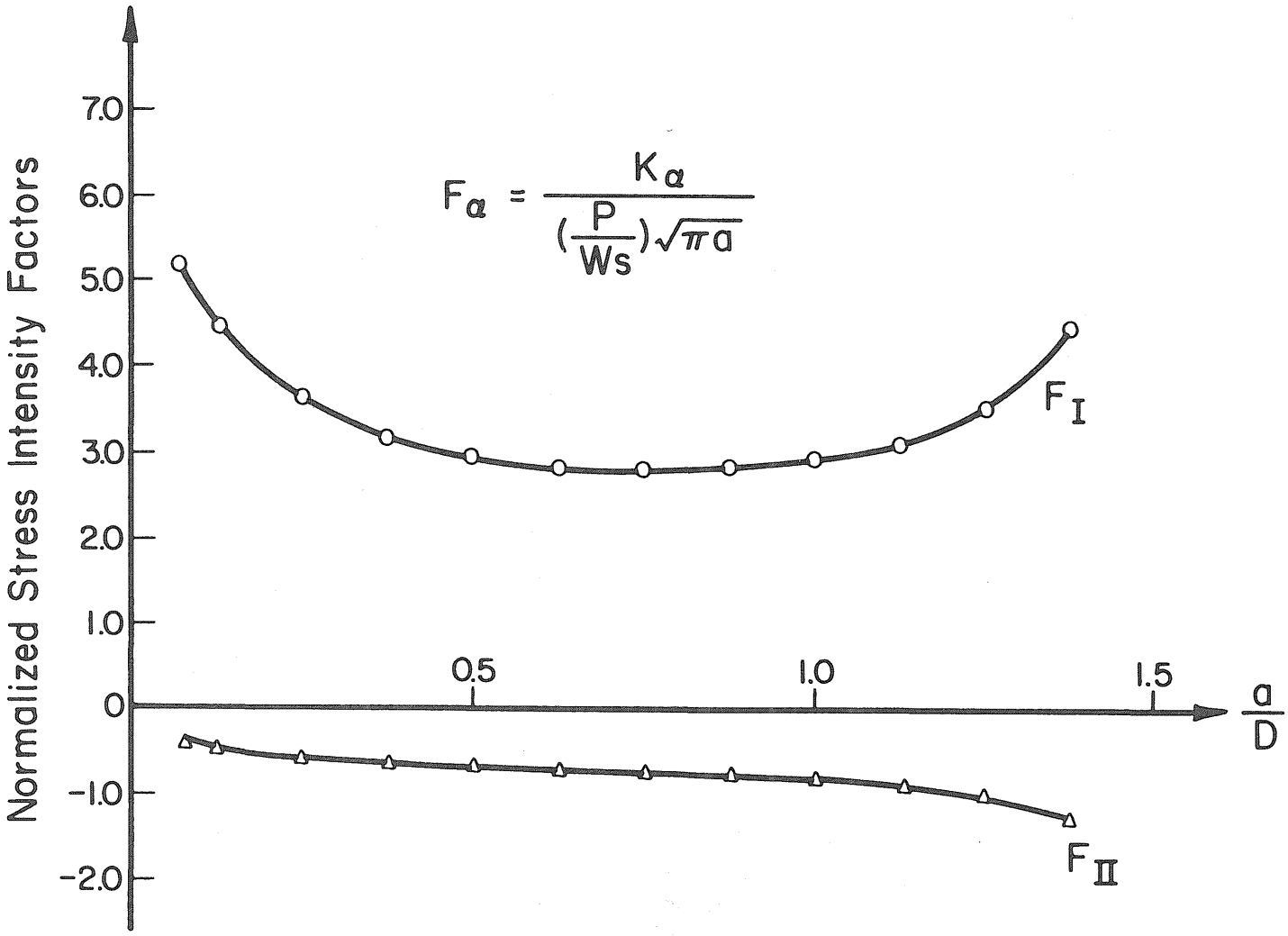

Figure 2.11 Individual Stress Intensity Factors vs. Crack Length

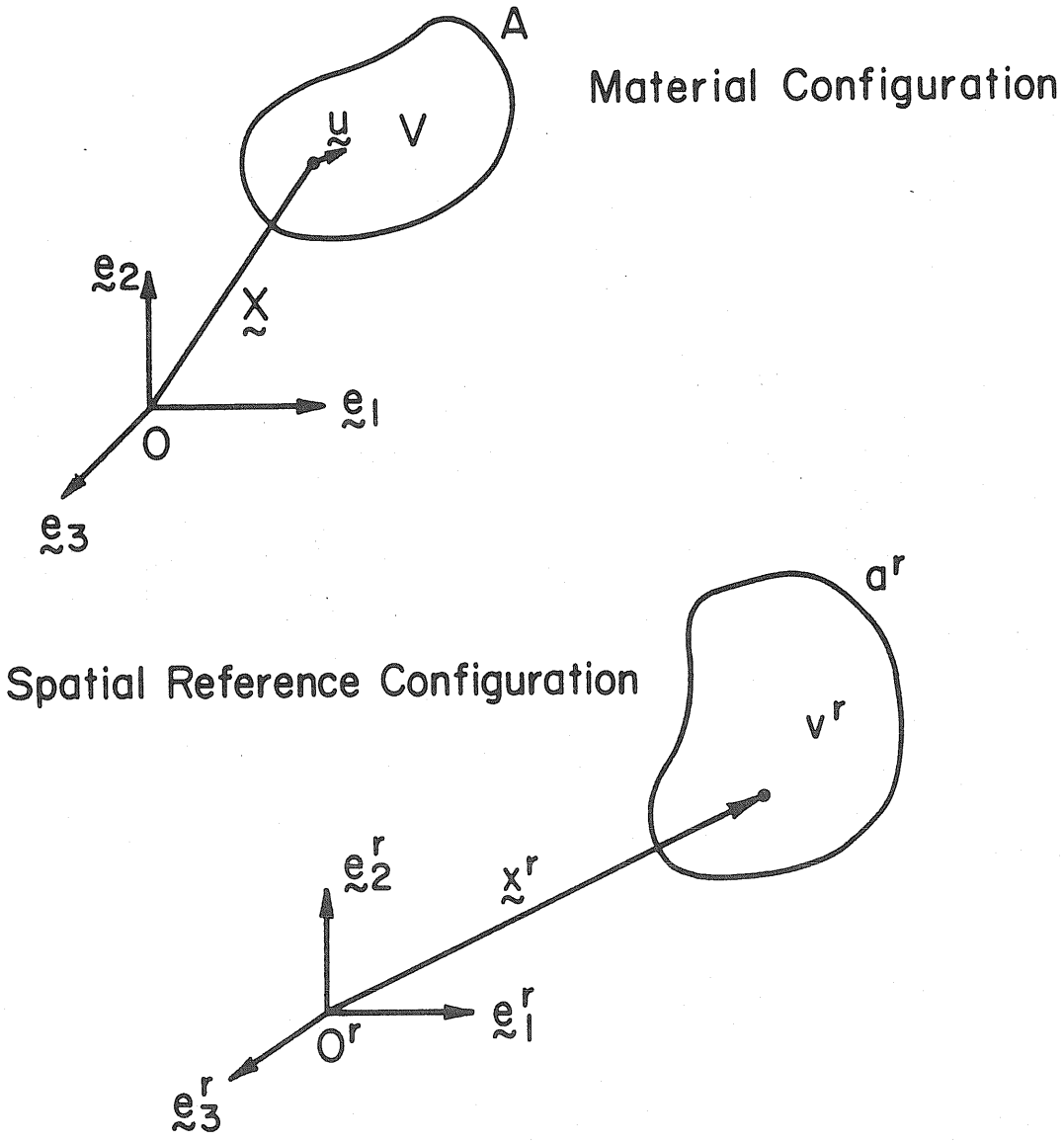

Figure 3.1 The Eulerian-Lagrangian Kinematic Model for Small-Deformation Analysis

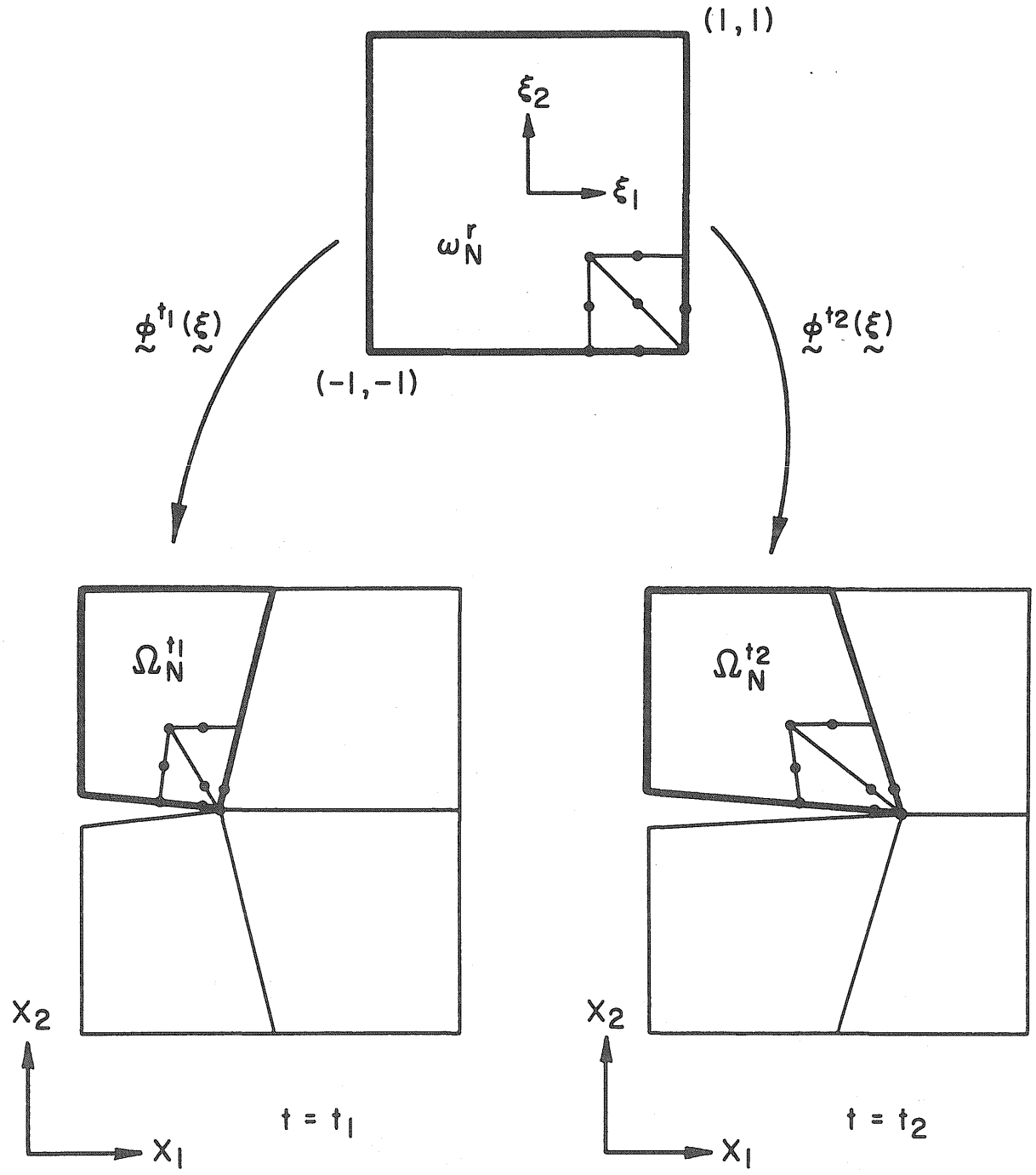

Figure 4.1 Auxiliary Geometric Mapping for Modeling the Crack-Tip Motion

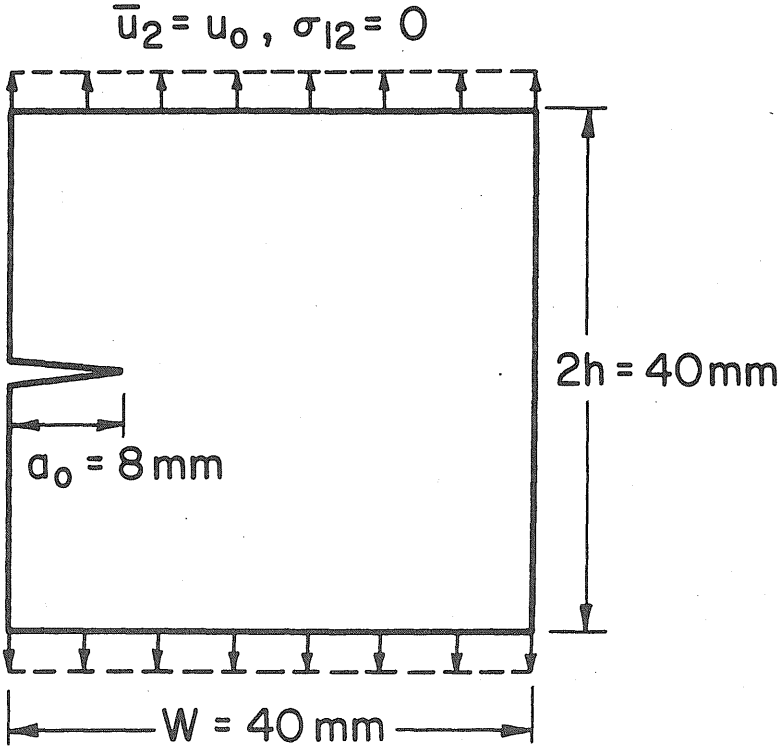

Young's Modulus (E): 7.56×10^{10} N/m^2
Poisson's Ratio (ν): 0.286
Shear Modulus (μ): 2.94×10^{10} N/m^2
Mass Density (ρ): 2.45×10^{3} Kg/m^3

Figure 4.2 Dimensions and Material Properties for a Mode-I Dynamic Crack Propagation Problem in a Finite Strip with Prescribed Boundary Displacements

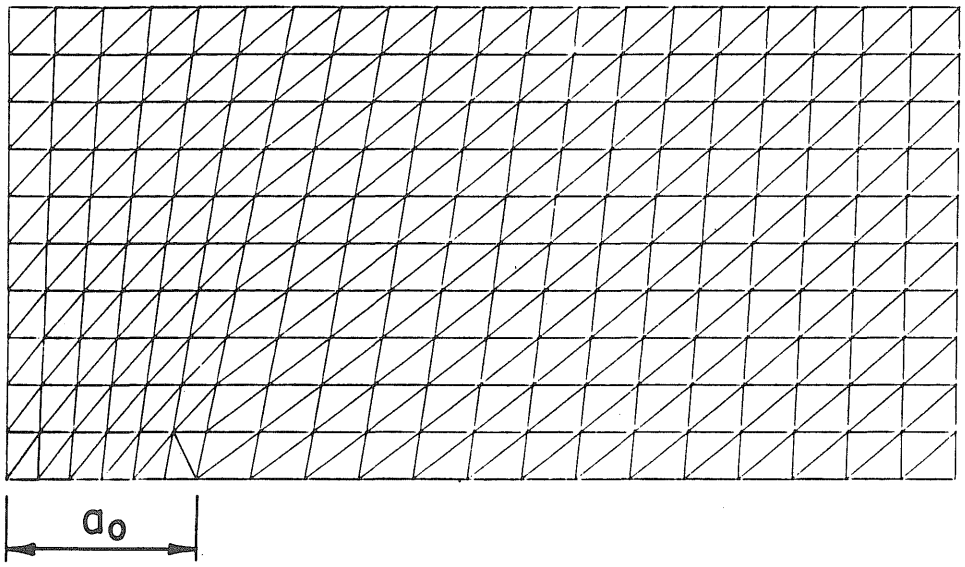

Figure 4.3 Finite Element Mesh for a Mode-I Dynamic Crack Propagation Problem in a Finite Strip

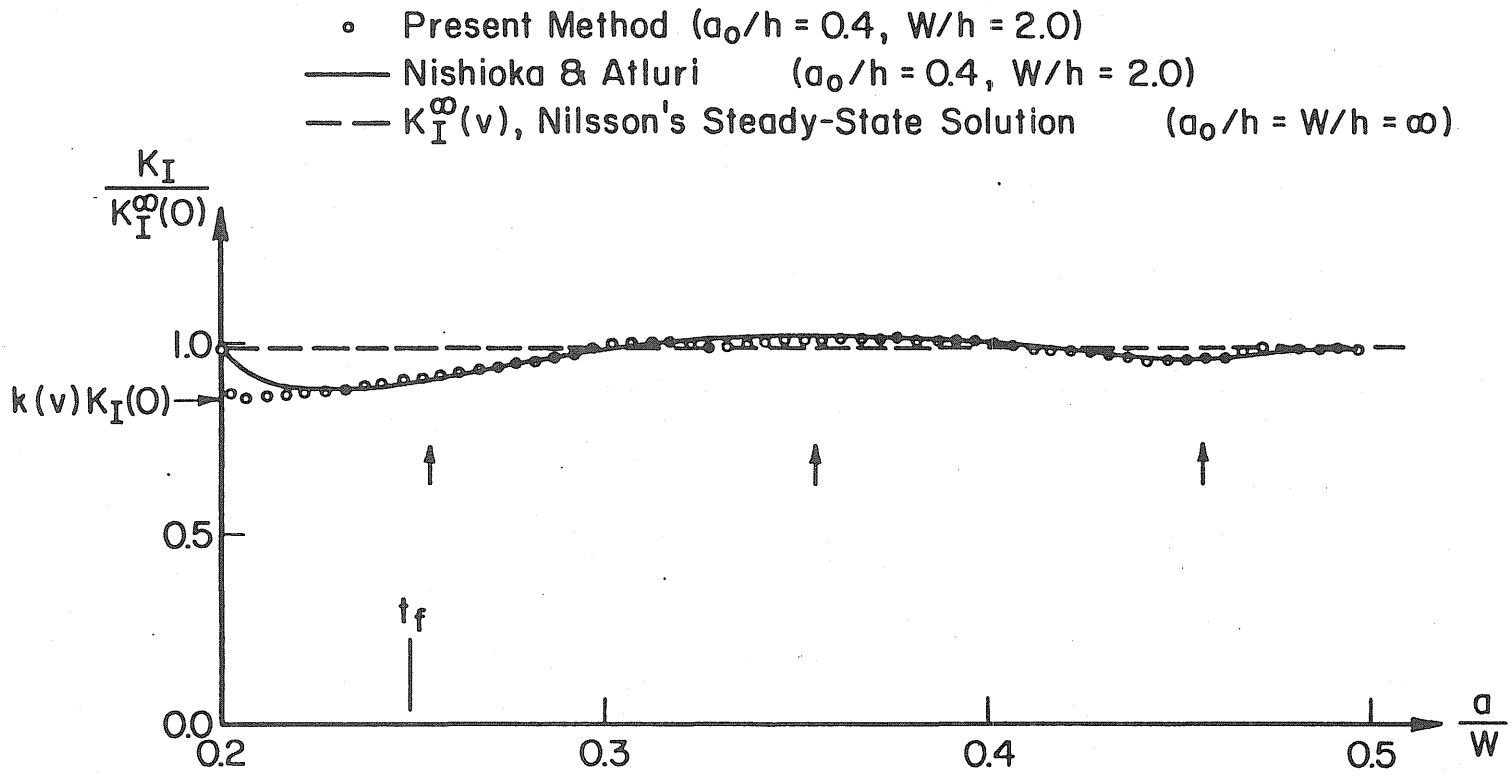

Figure 4.4 Normalized Stress Intensity Factor for Mode-I Dynamic Crack Propagation in a Finite Strip: ($v = 0.2\ C_s$)

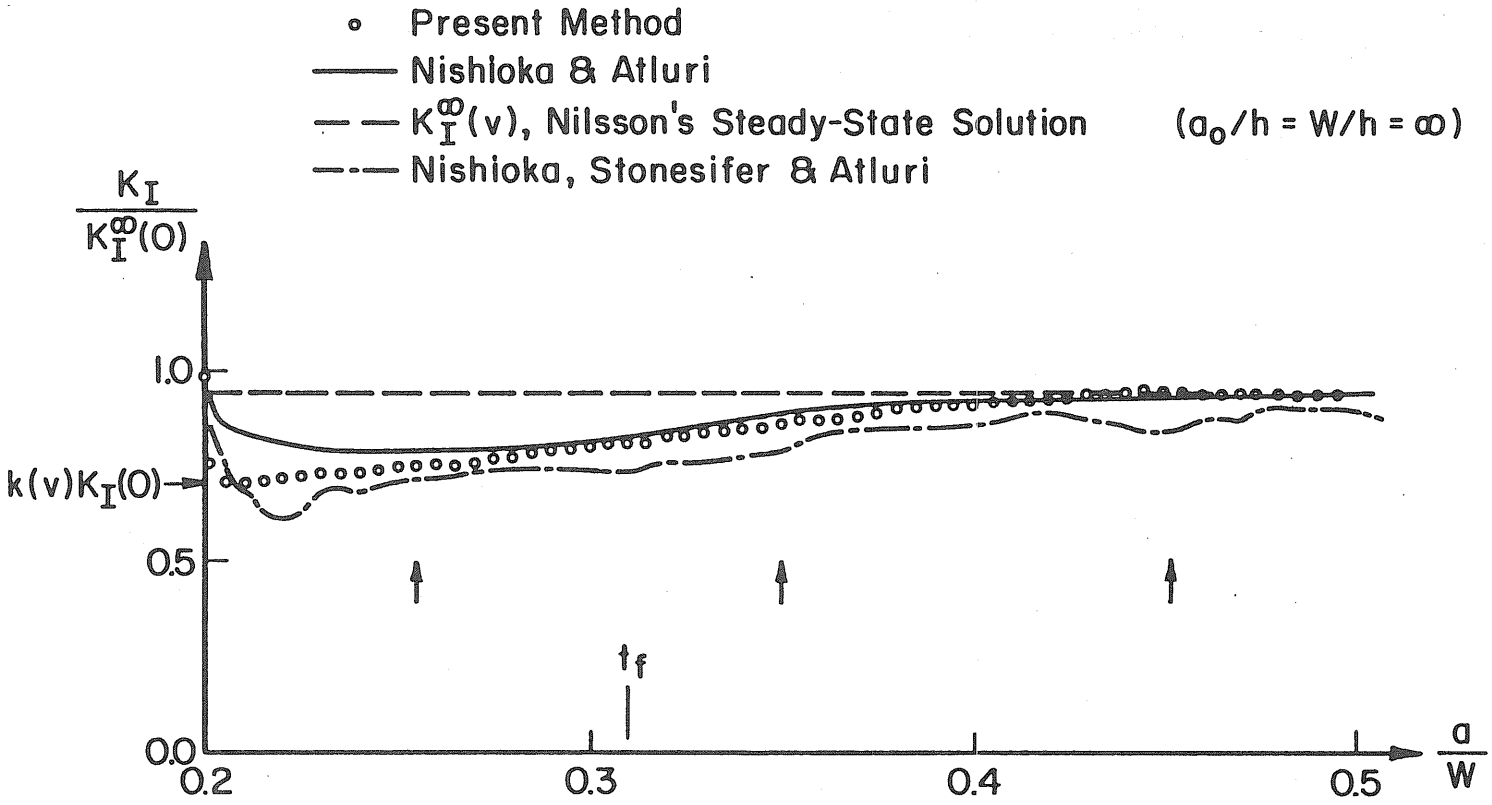

Figure 4.5 Normalized Stress Intensity Factor for Mode-I Dynamic Crack Propagation in a Finite Strip: ($v = 0.4\ C_S$)

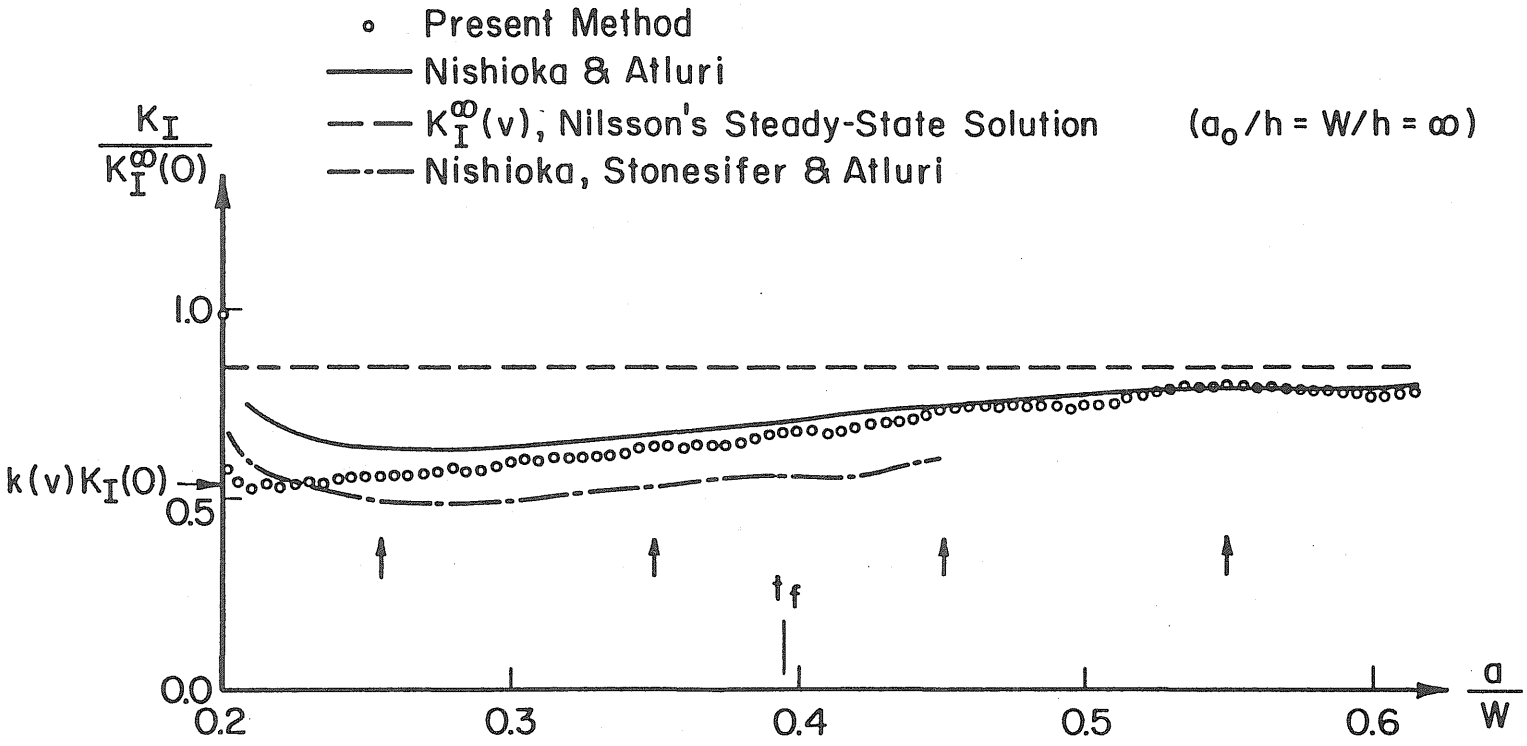

Figure 4.6 Normalized Stress Intensity Factor for Mode-I Dynamic Crack Propagation in a Finite Strip: ($v = 0.6\ C_s$)

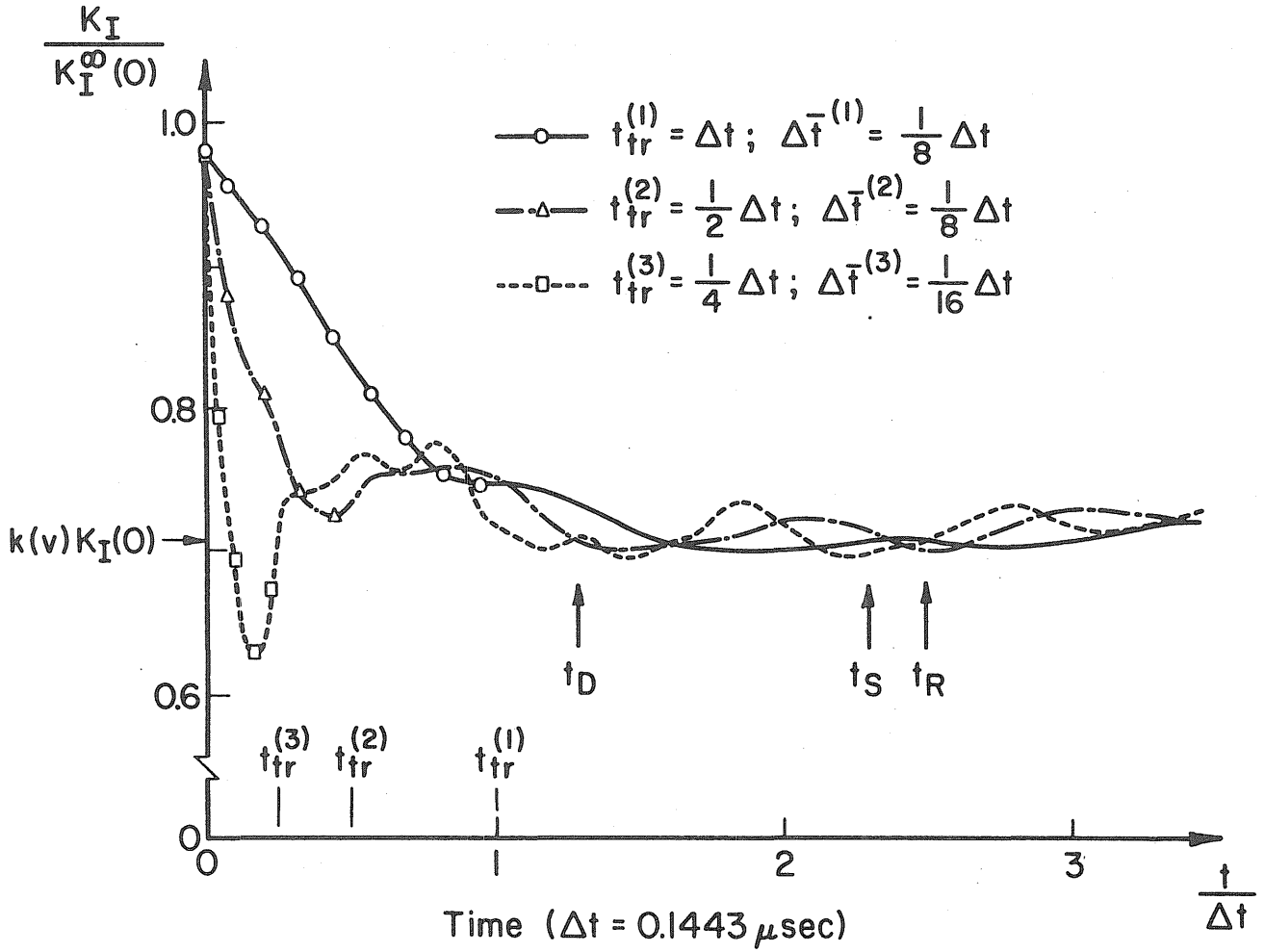

Figure 4.7 The Effect of Varying the Crack Acceleration Period on the Transient Response

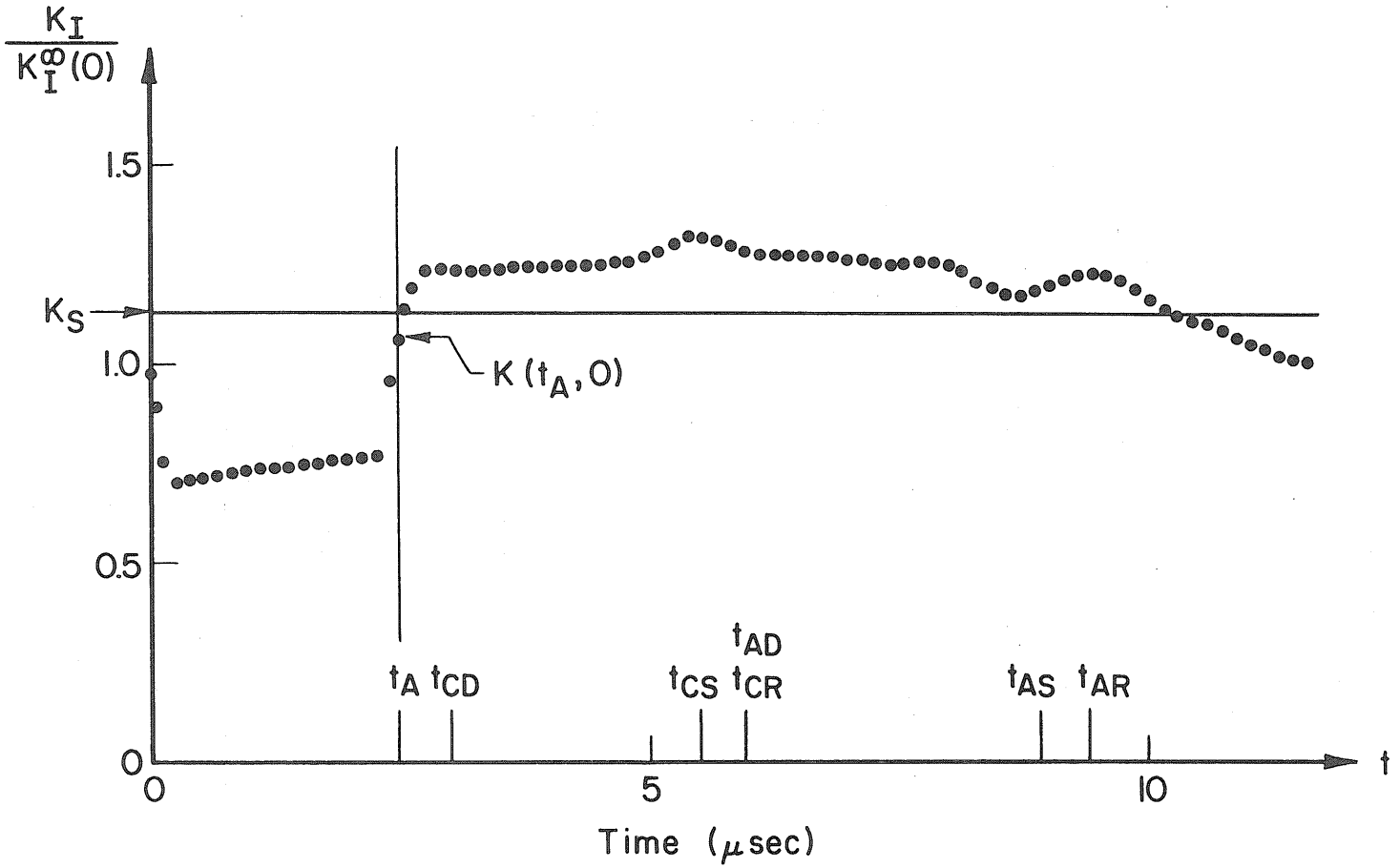

Figure 4.8 Normalized Stress Intensity Factor for a Crack Arrest Problem

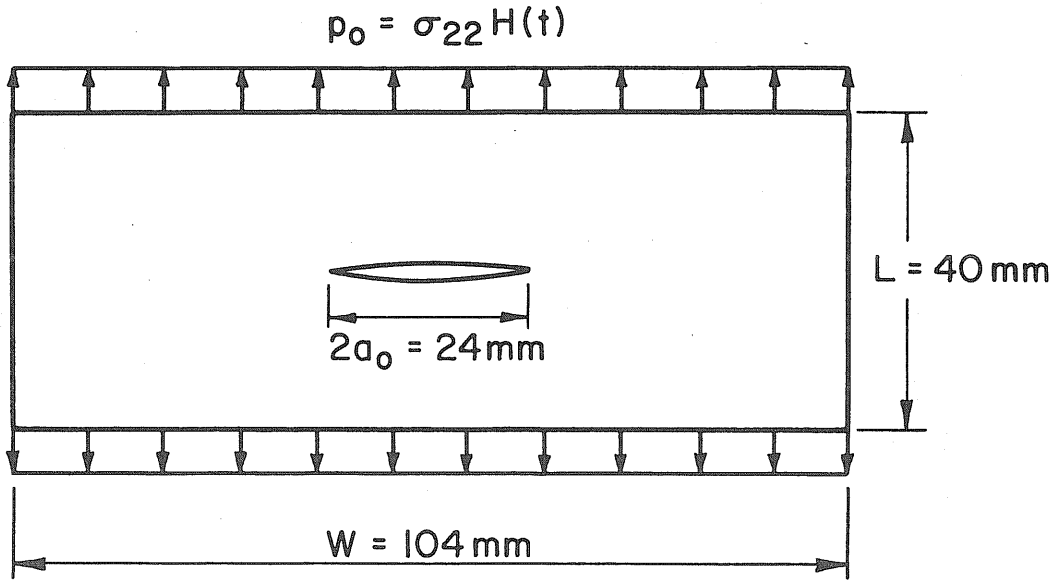

Young's Modulus (E): 7.56×10^{10} N/m^2

Poisson's Ratio (ν): 0.286

Shear Modulus (μ): 2.94×10^{10} N/m^2

Mass Density (ρ): 2.45×10^3 Kg/m^3

Figure 4.9 Dimensions and Material Properties for a Mode-I Dynamic Crack Propagation Problem in a Finite Plate with Stress-Wave Loading

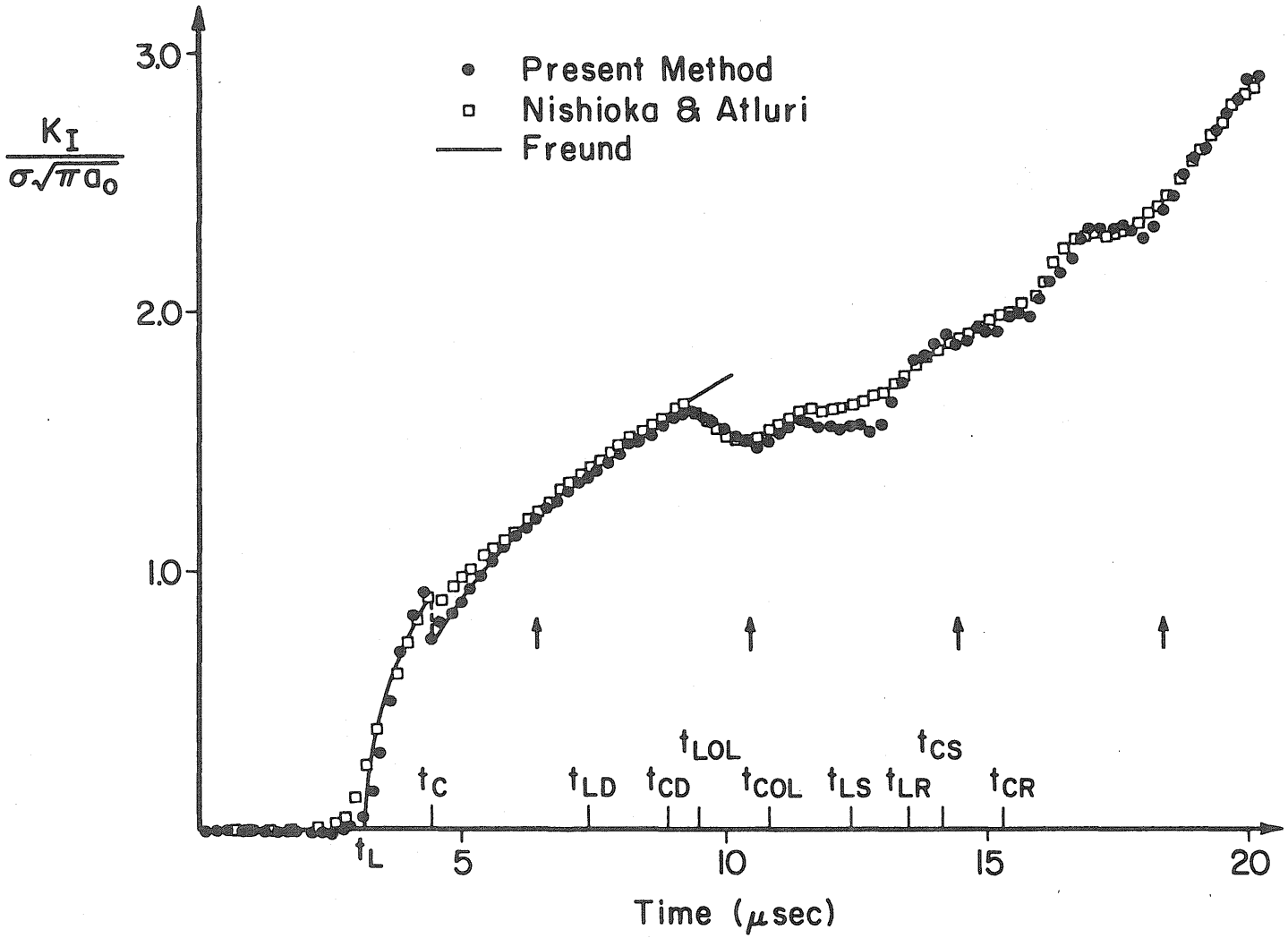

Figure 4.10 Normalized Stress Intensity Factor for Mode-I Dynamic Crack Propagation Problem in a Finite Plate with Stress-Wave Loading

APPENDIX A

FINITE ELEMENT MATRICES FOR COMPUTING THE ENERGY RELEASE RATES

This appendix presents finite element matrices for evaluating the mutual potential energy release rate (2.40) and the potential energy release rate (2.51). Field variables marked with superscripts (1) and (2) indicate quantities in the two independent equilibrium solutions used in the mutual potential energy formulation.

Isoparametric shape functions are used to interpolate the displacement field (2.34) and the element geometry (2.35). The Jacobian matrix is given by

$$\tilde{J} = \begin{bmatrix} \dfrac{\partial X_1}{\partial x_1^r} & \dfrac{\partial X_1}{\partial x_2^r} \\ \dfrac{\partial X_2}{\partial x_1^r} & \dfrac{\partial X_2}{\partial x_2^r} \end{bmatrix} = \begin{bmatrix} \tilde{J}_{11} & \tilde{J}_{12} \\ \tilde{J}_{21} & \tilde{J}_{22} \end{bmatrix} \tag{A.1}$$

$$\tilde{J}_{ij} = h_{\alpha,j} X_{i\alpha}; \quad \alpha = 1, N \tag{A.2}$$

and the inverse Jacobian matrix is

$$\bar{J} = \begin{bmatrix} \tilde{J}_{11} & \tilde{J}_{12} \\ \tilde{J}_{21} & \tilde{J}_{22} \end{bmatrix}^{-1} = \begin{bmatrix} \bar{J}_{11} & \bar{J}_{12} \\ \bar{J}_{21} & \bar{J}_{22} \end{bmatrix} \tag{A.3}$$

The stress and strain components for an axisymmetric problem are arranged in vector format as

$$\boldsymbol{\varepsilon}^T = \{e_{11}\ e_{22}\ 2e_{12}\ e_{33}\} \tag{A.4}$$

and

$$\begin{aligned} \boldsymbol{\tau}^T &= \{\sigma_{11}\ \sigma_{22}\ \sigma_{12}\ \sigma_{33}\} \\ &= \mathbf{E}\boldsymbol{\varepsilon} \end{aligned} \tag{A.5}$$

where $\mathbf{E}$ is the elasticity matrix. The terms in the strain vector are

$$\begin{aligned} e_{11} &= u_{1,1}\bar{J}_{11} + u_{1,2}\bar{J}_{21} \\ e_{22} &= u_{2,2}\bar{J}_{22} + u_{2,1}\bar{J}_{12} \\ 2e_{12} &= u_{1,1}\bar{J}_{12} + u_{1,2}\bar{J}_{22} + u_{2,2}\bar{J}_{21} \\ e_{33} &= u_1/r \end{aligned} \tag{A.6}$$

in which r is the radius from the axis of symmetry, and

$$u_{i,j} = h_{\alpha,j}u_{i\alpha};\quad \alpha = 1,\ N \tag{A.7}$$

Therefore, the strain-displacement transformation is

$$\boldsymbol{\varepsilon} = \mathbf{B}\mathbf{U}_e \tag{A.8}$$

where

$$\mathbf{B} = \begin{bmatrix} 1 & 0 & 0 & 0 & 0 \\ 0 & 0 & 0 & 1 & 0 \\ 0 & 1 & 1 & 0 & 0 \\ 0 & 0 & 0 & 0 & 1/r \end{bmatrix} \begin{bmatrix} \bar{J}_{11} & \bar{J}_{21} & 0 & 0 & 0 \\ \bar{J}_{12} & \bar{J}_{22} & 0 & 0 & 0 \\ 0 & 0 & \bar{J}_{11} & \bar{J}_{21} & 0 \\ 0 & 0 & \bar{J}_{12} & \bar{J}_{22} & 0 \\ 0 & 0 & 0 & 0 & 1 \end{bmatrix}$$

$$\cdot \begin{bmatrix} h_{1,1} & 0 & h_{2,1} & 0 & \cdots & h_{N,1} & 0 \\ h_{1,2} & 0 & h_{2,2} & 0 & \cdots & h_{N,2} & 0 \\ 0 & h_{1,1} & 0 & h_{2,1} & \cdots & 0 & h_{N,2} \\ 0 & h_{1,2} & 0 & h_{2,2} & \cdots & 0 & h_{N,2} \\ h_1 & 0 & h_2 & 0 & \cdots & h_N & 0 \end{bmatrix} \tag{A.9}$$

and

$$\mathbf{U}_e^T = \{u_{11}\ u_{21}\ u_{12}\ u_{22}\ \ldots u_{1N}\ u_{2N}\} \tag{A.10}$$

The scalars A_1 in (2.53) and $A_1^{(1,2)}$ in (2.41) can be expressed as

$$A_1 = \frac{1}{2}\, \boldsymbol{\varepsilon}^T \boldsymbol{\tau}\, \mathbf{J}^T\, \mathbf{v} \tag{A.11a}$$

$$A_1^{(1,2)} = \{\boldsymbol{\varepsilon}^{(1)}\}^T\, \boldsymbol{\tau}^{(2)}\, \mathbf{J}^T\, \mathbf{v} \tag{A.11b}$$

where

$$\mathbf{J}^T = \{\tilde{J}_{22}\ -\tilde{J}_{21}\ -\tilde{J}_{12}\ \tilde{J}_{11}\} \tag{A.12}$$

and

$$\mathbf{v} = \begin{bmatrix} h_{1,1} & 0 & h_{2,1} & 0 & \cdots & h_{N,1} & 0 \\ h_{1,2} & 0 & h_{2,2} & 0 & \cdots & h_{N,2} & 0 \\ 0 & h_{1,1} & 0 & h_{2,1} & \cdots & 0 & h_{N,1} \\ 0 & h_{1,1} & 0 & h_{2,2} & \cdots & 0 & h_{N,2} \end{bmatrix} \begin{bmatrix} D_{11} \\ D_{21} \\ D_{12} \\ D_{22} \\ \vdots \\ D_{1N} \\ D_{2N} \end{bmatrix} \tag{A.13}$$

in which values of the elements $D_{i\alpha}$ are given in (2.39).

The scalars A_2 in (2.54) and $A_2^{(1,2)}$ in (2.42) can be written as

$$A_2 = -\tau^T \mathbf{R}\, \mathbf{Q}\, \tilde{J} \tag{A.14a}$$

$$A_2^{(1,2)} = -(\{\tau^{(1)}\}^T \mathbf{R}^{(2)} + \{\tau^{(2)}\}^T \mathbf{R}^{(1)})\, \mathbf{Q}\, \tilde{J} \tag{A.14b}$$

where

$$\mathbf{R} = \begin{bmatrix} u_{1,1} & u_{1,2} & 0 & 0 & 0 \\ 0 & 0 & u_{2,1} & u_{2,2} & 0 \\ u_{2,1} & u_{2,2} & u_{1,1} & u_{1,2} & 0 \\ 0 & 0 & 0 & 0 & -u_1/r^2 \end{bmatrix} \tag{A.15}$$

$$\mathbf{Q} = \begin{Bmatrix} Q_1 \\ Q_2 \end{Bmatrix} \tag{A.16}$$

$$Q_1 = \begin{bmatrix} \bar{J}_{11}^2 & \bar{J}_{11}\bar{J}_{21} & \bar{J}_{11}\bar{J}_{12} & \bar{J}_{21}\bar{J}_{12} \\ & \bar{J}_{21}^2 & \bar{J}_{11}\bar{J}_{22} & \bar{J}_{21}\bar{J}_{22} \\ & \text{Symm.} & \bar{J}_{12}^2 & \bar{J}_{12}\bar{J}_{22} \\ & & & \bar{J}_{22}^2 \end{bmatrix} \mathbf{v} \tag{A.17}$$

and

$$Q_2 = \{h_1\ 0\ h_2\ 0\ \ldots\ h_N\ 0\} \begin{bmatrix} D_{11} \\ D_{21} \\ D_{12} \\ D_{22} \\ \vdots \\ D_{1N} \\ D_{2N} \end{bmatrix} \tag{A.18}$$

The energy release rate, (2.40) or (2.51), is numerically integrated over the crack-tip elements by evaluating (A.11) and (A.14) at the Gauss points.

For plane stress and plane strain problems the terms e_{33}, σ_{33} and Q_2, row 4 and column 4 of $\mathbf{E}$, row 4 and column 5 of $\mathbf{R}$ and row 4 of $\mathbf{B}$ are dropped.

APPENDIX B

FINITE ELEMENT MATRICES FOR THE DYNAMIC EULERIAN-LAGRANGIAN FORMULATION

This appendix presents matrices for general three-dimensional isoparametric finite element analysis based on the dynamic ELD kinematic model developed in Chapter 3. As in the text, the summation symbol indicates assembly over the number of elements. The consistent mass matrix in (3.33) is

$$\mathbf{M} = \sum \int_{v_e^r} \rho \, \mathbf{H}^T \mathbf{H} \, \tilde{J} dv_e^r \tag{B.1}$$

and the effective damping matrix is

$$\mathbf{C} = \sum \left(-\int_{v_e^r} 2\rho \, \mathbf{H}^T \mathring{\mathbf{A}} \mathbf{G} \, \tilde{J} dv_e^r\right) \tag{B.2}$$

where matrices $\mathring{\mathbf{A}}$ and $\mathbf{G}$ are

$$\mathring{\mathbf{A}} = \begin{bmatrix} \bar{J}_{1j}\mathring{X}_j & \bar{J}_{2j}\mathring{X}_j & \bar{J}_{3j}\mathring{X}_j & 0 & 0 & 0 & 0 & 0 & 0 \\ 0 & 0 & 0 & \bar{J}_{1j}\mathring{X}_j & \bar{J}_{2j}\mathring{X}_j & \bar{J}_{3j}\mathring{X}_j & 0 & 0 & 0 \\ 0 & 0 & 0 & 0 & 0 & 0 & \bar{J}_{1j}\mathring{X}_j & \bar{J}_{2j}\mathring{X}_j & \bar{J}_{3j}\mathring{X}_j \end{bmatrix} \tag{B.3}$$

$$\mathbf{G} = \begin{bmatrix} \mathbf{g} & \mathbf{0} & \mathbf{0} \\ \mathbf{0} & \mathbf{g} & \mathbf{0} \\ \mathbf{0} & \mathbf{0} & \mathbf{g} \end{bmatrix} \cdot \mathbf{H} \tag{B.4}$$

and

$$\mathbf{g}^T = \{\partial/\partial x_1^r \quad \partial/\partial x_2^r \quad \partial/\partial x_3^r\} \tag{B.5}$$

The stiffness matrix is defined as

$$\mathbf{K} = \sum \Big(\int_{v_e^r} \mathbf{B}^T\mathbf{E}\mathbf{B}\, \tilde{J} dv_e^r + \int_{v_e^r} \rho\, \mathbf{H}^T\mathbf{D}\mathbf{G}\, \tilde{J} dv_e^r - \int_{v_e^r} \rho\, \mathbf{H}^T\ddot{\mathbf{A}}\mathbf{G}\, \tilde{J} dv_e^r$$

$$+ \int_{a_e^r} \rho\, \mathbf{H}^T\mathring{\mathbf{A}}\mathbf{G}\, A_1 K_a da_e^r - \int_{v_e^r} \rho\, \mathbf{H}^T\mathbf{S}\mathbf{G}\, \tilde{J} dv_e^r - \int_{v_e^r} \rho\, \mathbf{G}^T\mathring{\mathbf{A}}^T\mathring{\mathbf{A}}\mathbf{G}\, \tilde{J} dv_e^r \Big) \tag{B.6}$$

Here, matrix $\ddot{\mathbf{A}}$ has the same form as $\mathring{\mathbf{A}}$ with $\dot{X}$ being replaced by $\ddot{X}$. **D** and **S** are defined by introducing the following two vectors:

$$\mathbf{b} = \mathring{\mathbf{A}}\mathbf{G}\dot{X}_e, \quad \mathbf{q} = a\,\mathbf{H}\dot{X}_e \tag{B.7}$$

where $a = \dot{X}_{\ell,m}\bar{J}_{m\ell}$. Then

$$\mathbf{D} = \begin{bmatrix} b_i\bar{J}_{1i} & b_i\bar{J}_{2i} & b_i\bar{J}_{3i} & 0 & 0 & 0 & 0 & 0 & 0 \\ 0 & 0 & 0 & b_i\bar{J}_{1i} & b_i\bar{J}_{2i} & b_i\bar{J}_{3i} & 0 & 0 & 0 \\ 0 & 0 & 0 & 0 & 0 & 0 & b_i\bar{J}_{1i} & b_i\bar{J}_{2i} & b_i\bar{J}_{3i} \end{bmatrix} \tag{B.8}$$

and matrix **S** is obtained by replacing b_i in **D** by q_i. When the mapping changes in the X_1-direction only, matrices **D** and **S** are identical, and the corresponding integrals in (B.6) cancel.

The scalar $A_1 K_a$ in (B.6), where $A_1 = \dot{X}_i n_i$, is expressed as,

$$A_1 K_a = \dot{X}_e^T \cdot H^T \cdot \begin{bmatrix} \tilde{J}_{22}\tilde{J}_{33} - \tilde{J}_{32}\tilde{J}_{23} \\ \tilde{J}_{32}\tilde{J}_{13} - \tilde{J}_{12}\tilde{J}_{33} \\ \tilde{J}_{12}\tilde{J}_{23} - \tilde{J}_{22}\tilde{J}_{13} \end{bmatrix} \tag{B.9}$$

Note that the surface integral in (B.6) will vanish for finite bodies by (3.29).

The load vector in (3.33) is

$$P = \sum \left(\int_{v_e^r} H^T F_e \tilde{J} dv_e^r + \int_{a_T^r} H^T \bar{T}_e K_a da_e^r \right) \tag{B.10}$$

where F_e and $\bar{T}_e$ are vectors containing nodal intensities of body force and surface traction for each element.

REFERENCES

1. Rice, J. R., "An Examination of the Fracture Mechanics Energy Balance From the Point of View of Continuum Mechanics," Proceedings of the First International Conference on Fracture, Sendai, pp. 309-340 (1965)

2. Griffith, A. A., "The Phenomena of Rupture and Flow in Solids," Philosophical Transactions of the Royal Society of London, Series A, Vol 221, pp. 163-198 (1920)

3. Mott, N. F., "Fracture of Metals: Theoretical Considerations," Engineering, Vol. 165, pp. 16-18 (1948)

4. Irwin, G. R., "Fracture," in Handbuch der Physik, Vol. 6, pp. 551-590 (1958)

5. Orowan, E., "Fracture and Strength of Solids," Reports on Progress in Physics, Vol. 12, p. 185 (1948)

6. Irwin, G. R., "Analysis of Stresses and Strains Near the End of a Crack Traversing a Plate," Journal of Applied Mechanics, Transactions of ASME, Vol. 24, pp. 361-364 (1957)

7. Nilsson, F., "A Note on the Stress Singularity at a Non-Uniformly Moving Crack Tip," Journal of Elasticity, Vol. 4, pp. 73-75 (1974)

8. Knauss, W. G. and Ravi-Chandar, K., "Some Basic Problems in Stress Wave Dominated Fracture," International Journal of Fracture, Vol. 27, pp. 127-143 (1985)

9. Paris, P. C. and Sih, G. C., "Stress Analysis of Cracks," in Fracture Toughness Testing and its Applications, ASTM STP, No. 381, pp. 30-81 (1965)

10. Rice, J. R., "Mathematical Analysis in the Mechanics of Fracture," Chapter 3 in Fracture, Vol. II (Ed. Liebowitz, H.), Academic Press, New York (1968)

11. Freund, L. B., "Dynamic Crack Propagation," The Mechanics of Fracture (Ed. Erdogan, F.), ASME AMD, Vol. 19, pp. 105-134 (1976)

12. Rose, L. R. F., "Recent Theoretical and Experimental Results on Fast Brittle Fracture," International Journal of Fracture, Vol. 12, pp. 799-813 (1976)

13. Ma, C. C. and Freund, L. B., "The Extent of the Stress Intensity Factor Field in Dynamic Crack Growth," Report to NSF, Brown University (1984)

14. Gallagher, R. H., "A Review of Finite Element Techniques in Fracture Mechanics," Numerical Methods in Fracture Mechanics (Ed. Luxmoore, A. R. and Owen, D. R.), Swansea, pp. 1-25 (1978)

15. Kanninen, M. F., "A Critical Appraisal of Solution Techniques in Dynamic Fracture Mechanics," Numerical Methods in Fracture Mechanics (Ed. Luxmoore, A. R. and Owen, D. R.), Swansea, pp. 612-633 (1978)

16. Atluri, S. N. and Nishioka, T., "Numerical Studies in Dynamic Fracture Mechanics," International Journal of Fracture, Vol. 27, pp. 127-143 (1985)

17. Haber, R. B., "A Mixed Eulerian-Lagrangian Displacement Model for Large-Deformation Analysis in Solid Mechanics," Computer Methods in Applied Mechanics and Engineering, Vol. 43, pp. 277-292 (1984)

18. Haber, R. B. and Hariandja, B. H., "An Eulerian-Lagrangian Finite Element Approach to Large-Deformation Frictional Contact," Computers and Structures, Vol. 20, pp. 193-201 (1985)

19. Hariandja, B. H., "Adaptive Finite Element Analysis of Nonlinear Frictional Contact with Mixed Eulerian-Lagrangian Coordinates," Thesis submitted in partial fulfillment of the requirements for the degree of Doctor of Philosophy in Civil Engineering in the Graduate College of the University of Illinois at Urbana-Champaign, Urbana, Illinois (1986)

20. Bergkvist, H. and Guex, L., "Curved Crack Propagation," International Journal of Fracture, Vol. 15, pp. 429-441 (1979)

21. Rice, J. R., "A Path Independent Integral and the Approximate Analysis of Strain Concentration by Notches and Cracks," Journal of Applied Mechanics, Transactions of ASME, Vol. 35, pp. 379-386 (1968)

22. Haber, R. B. and Koh, H. M., "Explicit Expressions for Energy Release Rates Using Virtual Crack Extensions," International Journal for Numerical Methods in Engineering, Vol. 21, pp. 301-315 (1985)

23. Haber, R. B. and Koh, H. M., "An Eulerian-Lagrangian Virtual Crack Extension Method for Mixed-Mode Fracture Problems," Proceedings of the 25th Structures, Structural Dynamics and Materials Conference, AIAA/ASME/ASCE/AHS, Part I, Palm Springs, CA, pp. 116-122 (1984)

24. Henshell, R. D. and Shaw, K. G., "Crack Tip Elements Are Unnecessary," International Journal for Numerical Methods in Engineering, Vol. 9, pp. 495-507 (1975)

25. Barsoum, R. S., "On the Use of Isoparametric Finite Elements in Linear Fracture Mechanics," International Journal for Numerical Methods in Engineering, Vol. 10, pp. 25-37 (1976)

26. Akin, J. E., "The Generation of Elements with Singularities," International Journal for Numerical Methods in Engineering, Vol. 10, pp. 1249-1259 (1976)

27. Hibbit, H. D., "Some Properties of Singular Isoparametric Elements," International Journal for Numerical Methods in Engineering, Vol. 11, pp. 180-184 (1977)

28. Yamada, Y., Ezawa, Y., Nishiguchi, I. and Okabe, M., "Reconsiderations on Singularity or Crack Tip Elements," International Journal for Numerical Methods in Engineering, Vol. 14, pp. 1525-1544 (1979)

29. Lynn, P. P. and Ingraffea, A. R., "Transition Elements to be Used with Quarter-Point Crack-Tip Elements," International Journal for Numerical Methods in Engineering, Vol. 12, pp. 1031-1036 (1978)

30. Tong, P., Pian, T. H. H. and Lasry, S. J., "A Hybrid-Element Approach to Crack Problems in Plane Elasticity," International Journal for Numerical Methods in Engineering, Vol. 7, pp. 297-308 (1973)

31. Blackburn, W. S., "Calculation of Stress Intensity Factors at Crack Tips Using Special Finite Elements," in The Mathematics of Finite Elements and Applications (Ed. Whiteman, J. R.), Academic Press, New York (1973)

32. Tracey, D. M. and Cook, T. S., "Analysis of Power Type Singularities Using Finite Elements," International Journal for Numerical Methods in Engineering, Vol. 11, pp. 1225-1233 (1977)

33. Chan, S. K., Tuba, I. S. and Wilson, W. K., "On the Finite Element Method in Linear Fracture Mechanics," Engineering Fracture Mechanics, Vol. 2, pp. 1-17 (1970)

34. Tracey, D. M., "Finite Elements for Determination of Crack Tip Elastic Stress Intensity Factors," Engineering Fracture Mechanics, Vol. 3, pp. 255-265 (1972)

35. Gifford, L. N., Jr. and Hilton, P. D., "Stress Intensity Factors by Enriched Finite Elements," Engineering Fracture Mechanics, Vol. 10, pp. 485-496 (1978)

36. Watwood, V. B., Jr., "The Finite Element Method for Prediction of Crack Behavior," Nuclear Engineering and Design, Vol. 11, pp. 323-332 (1969)

37. Parks, D. M., "A Stiffness Derivative Finite Element Technique for Determination of Crack Tip Stress Intensity Factors," International Journal of Fracture, Vol. 10, pp. 487-502 (1974)

38. Hellen, T. K., "On the Method of Virtual Crack Extensions," International Journal for Numerical Methods in Engineering, Vol. 9, pp. 187-207 (1975)

39. Yau, J. F., Wang, S. S. and Corten, H. T., "A Mixed-Mode Crack Analysis of Isotropic Solids Using Conservation Laws of Elasticity," Journal of Applied Mechanics, Transactions of ASME, Vol. 47, pp. 335-341 (1980)

40. Cook, R. D., Concepts and Applications of Finite Element Analysis, 2nd Edition, Wiley, New York (1981)

41. Bueckner, H. F., Discussion on Reference 9, in ASTM STP No. 381, pp. 82-83 (1965)

42. Tong, P. and Pian, T. H. H., "On the Convergence of the Finite Element Method for Problems with Singularity," International Journal of Solids and Structures, Vol. 9, pp. 313-321 (1973)

43. Liu, A. F. and Kan, H. P., "Test and Analysis of Cracked Lug," Advances in Research on the Strength and Fracture of Materials (Ed. Taplin, D. M. R.), pp. 657-664 (1978)

44. Paris, P. and Erdogan, F., "A Critical Analysis of Crack Propagation Laws," Journal of Basic Engineering, Transactions of ASME, Series D, Vol. 85, No. 3, pp. 528-534 (1963)

45. Nishioka, T. and Atluri, S. N., "Numerical Modeling of Dynamic Crack Propagation in Finite Bodies, by Moving Singular Elements, Part 1: Formulation," Journal of Applied Mechanics, Transactions of ASME, Vol. 47, pp. 570-576 (1980)

46. Bazant, Z. P., Glazik, J. I., Jr. and Achenbach, J. D., "Elastodynamic Fields Near Running Cracks by Finite Elements," Computers and Structures, Vol. 8, pp. 193-198 (1978)

47. Bazant, Z. P., Glazik, J. I., Jr. and Achenbach, J. D., "Finite Element Analysis of Wave Diffraction by a Crack," Journal of Engineering Mechanics Division, ASCE, Vol. 102, EM3, pp. 479-496 (1976)

48. Freund, L. B., "The Analysis of Elastodynamic Crack Tip Stress Fields," in Mechanics Today (Ed. Nemat-Nasser, S.), Vol. 3, pp. 55-91 (1976)

49. Freund, L. B. and Clifton, R. J., "On the Uniqueness of Plane Elastodynamic Solutions for Running Cracks," Journal of Elasticity, Vol. 4, pp. 293-299 (1974)

50. Freund, L. B., "Crack Propagation in an Elastic Solid Subjected to General Loading -- III. Stress Wave Loading," Journal of the Mechanics of Physics and Solids, Vol. 21, pp. 47-61 (1973)

51. Freund, L. B., "Crack Propagation in an Elastic Solid Subjected to General Loading -- I. Constant Rate of Extension," Journal of the Mechanics of Physics and Solids, Vol. 20, pp. 129-140 (1972)

52. Kostrov, B. V., "On the Crack Propagation with Variable Velocity," International Journal of Fracture, Vol. 11, pp. 47-56 (1975)

53. Bergkvist, H., "The Motion of a Brittle Crack," Journal of the Mechanics of Physics and Solids, Vol. 21, pp. 229-239 (1973)

54. Freund, L. B., "Energy Flux into the Tip of an Extending Crack in an Elastic Solid," Journal of Elasticity, Vol. 2, pp. 341-349 (1972)

55. Nishioka, T. and Atluri, S. N., "Path-Independent Integrals, Energy Release Rates, and General Solutions of Near-Tip Fields in Mixed-Mode Dynamic Fracture Mechanics," Engineering Fracture Mechanics, Vol. 18, pp. 1-22 (1983)

56. Erdogan, F., "Crack-Propagation Theories," Chapter 5 in Fracture, Vol. II (Ed. Liebowitz, H.), Academic Press, New York (1968)

57. Achenbach, J. D., "Dyanmic Effects in Brittle Fracture," Mechanics Today (Ed. Nemat-Nasser, S.), Vol. 1, pp. 1-57 (1974)

58. Keegstra, P. N. R., Head, J. L. and Turner, C. E., "A Two Dimensional Dynamic Linear Elastic Finite Element Program for the Analysis of Unstable Crack Propagation and Arrest," Numerical Methods in Fracture Mechanics (Ed. Luxmoore, A. R. and Owen, D. R.), Swansea, pp. 634-647 (1978)

59. Kobayashi, A. S., "Dynamic Fracture Analysis by Dynamic Finite Element Method - Generation and Propagation Analysis," Nonlinear and Dynamic Fracture Mechanics, ASME AMD, Vol. 35, pp. 19-36 (1979)

60. Hodulak, L., Kobayashi, A. S. and Emery, A. F., "A Critical Examination of a Numerical Fracture Dynamic Code," Fracture Mechanics: Twelfth Conference, ASTM STP 700, pp. 174-188 (1980)

61. Malluck, J. F. and King, W. W., "Fast Fracture Simulated by Conventional Finite Elements: A Comparison of Two Energy-Release Algorithms," Crack Arrest Methodology and Applications, ASTM STP 711, pp. 38-53 (1980)

62. Caldis, E. S., Owen, D. R. J. and Zienkiewicz, O. C., "Nonlinear Dynamic Transient Methods in Crack Propagation Studies," Nonlinear and Dynamic Fracture Mechanics, ASME AMD, Vol. 35, pp. 1-17 (1979)

63. Brickstad, B. and Nilsson, F., "Explicit Time Integration in FEM-analysis of Dynamic Crack Propagation," Numerical Methods in Fracture Mechanics (Ed. Luxmoore, A. R. and Owen, D. R.), Swansea, pp. 7-11 (1980)

64. Gunther, C. K., Holsapple, K. A. and Kobayashi, A. S., "Elastodynamic Analysis of Cracked Finite Bodies by the Finite Element Method," Proceedings of the 21st Structures, Structural Dynamics, and Materials Conference, AIAA/ASME/ASCE/AHS, Part I, Seattle, pp. 334-344 (1980)

65. Nishioka, T., Stonesifer, R. B. and Atluri, S. N., "An Evaluation of Several Moving Singularity Finite Element Models for Fast Fracture Analysis," Engineering Fracture Mechanics, Vol. 15, pp. 205-218 (1981)

66. Atluri, S. N., "Path-Independent Integrals in Finite Elasticity and Inelasticity, with Body Froces, Inertia, and Arbitrary Crack-Face Conditions," Engineering Fracture Mechanics, Vol. 16, pp. 341-364 (1982)

67. Nishioka, T. and Atluri, S. N., "Dynamic Crack Propagation Analysis Using a New Path-Independent Integral and Moving Isoparametric Elements," Proceedings of the 24th Structures, Structural Dynamics and Materials Conference, AIAA/ASME/ASCE/AHS, Lake Tahoe, pp. 180-190 (1983)

68. Haber, R. B. and Abel, J., "Discrete Transfinite Mappings for the Description of Three-Dimensional Surfaces Using Interactive Computer Graphics." International Journal for Numerical Methods in Engineering, Vol. 18, pp. 41-66 (1982)

69. Nilsson, F., "Dynamic Stress-Intensity Factors for Finite Strip Problems," International Journal of Fracture Mechanics, Vol. 8, pp. 403-411 (1972)

70. Nishioka, T. and Atluri, S. N., "Numerical Modeling of Dynamic Crack Propagation in Finite Bodies, by Moving Singular Elements, Part 2: Results," Journal of Applied Mechanics, Transactions of ASME, Vol. 47, pp. 577-582 (1980)

71. Eshelby, J. D., "The Elastic Field of a Crack Extending Non-Uniformly Under General Anti-Plane Loading," Journal of Mechanis of Physics and Solids, Vol. 17, pp. 177-199 (1969)

72. Kalthoff, J. F., Beinert, J., Winkler, S. and Klemm, W., "Experimental Analysis of Dynamic Effects in Different Crack Arrest Test Specimens," Crack Arrest Methodology and Applications, ASTM STP 711, pp. 109-127 (1980)

73. Hussain, M. A., Coffin, L. F. and Zaleski, K. A., "Three Dimensional Singular Element," Computers and Structures, Vol. 13, pp. 595-599 (1981)

74. Manu, C., "Quarter-point Elements for Curved Crack Fronts," Computers and Structures, Vol. 17, pp. 227-231 (1983)

75. Peano, A. and Pasini, A., "A Warning Against Misuse of Quarter-Point Elements," International Journal for Numerical Methods in Engineering, Vol. 18, pp. 314-320 (1982)

76. Wilson, E. L., Bathe, K. J. and Peterson, F. E., "Finite Element Analysis of Linear and Nonlinear Heat Transfer," Nuclear Engineering and Design, Vol. 29, pp. 110-124 (1974)

77. Döll, W., "Application of an Energy Balance and an Energy Method to Dynamic Crack Propagation," International Journal of Fracture, Vol. 12, pp. 595-605 (1976)

78. Weichert, R. and Schönert, K., "On the Temperature Rise at the Tip of a Fast Running Crack," Journal of Mechanics of Physics and Solids, Vol. 22, pp. 127-133 (1974)

79. Weichert, R. and Schönert, K., "Heat Generation at the Tip of a Moving Crack," Journal of Mechanics of Physics and Solids, Vol. 26, pp. 151-161 (1978)